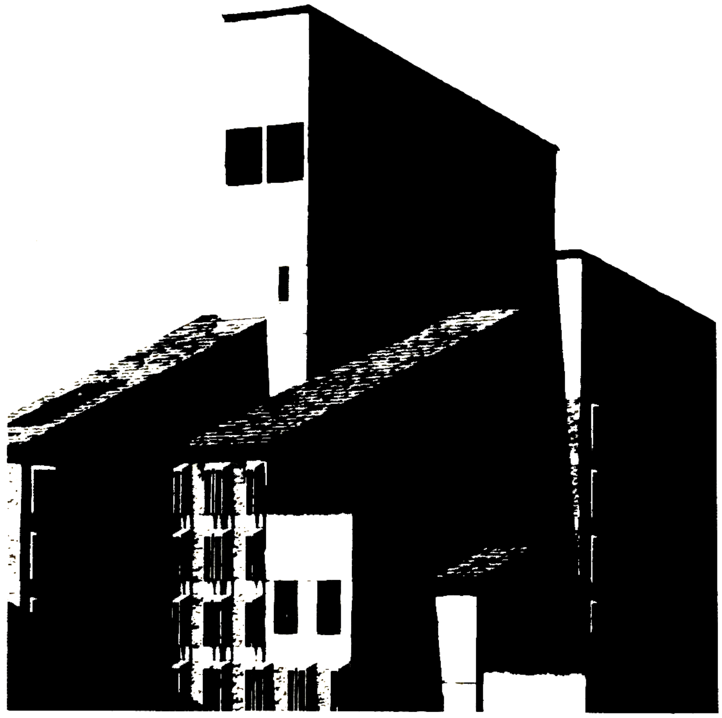

NEESR-SG Project
Seismic Performance Assessment and Retrofit of Non-Ductile RC Frames With Infill Walls

Ben Blackard, Dr. Sivaselvan Mettupalayam, Dr. Kaspar Willam

SESM No. 03-2009

Department of Civil, Environmental,
and Architectural Engineering

College of Engineering
and Applied Science

University of Colorado at Boulder

Table of Contents

Chapter 1: Introduction

Six infilled frame tests have been conducted at the University of Colorado Structural Engineering lab. Solid infill walls, walls with openings, and retrofitted walls have been tested. Table 1.1 summarizes the test program. In addition to the infilled RC frame tests, several masonry tests were conducted on bricks, mortar, and masonry prisms. The material test results are include in chapter 3. Chapter 4 addresses the details of the RC frames, which had the same geometry but different concrete strengths (unintentional). Chapters 5 through 10 cover individual RC frame test results. Comparisons of the six tests are given in chapter 11.

Table 1.1: Infilled Frame Test Program

Test	Test Date	Opening	Retrofit
1	10-10-2007	no opening	no retrofit
2	03-07-2008	small window	no retrofit
3	09-09-2008	small window	½" ECC
4	12-09-2008	no opening	1" ECC
5	07-03-2009	door	no retrofit
6	06-10-2009	large window	no retrofit

Chapter 2: Literature Review

The current study is concerned with the behavior of reinforced concrete frames (RC frames) with unreinforced clay brick infill panels. Numerous parameters determine the response of such structures to in-plane shear loads. The frame itself is a composite consisting of concrete and reinforcing steel. The masonry infill wall is a brick and mortar composite. When the two are combined, the result is a composite of composite structures. If a layer of reinforced retrofit is added, a third composite is added to the system. It is clear that such a complex system is quite difficult to fully understand.

RC Frame

Reinforced concrete frames have been studied for many decades. This is due to the fact that these are structural systems which are used widely throughout the world. Unlike the masonry infills, which are generally considered architectural, the frames support gravity, wind, and earthquake loads. As such countless experiments have been performed to better understand their behavior. The result is a rich body of knowledge and design guidelines related to the analysis and design of RC frames. A typical RC frame without infill will generally yield a ductile behavior in shear because of the formation of plastic hinges. Figure 2.1 shows a typical response from a RC frame with no infill (Mehrabi 1994).

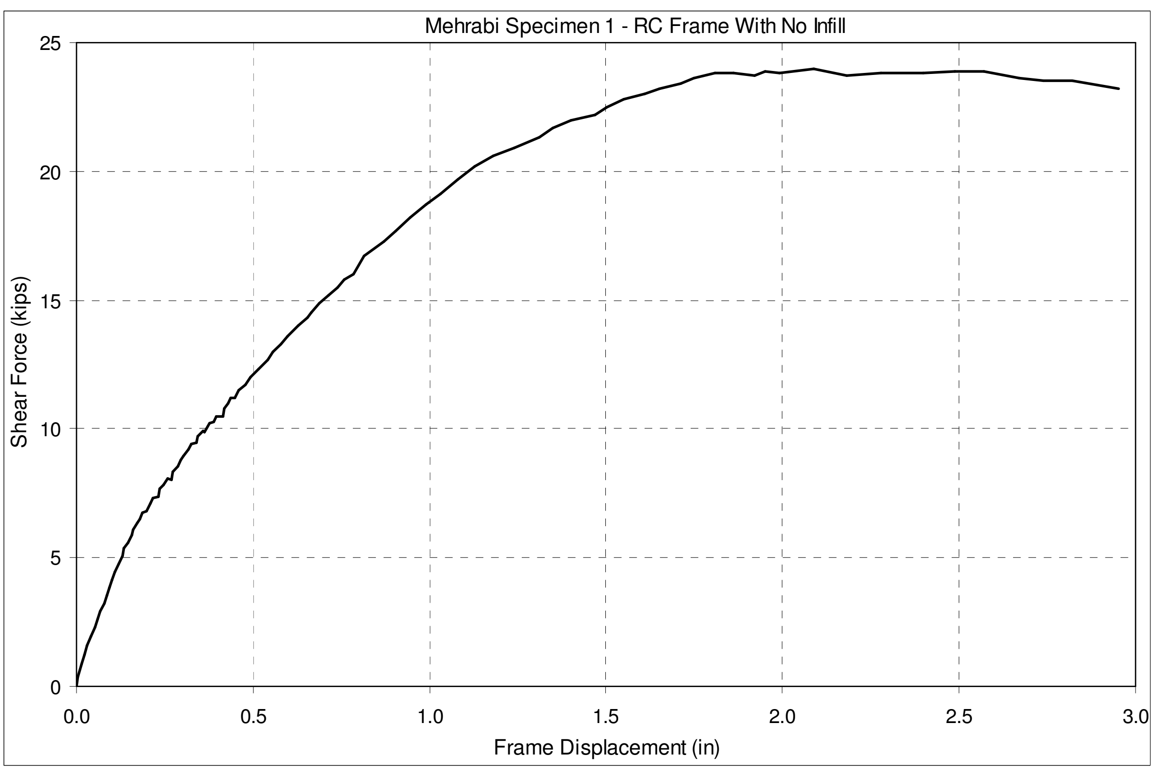

Figure 2.1: Typical Bare RC Frame Shear Response

Masonry Shearwall

Clay brick masonry historically has been used to support vertical loads. Thus the main consideration in the past was regarding the compressive strength of masonry prisms. In more modern times the advent of reinforced concrete frame structures has given masonry walls a different roll. Masonry is often used as an architectural infill for the RC frames. There seems to be little need for any thorough understanding for the structural behavior of these "architectural features". A problem arises when the RC frame and infill wall act together during an earthquake. The architectural wall often reacts with the frame in non-beneficial manners, changing the response of the structure considerably. Thus the masonry is not as non-structural during an earthquake as desired. As a result, there is a need to understand the response of unreinforced brick masonry walls, particularly with respect to in plane shear loading.

The tensile strength of the brick/mortar interface can influence the behavior of a masonry shearwall to some extent. In particular the opening of head joints during the formation of wall cracks dissipates energy and can increase the peak shear strength of the wall by a small amount. Several test procedures are available. Three such procedures are the bond wrench test (ASTM C 1072-05b), beam test (ASTM E 518-03), and cross brick test (ASTM C 952-02). Table 2.1 illustrates a sample of test results. The extensive variation in the tensile strength is quite prominent, even within a particular test program. Van der Pluijm (1993) conducted direct tension tests similar to the cross brick test. Three types of brick and two mortars were used. Rao (1996) carried out an extensive set of tests using the bond wrench procedure. Three types of blocks were used, burnt bricks, stabilized mud blocks, and stabilized soil-sand blocks. Only the results of the burnt brick tests are displayed here. Five different mortars were used for one series of tests, then two mortars were used with varying moisture content of the bricks. The bricks were considered completely saturated at 17% moisture content. It is interesting to see the effect of dry, wet, and saturated bricks at the time of the masonry construction. An increase in the brick moisture content initially increases the tensile strength of the masonry. But then if the bricks are at or near saturation the tensile strength decreased considerably. This variation exists outside of the laboratory as well. Differing construction techniques, climates, and material storage practices can have a significant effect on the brick/mortar tensile strength.

Table 2.1: Brick/Mortar Interface Tensile Strength

Source	type of test	tensile strength (psi)	Comments
Van der Pluijm 1993	direct tension	15	specimen VE.B
		51	specimen VE.C
		90	specimen JG.B
		207	specimen JG.C
		2.9	specimen CS.B
		8.7	specimen CS.C
			(see van der Pluijm 1993)
Rao 1996	bond wrench	15	mortar A
		12	mortar B
		7.3	mortar C
		16	mortar D
		12	mortar E
		8.7	mortar A, MC = 0%
		8.7	mortar A, MC = 2%
		12	mortar A, MC = 9%
		15	mortar A, MC = 14%
		4.5	mortar A, MC = 17%
		8.7	mortar D, MC = 0%
		8.7	mortar D, MC = 2%
		13	mortar D, MC = 9%
		17	mortar D, MC = 14%
		4.5	mortar D, MC = 17%
			(see Rao 1996)
Current study	cross brick	18	dry bricks
		56	wet bricks

Probably the most important behavior of the shear wall is the bedjoint shear response. This is predominately the property of the brick/mortar interface. Many factors influence this shear response, including the mortar mix, texture of the brick contact surface, and the masonry construction practice to name a few. The shear resistance has two components, the peak strength and residual strength. Generally the shear resistance behaves nearly linearly until a peak strength is reached. This is followed by a rapid decay of strength until a residual value is attained. The residual strength is nearly constant for large shear deformations in most cases. Both of these strengths are dependent on the degree of normal compressive stress present across the interface. A higher applied compressive stress results in greater peak and residual shear strengths. It is not a common practice to perform shear tests on masonry specimens, particularly in commercial construction. Even in research such tests are rare. However, when these tests are conducted several specimens are tested with a range of applied normal stresses. The shear strength vs. normal stress results are plotted for both the peak and residual. From the results separate regression lines are obtained for the peak and residual responses. The intercept of these lines with the shear strength axis are the "cohesive" strengths of the interface. The slope of these two lines are the tangent of the "friction angles". The notations c_p, ϕ_p, c_r, ϕ_r are commonly used for these four values.

Several test methods are used to determine the shear response of the brick/mortar interface. For a discussion of some of these methods see Atkinson 1987. Various cohesion and friction results are displayed in table 2.2. Nuss (1978) examined the peak shear response of the brick/mortar interface using prisms with diagonal bed joints. Mortar properties, water absorption of the bricks, and the bed joint angle were varied. Atkinson (1987) used a direct shear apparatus constructed at the University of Colorado, Boulder. Two loading scenarios were used for these tests, type I consisted of large displacement monotonic loading, and type II used small pre-peak displacement cycles followed by large displacement monotonic displacements. Two types of clay bricks were used in Atkinson (1989) using the same direct shear apparatus. In addition, the mortar mix and mortar joint thickness varied. Van der Pluijm (1993) used three types of bricks and two mortar mix designs. The specimens consisted of two bricks and a single mortar joint. Mehrabi (1994) tested concrete bricks and the direct shear apparatus in support of a series of infilled frame tests. Manzouri tested clay bricks using the direct shear apparatus, these tests were in collaboration with a series of masonry wall tests. It is quite evident from table 2.2 that shear behavior varies considerably, particularly for the peak cohesion.

Table 2.2: Brick/Mortar Interface Cohesion and Friction

Source	type of test	c_p (psi)	ϕ_p	c_r (psi)	ϕ_r	Comments
Nuss 1978	diagonal joint	705	37°			series 1-M-28
	prism	687	37°			series 1-S-28
		496	39°			series 1-N-28
		183	40°			series 1-O-28
		407	40°			series 1-M-14
		498	39°			series 1-S-14
		308	40°			series 1-N-14
		213	38°			series 1-O-14
		1050	34°			series M-140
		760	39°			series M-120
		665	41°			series M-110
		830	30°			series N-140
		725	31°			series N-120
		375	37°			series N-110
		524	41°			series M-Wet
		525	39°			series N-Wet
		320	38°			series O-Wet
		215	37°			series M-Dry
		248	40°			series N-Dry
		150	41°			series O-Dry
Atkinson	direct shear	11	35°	-8.1	35°	type I test
1987		42	34°	-1.9	34°	type II test

Table 2.2: Brick/Mortar Interface Cohesion and Friction (Continued)

Source	type of test	c_p (psi)	ϕ_p	c_r (psi)	ϕ_r	Comments
Atkinson 1989	direct shear	31	33°	5.5	35°	old bricks, 1:2:9 mortar, 0.27" joint
		18	35°	3.3	34°	old bricks, 1:2:9 mortar, 0.51" joint
		117	37°	5.4	37°	new bricks, 1:1.5:4.5 mortar, 0.27" joint
Van der Pluijm 1993	brick pair	15	40°	≈0	41°	specimen VE.B
		123	51°	≈0	45°	specimen VE.C
		127	36°	≈0	37°	specimen JG.B
		268	44°	≈0	36°	specimen JG.C
		22	45°	≈0	40°	specimen CS.B
		41	37°	≈0	41°	specimen CS.C
Mehrabi 1994	direct shear	15	49°	≈0	42°	
Manzouri 1995	direct shear	62	51°	6	43°	

Several tests have been conducted with masonry walls subjected to normal compressive stress and shear displacement. Manzouri (1995) tested unreinforced masonry walls of approximately ½ scale. The program consisted of 3 wythe thick walls with and without openings. The shear strength results for the three solid walls are shown in table 2.3. The values for the peak cohesion and friction angle were found to be $c_p = 12$ psi $\phi_p = 34°$.

Vermeltfoort (1993) tested several small masonry walls in a similar manner to Manzouri. Results from walls with no openings appear in table 2.3. The peak cohesion and shear for this set of data are $c_p = -20$ psi $\phi_p = 39°$.

Table 2.3: Shear Wall Results

Source	Vertical Load (psi)	Peak Shear Force (kips)	Peak Shear Strength (psi)	Comments
Manzouri 1995	150	156	115	Wall W1
	55	73	54	Wall W2
	85	82	61	Wall W3
Vermeltfoort 1993	143	14.8	96	Wall V1D
	156	17.5	113	Wall V3D
	138	13.9	90	Wall V4D
	173	19.6	127	Wall J3D
	114	11.5	74	Wall J4D
	154	11.9	77	Wall J5D

Because the compression test of masonry prisms is fairly common in commercial construction, the question of a relationship between the shear properties and the prism compression strength arises. This relationship is considered in table 2.4 and figures 2.2 and 2.3. As can be seen, the relationship between f'_m and the peak cohesive strength is tenuous. Furthermore the relationship between the peak friction angle and f'_m is essentially non-existent, at least in view of this modest set of data.

Table 2.4: Relationship Between Interface Shear Properties and Prism Compressive Strength

Source	type of test	c_p (psi)	ϕ_p	c_r (psi)	ϕ_r	f'_m (psi)	Comments
Nuss 1978	diagonal	705	37°			12,420	series 1-M-28
	joint	687	37°			8,710	series 1-S-28
	prism	496	39°			6,743	series 1-N-28
		183	40°			4,893	series 1-O-28
		407	40°			11,730	series 1-M-14
		498	39°			7,830	series 1-S-14
		308	40°			6,220	series 1-N-14
		213	38°			4,215	series 1-O-14
		1050	34°			12,420	series M-140
		760	39°			13,265	series M-120
		665	41°			12,080	series M-110
		830	30°			6,995	series N-140
		725	31°			7,436	series N-120
		375	37°			7,810	series N-110
		524	41°			7,845	series M-Wet
		525	39°			6,285	series N-Wet
		320	38°			4,865	series O-Wet
		215	37°			8,343	series M-Dry
		248	40°			5,753	series N-Dry
		150	41°			4,839	series O-Dry
Mehrabi 1994	direct shear	15	49°	≈0	42°	1,934	
Manzouri 1995	direct shear	62	51°	6	43°	2,125	

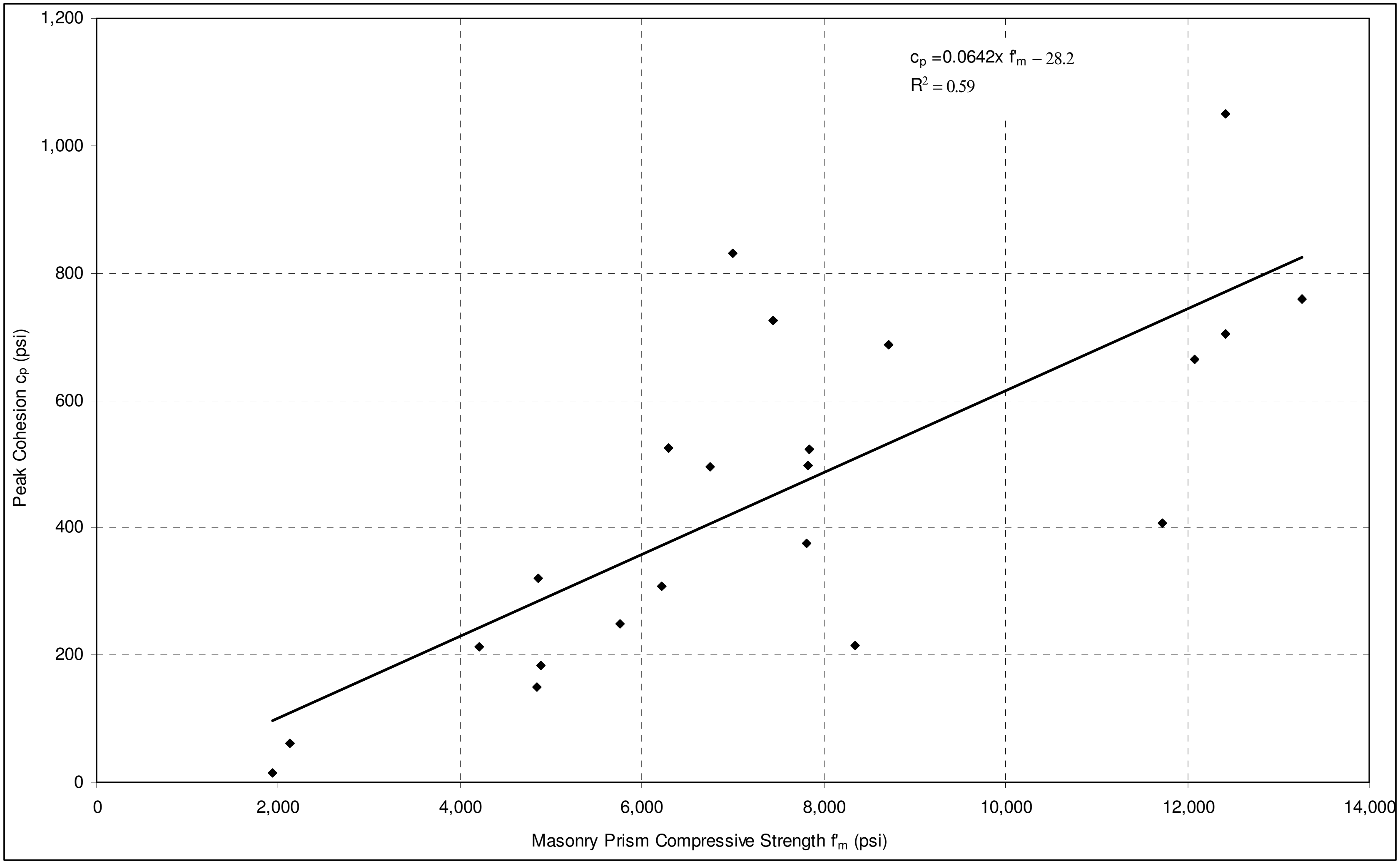

Figure 2.2: Relationship Between Peak Cohesion and Masonry Prism Strength

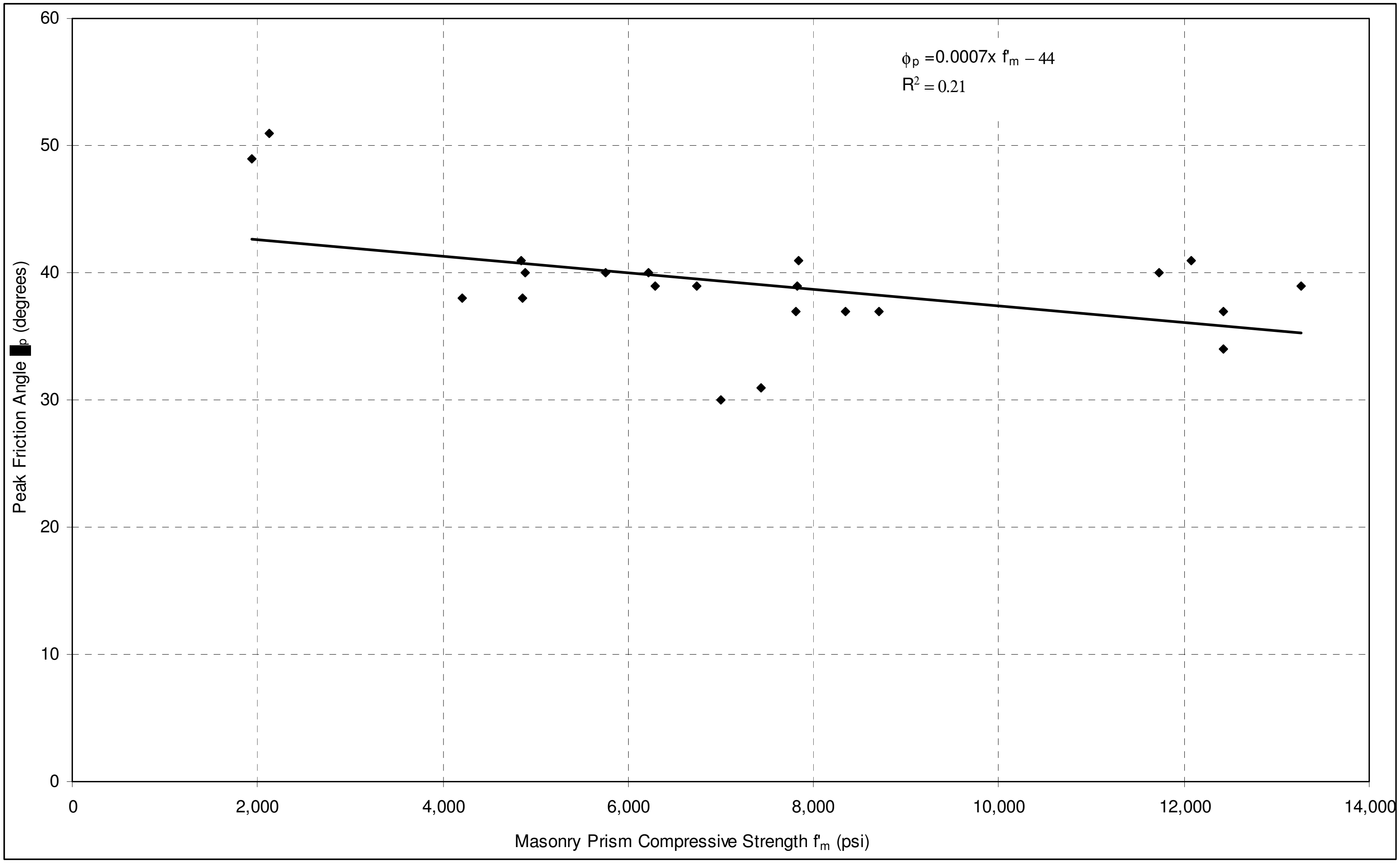

Figure 2.3: Relationship Between Peak Friction Angle and Masonry Prism Strength

Infilled Frames

Infilled RC frames are the main topic of the current study. There are many parameters that govern the behavior of an infilled RC frame. The longitudinal and transverse reinforcing in the columns and beams certainly effect the strength, stiffness and ductility. The concrete strength and aspect ratio of the frames also influence the behavior. The infill wall plays a leading role in the response of the structure. The masonry compressive strength can be important for some failure scenarios. Probably the most important aspect of the infill wall is the response of the brick/mortar joint interface. In particular the tensile behavior and the peak and residual shear response of the interface. The presence of openings and their location and geometry is quite significant. All of these factors leads to a complex behavior of the structural system. Bare RC frames generally respond in a ductile manner, forming plastic hinges in a flexural response. The presence of infill walls has been seen to change this ductile response to a more brittle behavior through the introduction of column shear. Figure 2.1 in the Mehrabi dissertation (Mehrabi 1994) illustrates a classification of the failure mechanisms of masonry infilled RC frames into 24 categories. The categories include combinations several crack patterns in the infill wall, plastic hinges in the RC frame, and column shear in the RC frame.

Mehrabi (1994) conducted 14 tests on ½ scale frames, of which all were infilled except the first bare frame test. Two frame aspect ratios were considered, as well as two different reinforcing details which were termed “strong” and “weak” frames. Both solid and hollow concrete bricks were used. Vertical loads were included in all tests. The column transverse reinforcing was quite heavy compared to the current study. As a result, column shear was not witnessed and the response of most of the the infilled frames can best be classified as ductile.

Al-Chaar (2002) carried out 5 tests on ½ scale frames, with 4 tests incorporating concrete and clay brick infill walls. No windows or vertical loads were implemented. One, two, and three bay specimens were part of the test program. The column transverse reinforcing was moderately light (6 gage wire at 5” spacing). The single bay specimen with concrete masonry infill experienced column shear but ductile behavior. The single bay specimen with brick infill experienced ductile behavior with no column shear. The multiple bay specimens experienced column shear and brittle behavior (see figure 2 pages 1058-1059 in Al-Chaar 2002).

Colangelo (2005) performed 13 tests on ½ scale infilled frames with two aspect ratios and six reinforcing details. Vertical loads were included but no openings were present in the walls. The frames were not generally pushed to a large enough displacement into the residual regime, so it is difficult to assess the ductility of the specimens.

Kakaletsis (2009) performed 10 tests on 1/3 scale frames. The first test was on a bare frame, the second on a solid infilled frame, and the rest were infilled frames with openings. The size, shape, and location of the openings was varied. Hollow clay bricks were used and a vertical load was applied. Column ties were closely spaced. Only the solid infilled frame and the frame with a small concentric window opening showed a brittle response.

Chapter 3: Material Test Results

Standard concrete and masonry material tests were performed for each infilled frame specimen. In addition, several masonry material tests were conducted before the first RC frame was constructed. This chapter summarizes the material test results.

Concrete compression tests were conducted with 4”x8” cylinders. The results are shown in table 3.1 with compressive strength vs age shown in figures 3.1 and 3.2 for infilled frames 3 and 5. As can be seen in table 3.1 there was considerable variation in the compressive strength of the concrete between batches. Reinforcing steel tensile test results are shown in figure 3.3. The average yield strength of #4 rebar is seen to be approximately 68,000 psi. The mortar and masonry prism compression strengths are shown in tables 3.14 and 3.15 for the masonry of the infilled frames. Note that the mortar mix design used in the tests and the masonry infill walls consists of a 1:1:5 ratio of cement:lime:sand.

Prior to the infilled frame tests bricks were tested for compressive and tensile strength, as well as modulus of elasticity and Poisson ratio. The results are shown in tables 3.2 through 3.5. Similarly results of mortar tests appear in tables 3.6 through 3.9. Stress vs strain plots for bricks and mortar specimens are shown in figures 3.4 and 3.5, both showing a gradual softening. Figure 3.6 shows a comparison of the stress strain response for the mortar and bricks along with that of 5-brick prisms. It is interesting to see the highly brittle prism behavior resulting from a composite of two somewhat ductile materials. An important aspect of masonry behavior is the tensile strength of the brick/mortar interface. A total of 28 cross brick tests were conducted. Half of the specimens were built from completely dry bricks and the other half used bricks that were soaked for approximately 1 minute before construction. A photograph of the cross-brick test is shown in figure 3.7, with the tensile strength results given in table 3.10. Prism were also tested before the wall tests started. Table 3.11 and 3.12 show results of prism tests for compressive strength and average modulus of elasticity.

The shear response of the brick/mortar interface is also very important for understanding the behavior of a masonry shear wall. Direct shear tests and triplet tests are excellent methods for testing the shear response corresponding to a variety of applied normal stresses. However, the cost of such test apparatus prohibited their use in the current project. Several prisms were constructed with sloped bed joints in order to achieve a state of shear and normal stresses in the brick/mortar interface. Figure 3.8 shows a photograph of these specimens and the results are displayed in table 3.13. Table 3.13 shows the results of the normal vs shear stress at peak. It should be noted that the prisms did not fail predominately from shear failure in the brick/mortar interface. Instead they mainly failed via lateral tension in the bricks, the same as the rectilinear prisms.

Several masonry prism were tested in compression while “filmed” using a Vic-2D digital imaging system. Figures 3.9 and 3.10 show the result of one such test. The mismatch of elastic moduli and Poisson ratios cause the mortar to be in a state of triaxial compression while the brick experiences lateral tension. The tension in the brick ultimately causes the brick to fail in tension. This is clearly seen in figure 3.10.

Table 3.1: LaFarge Mix RMXRE30DC5I Compressive Strength

Frame	Pour Date	Age (days)	Compressive Strength (ksi)
1	7/31/07	28	4.3
		66	4.3
2	11/08/07	28	2.2
		119	2.8
3	6/05/08	28	2.3
		95	2.3
4	8/19/08	28	3.2
		136	4.0
5	5/02/08	28	1.8
		300	2.2
6	4/21/09	7	1.7
		28	2.4
		48	2.4

Table 3.2: Brick Compression Strength

Specimen Designation	Comp Strength (ksi)	Avg Comp Strength (ksi)	Std Dev (ksi)	C.O.V.	Comments
A1	4.11				Capped Half - Bricks
A2	4.29				
A3	4.68				
A4	5.22				
A5	5.92				
		4.84	0.737	15%	
B1	3.83				Capped Half - Bricks
B2	4.44				
B3	4.39				
B4	3.61				
B5	3.88				
		4.03	0.367	9.1%	
C1	2.44				Uncapped Half - Bricks
C2	3.37				
C3	3.55				
C4	3.71				
C5	4.11				
		3.44	0.620	18%	
D1	4.31				Uncapped Half - Bricks
D2	5.35				
D3	4.59				
D4	4.24				
D5	4.9				
		4.68	0.457	9.8%	

Table 3.3: Brick Tension Strength

Specimen Designation	Tensile Strength (ksi)	Avg Tensile Strength (ksi)	Std Dev (ksi)	C.O.V.	Comments
S1	0.363				Brick Splitting Test
S2	0.434				
S3	0.395				
S4	0.319				
S5	0.299				
S6	0.435				
S7	0.360				
S8	0.387				
S9	0.354				
		0.372	0.0464	12%	
M1	0.628				MOR Test
M2	0.569				
M3	0.657				
M4	0.588				
M5	~~0.355~~				
M6	~~0.373~~				
M7	0.697				
M8	0.702				
		0.640	0.0553	8.6%	

Table 3.4: Brick Modulus of Elasticity

Specimen Designation	E (ksi)	Avg E (ksi)	Std Dev (ksi)	C.O.V.	Comments
H1	108				Half Bricks With LVDTs
H2	139				
H3	149				
H4	115				
H5	129				
		128	16.7	13%	
F1	224				Full Bricks Standing Vertically With LVDTs
F2	252				
F3	255				
F4	320				
F5	287				
		268	37.0	14%	
V1	2,103				Full Bricks Standing Vertically VIC-2D
V2	1,702				
V3	2,175				
V4	2,532				
V5	2,212				
		2,145	297	14%	

Table 3.5: Brick Poisson Ratio (using VIC-2D)

Specimen Designation	E (ksi)	Avg E (ksi)	Std Dev (ksi)	C.O.V.	Comments
33% of σ_{max}					Full Bricks Standing Vertically
P33-1	0.07				
P33-2	0.22				
P33-3	~~0.70~~				
P33-4	0.09				
P33-5	0.10				
		0.12	0.068	57%	
50% of σ_{max}					Full Bricks Standing Vertically
P50-1	0.11				
P50-2	0.18				
P50-3	~~0.60~~				
P50-4	0.12				
P50-5	0.15				
		0.14	0.032	23%	

Table 3.6: Mortar Compression Strength

Specimen Designation	Comp Strength (ksi)	Avg Comp Strength (ksi)	Std Dev (ksi)	C.O.V.	Comments
A1	~~1.146~~				4"x8" Cyls
A2	0.72				
A3	0.69				
A4	0.821				
A5	0.695				
		0.732	0.061	8.3%	
B1	1.36				2"x4" Cyls
B2	1.49				
B3	1.30				
B4	1.23				
B5	1.30				
		1.34	0.098	7.3%	
C1	0.57				2"x2"x2" Cubes
C2	0.72				
C3	0.51				
C4	0.49				
C5	0.57				
		0.57	0.09	16%	
D1	1.15				4"x8" Cyls Capped
D2	1.07				
D3	1.02				
D4	1.08				
		1.08	0.054	5.0%	
E1	1.01				4"x8" Cyls Uncapped
E2	0.99				
E3	1.03				
		1.01	0.020	2.0%	
F1	1.15				4"x8" Cyls
F2	1.17				
F3	1.12				
F4	1.19				
F5	1.15				
		1.16	0.026	2.2%	

Table 3.7: Tensile Strength of Mortar (Brazilian Test)

Specimen Designation	Tensile Strength (ksi)	Avg Tensile Strength (ksi)	Std Dev (ksi)	C.O.V.	Comments
A1	0.127				
A2	0.121				
A3	0.134				
A4	0.132				
A5	0.092				
		0.121	0.0171	14%	4” dia x 2” long cylinders
B1	0.141				
B2	0.146				
B3	0.134				
B4	0.144				
B5	0.141				
		0.141	0.0045	3.2%	4” dia x 4” long cylinders
C1	0.289				
C2	0.234				
C3	0.281				
C4	0.261				
C5	0.258				
		0.265	0.0215	8.1%	2” dia x 4” long cylinders

Table 3.8: Mortar Modulus of Elasticity

Specimen Designation	E (ksi)	Avg E (ksi)	Std Dev (ksi)	C.O.V.	Comments
A1	1,426				4”x8” cylinders secant at 50% of σ_{max}
A2	1,564				
A3	1,342				
A4	1,399				
A5	1,384				
		1,423	84.5	5.9%	
B1	417				2”x4” cylinders secant at 50% of σ_{max}
B2	449				
B3	304				
B4	386				
B5	174				
		346	110	32%	
C1	1,671				2”x2” x2” cubes VIC-2D
C2	1,285				
C3	1,832				
C4	962				
C5	1,378				
		1,426	340	24%	
D1	1,075				capped 4”x8” cyls
D2	1,085				
D3	973				
D4	998				
		1,033	56	5.4%	
E1	905				uncapped 4”x8” cyls
E2	1,105				
E3	1,040				
		1,017	102	10%	

Table 3.9: Mortar Poisson Ratio (using VIC-2D)

Specimen Designation	ν (ksi)	Avg ν (ksi)	Std Dev (ksi)	C.O.V.	Comments
33% of σ_{max}					
P33-1	0.29				2”x2”x2” cubes
P33-2	0.28				
P33-3	~~0.6~~				
P33-4	0.13				
P33-5	0.09				
		0.278	0.20	72%	
50% of σ_{max}					
P50-1	0.24				2”x2”x2” cubes
P50-2	0.21				
P50-3	0.24				
P50-4	0.19				
P50-5	0.20				
		0.216	0.023	11%	

Table 3.10: Brick/Mortar Interface Tensile Strength

Specimen Designation	Tensile Strength (psi)	Avg Tensile Strength (psi)	Std Dev (psi)	C.O.V.	Comments
D1	17.90				constructed from dry bricks
D2	42.50				
D3	37.17				
D4	23.27				
D5	17.86				
D6	25.55				
D7	27.32				
D8	21.59				
D9	23.28				
D10	11.16				
D11	2.13				
D12	1.90				
D13	0.00				
D14	0.00				
		17.97	13.55	75%	
W1	47.41				constructed from wet bricks
W2	59.98				
W3	48.12				
W4	71.32				
W5	57.49				
W6	76.15				
W7	39.74				
W8	75.87				
W9	60.15				
W10	73.69				
W11	48.08				
W12	38.81				
W13	47.64				
W14	37.37				
		55.84	14.03	25%	

Table 3.11: Prism Compression Strength

Specimen Designation	Comp Strength (psi)	Avg Comp Strength (ksi)	Std Dev (ksi)	C.O.V.	Comments
prism 1	2.81				
prism 2	2.49				
prism 3	3.00				
		2.76	0.257	9.3%	

Table 3.12: Prism Modulus of Elasticity

Specimen Designation	E (ksi)	Avg E (ksi)	Std Dev (ksi)	C.O.V.	Comments
prism 1	1,330				
prism 2	899				
prism 3	1,330				
		1,186	249	21%	

Table 3.13: Sloped Bedjoint Prism Test Results

Specimen Designation	Peak Bedjoint Normal Stress (psi)	Peak Bedjoint Shear Stress (ksi)	Peak Shear Strength/ Normal Stress
I-1 (30°)	1,877	1,083	173%
I-2 (30°)	1,508	870	173%
I-3 (30°)	1,572	907	173%
I-4 (30°)	1,828	1,055	173%
I-5 (30°)	1,739	1,004	173%
II-1 (15°)	2,132	571	373%
II-2 (15°)	2,544	682	373%
II-3 (15°)	1,738	466	373%
II-4 (15°)	2,535	679	373%
II-5 (15°)	1,841	493	373%

Table 3.14: Infilled Frame Mortar Test Results

Specimen Designation	Comp Strength (psi)	Avg Comp Strength (psi)	Std Dev (psi)	C.O.V.	Comments
frame 1:					4"x8" cylinders 23 days old
cylinder 1	1,330				
cylinder 2	1,350				
		1,340	14	1.0%	
frame 2:					4"x8" cylinders 28 days old
cylinder 1	3,660				
cylinder 2	3,380				
cylinder 3	3,240				
		3,430	214	6.2%	
frame 3:					4"x8" cylinders 28 days old
cylinder 1	1,410				
cylinder 2	1,350				
cylinder 3	1,420				
cylinder 4	1,410				
cylinder 5	1,370				
cylinder 6	1,450				
cylinder 7	1,380				
cylinder 8	1,340				
		1,390	37	2.7%	
frame 4:					4"x8" cylinders 28 days old
cylinder 1	912				
cylinder 2	982				
cylinder 3	946				
cylinder 4	1,080				
cylinder 5	930				
		970	67	6.9%	
frame 5:					4"x8" cylinders 27 days old
cylinder 1	650				
cylinder 2	630				
cylinder 3	660				
		647	15	2.3%	

Table 3.14: Infilled Frame Mortar Test Results (continued)

Specimen Designation	Comp Strength (psi)	Avg Comp Strength (psi)	Std Dev (psi)	C.O.V.	Comments
frame 6:					
cylinder 1	744				4”x8” cylinders 31 days old
cylinder 2	749				
cylinder 3	856				
cylinder 4	865				
cylinder 5	754				
		793	61	7.7%	

Table 3.15: Infilled Frame Prism Test Results

Specimen Designation	Comp Strength (psi)	Avg Comp Strength (psi)	Std Dev (ksi)	C.O.V.	Comments
frame 1:					4.5"x3.75" prisms 23 days old
prism 1	3,070				
prism 2	3,640				
prism 3	3,880				
		3,530	416	12%	
frame 2:					4.5"x3.75" prisms 28 days old
prism 1	2,600				
prism 2	1,210				
prism 3	2,950				
		2,250	915	41%	
frame 3:					4.5"x3.75" prisms 28 days old
prism 1	2,930				
prism 2	2,820				
prism 3	3,050				
		2,940	111	3.8%	
frame 4:					4.5"x3.75" prisms 28 days old
prism 1	2,440				
prism 2	2,960				
prism 3	2,570				
		2,650	271	10%	
frame 5:					7.75"x3.75" prisms 27 days old
prism 1	1,740				
prism 2	2,470				
		2,100	516	25%	

frame 6:
A data collection malfunction with the south 110 MTS machine occurred.
As a result, there is no data from the prism compression tests for infilled frame 6.

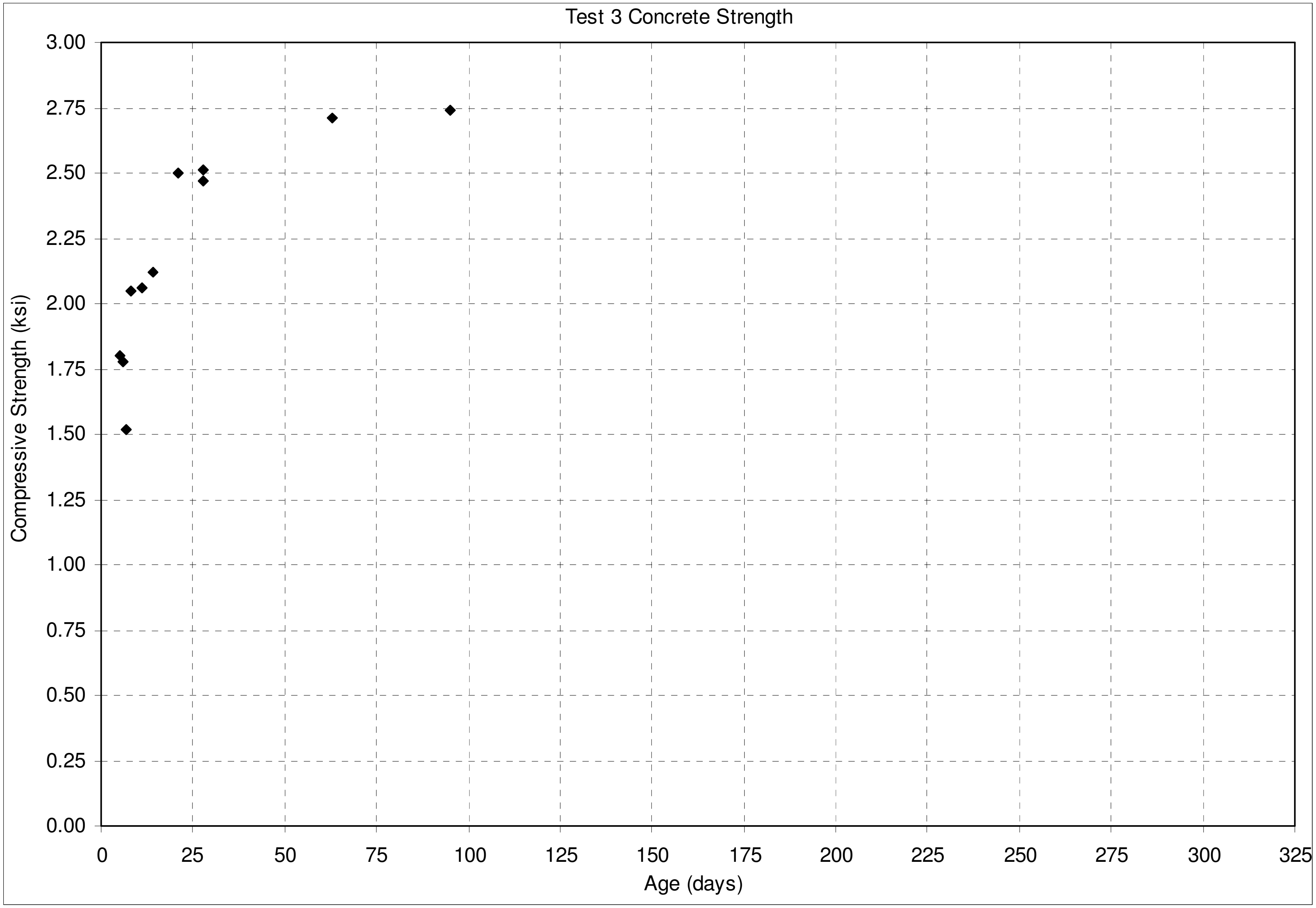

Figure 3.1: Test 3 Concrete Strength

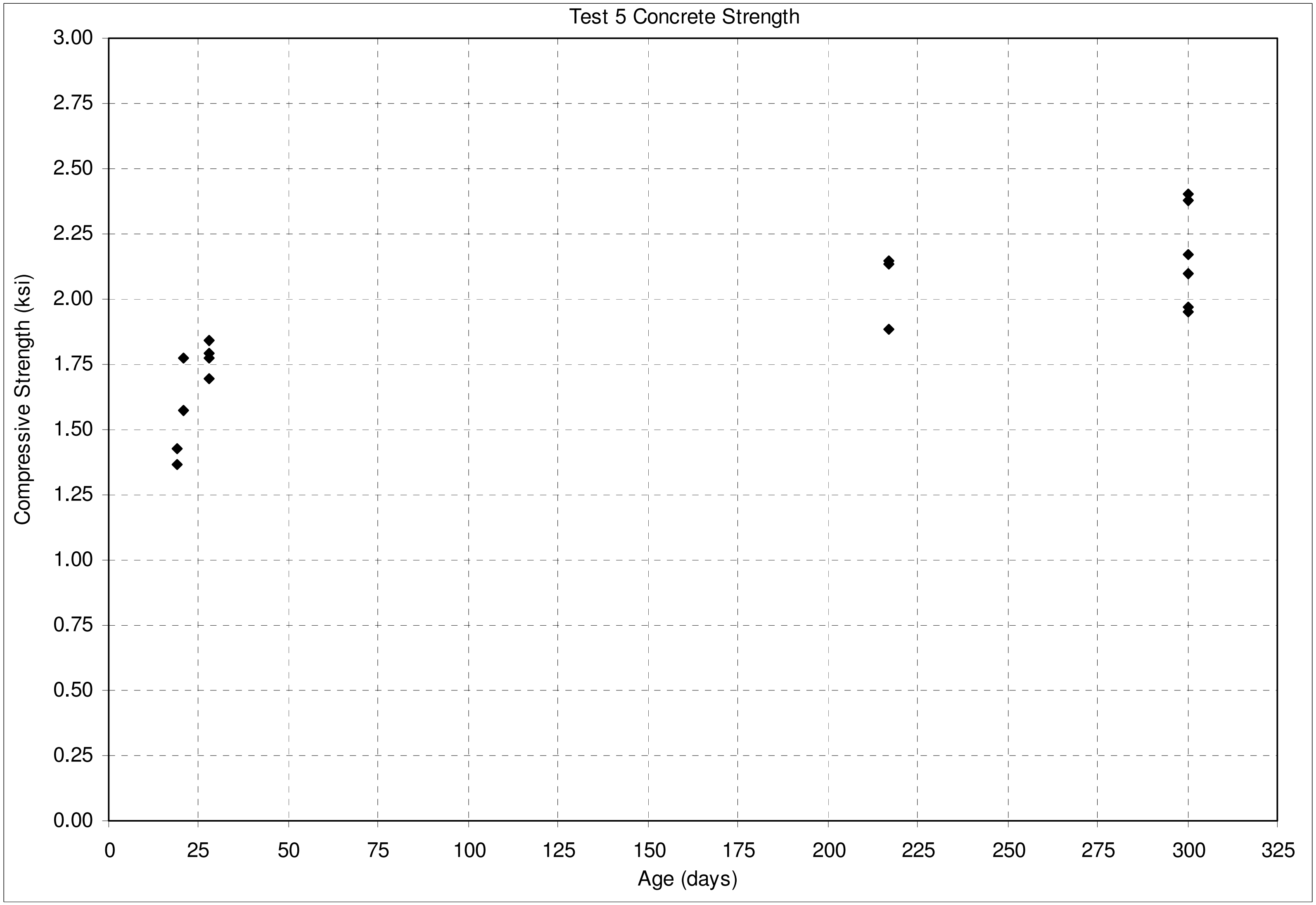

Figure 3.2: Test 5 Concrete Strength

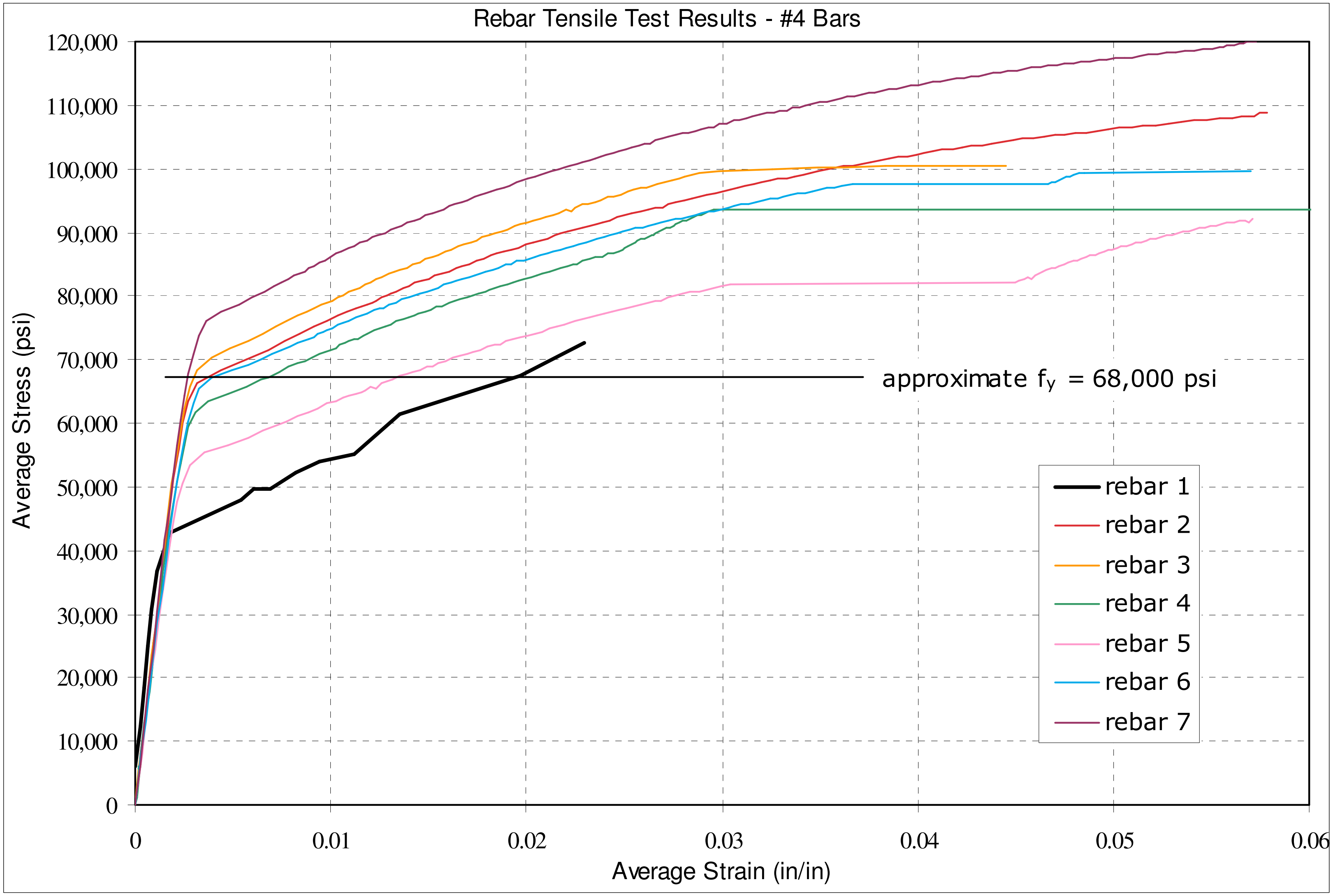

Figure 3.3: Rebar Tensile Test Results

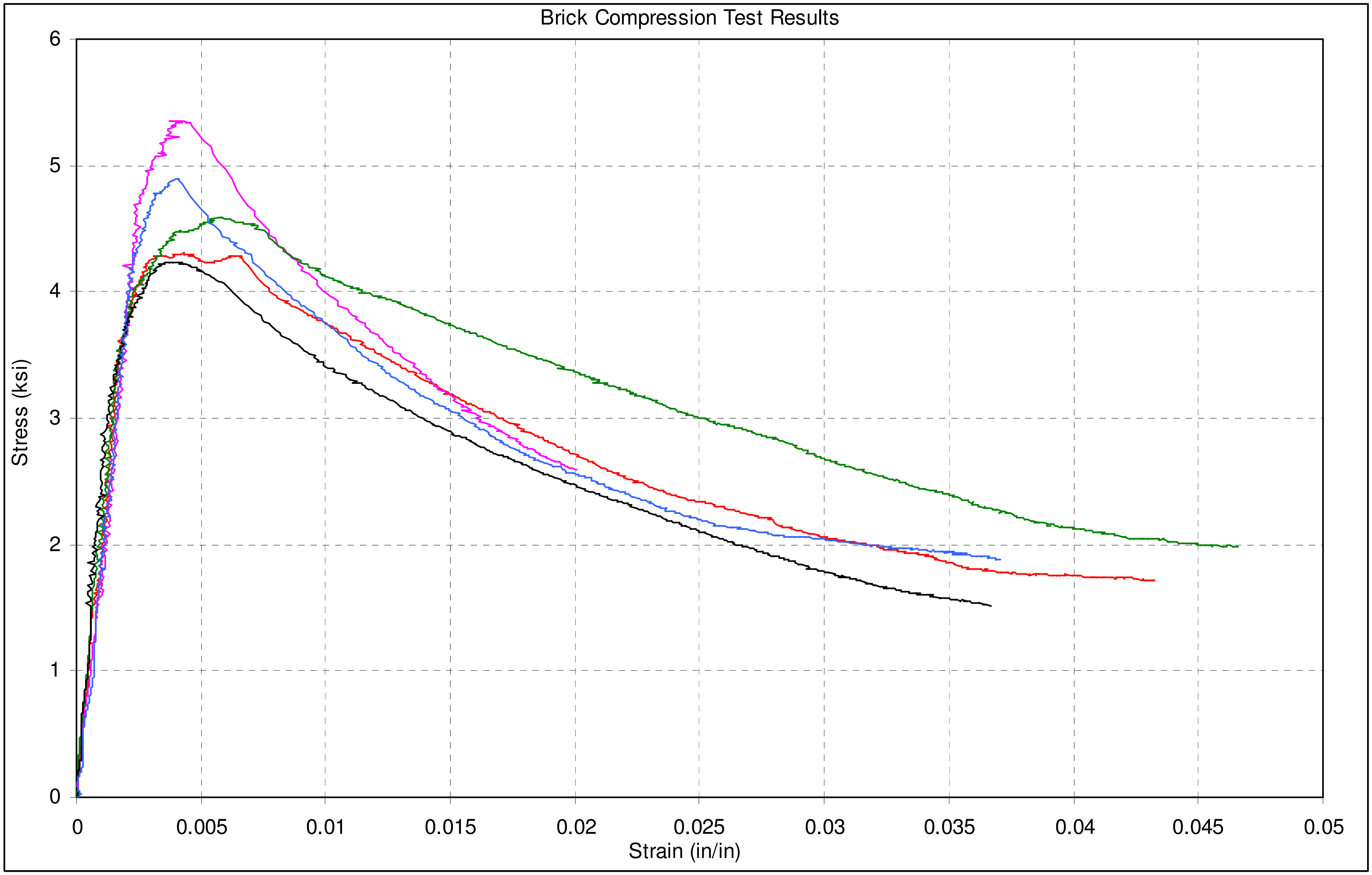

Figure 3.4: Brick Compression Test Results – D Series Half Bricks

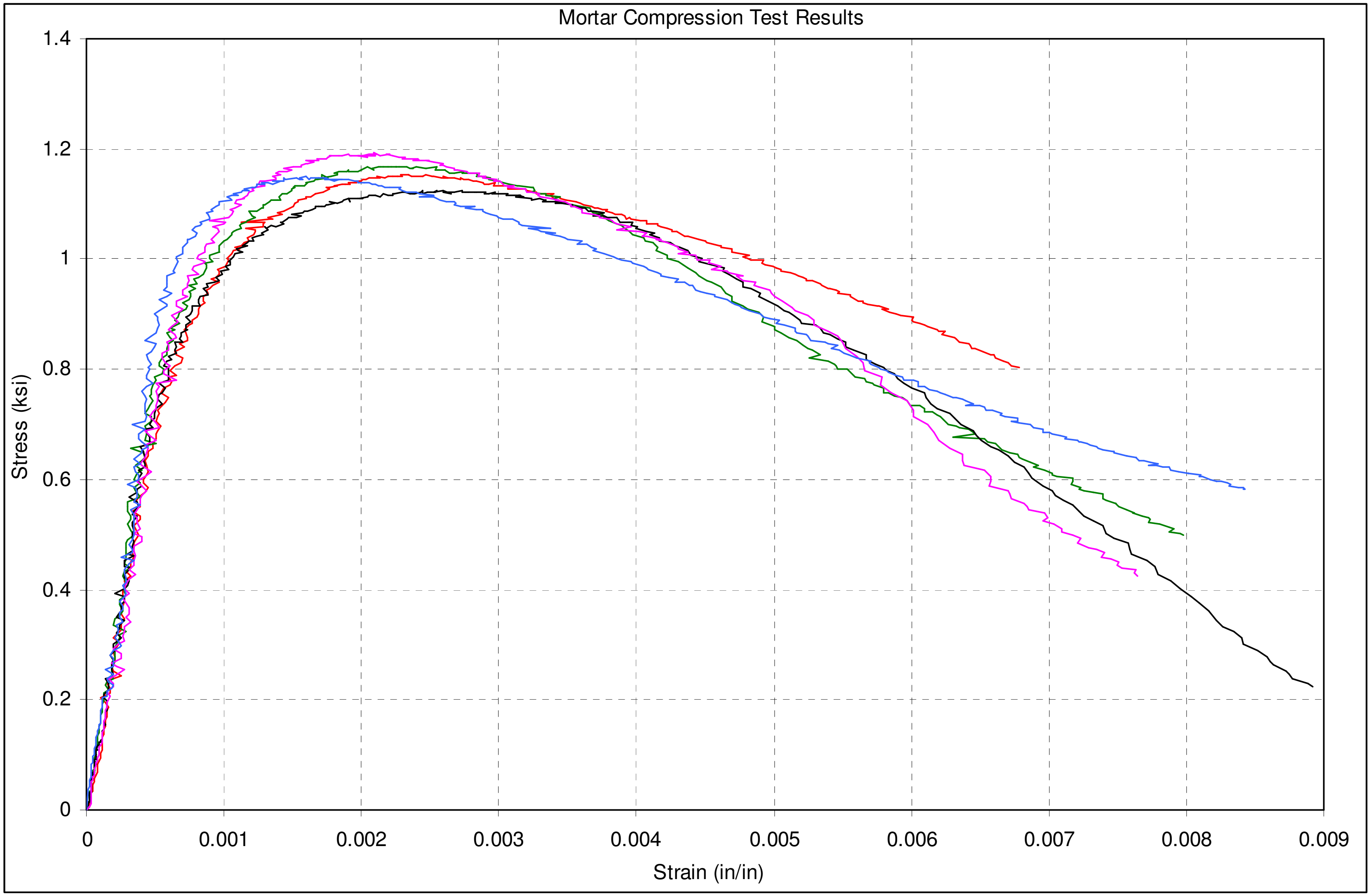

Figure 3.5: Mortar Compressive Strength – F Series Cylinders

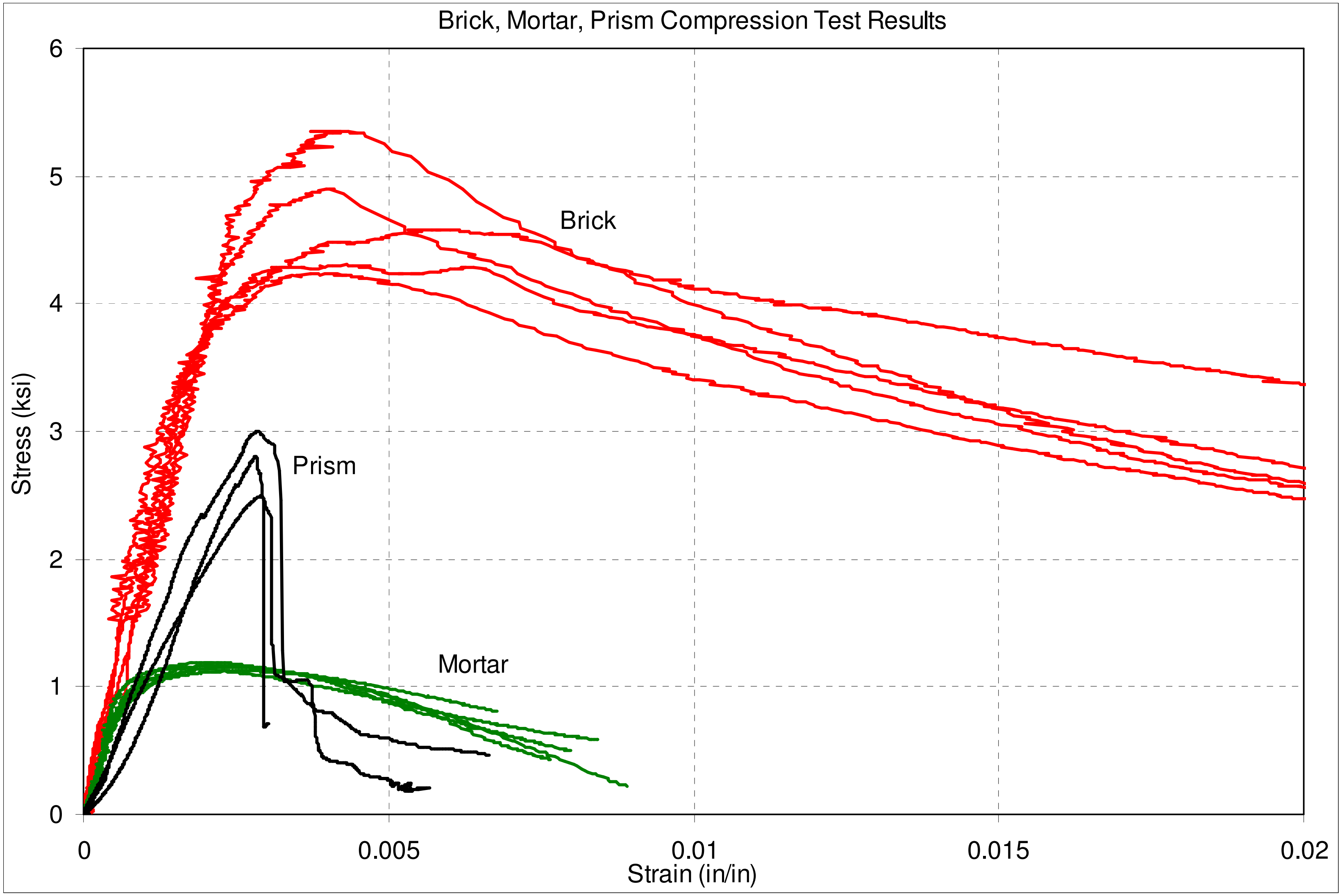

Figure 3.6: Brick, Mortar, Prism Compression Results

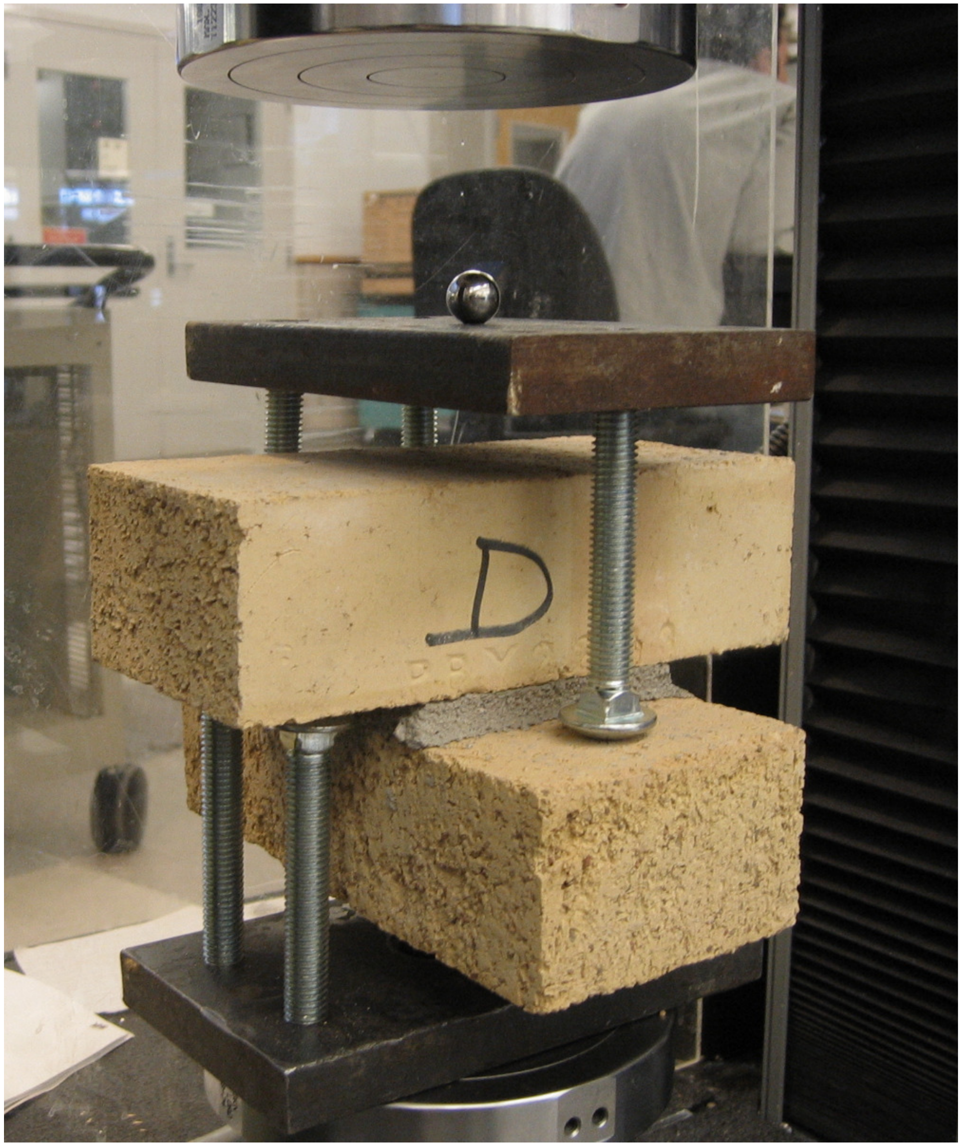

Figure 3.7: Cross Brick Test Setup

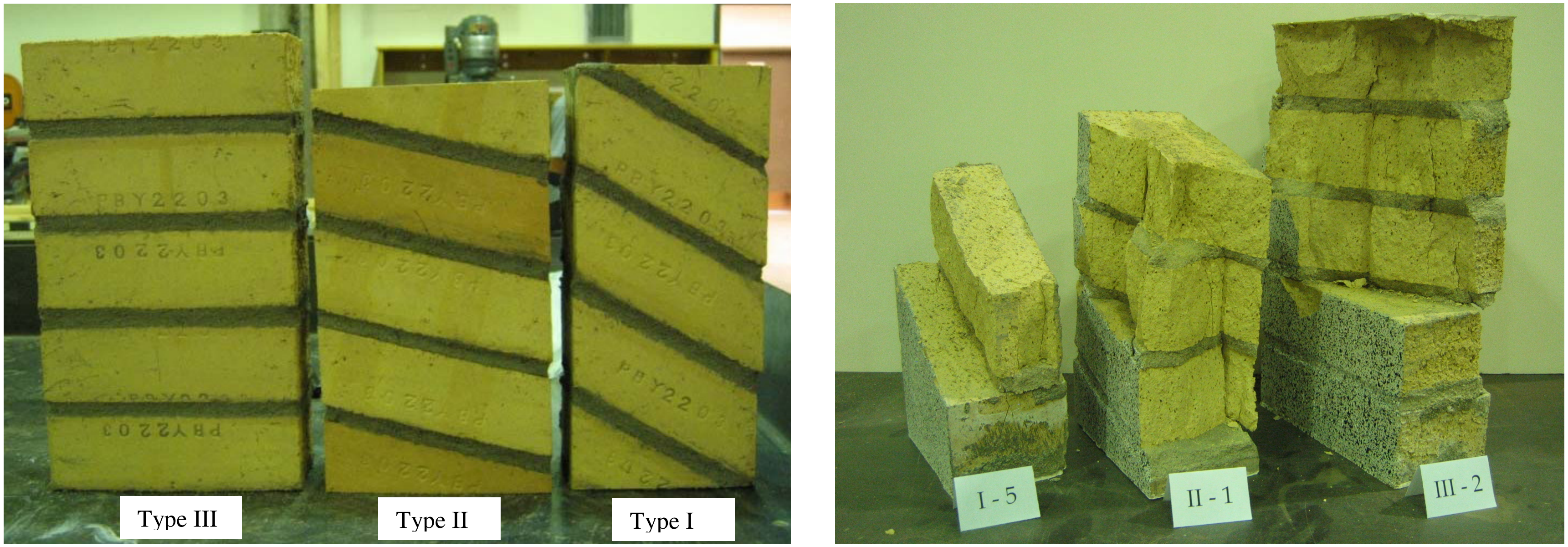

Figure 3.8: Prisms With Sloped Bed Joints

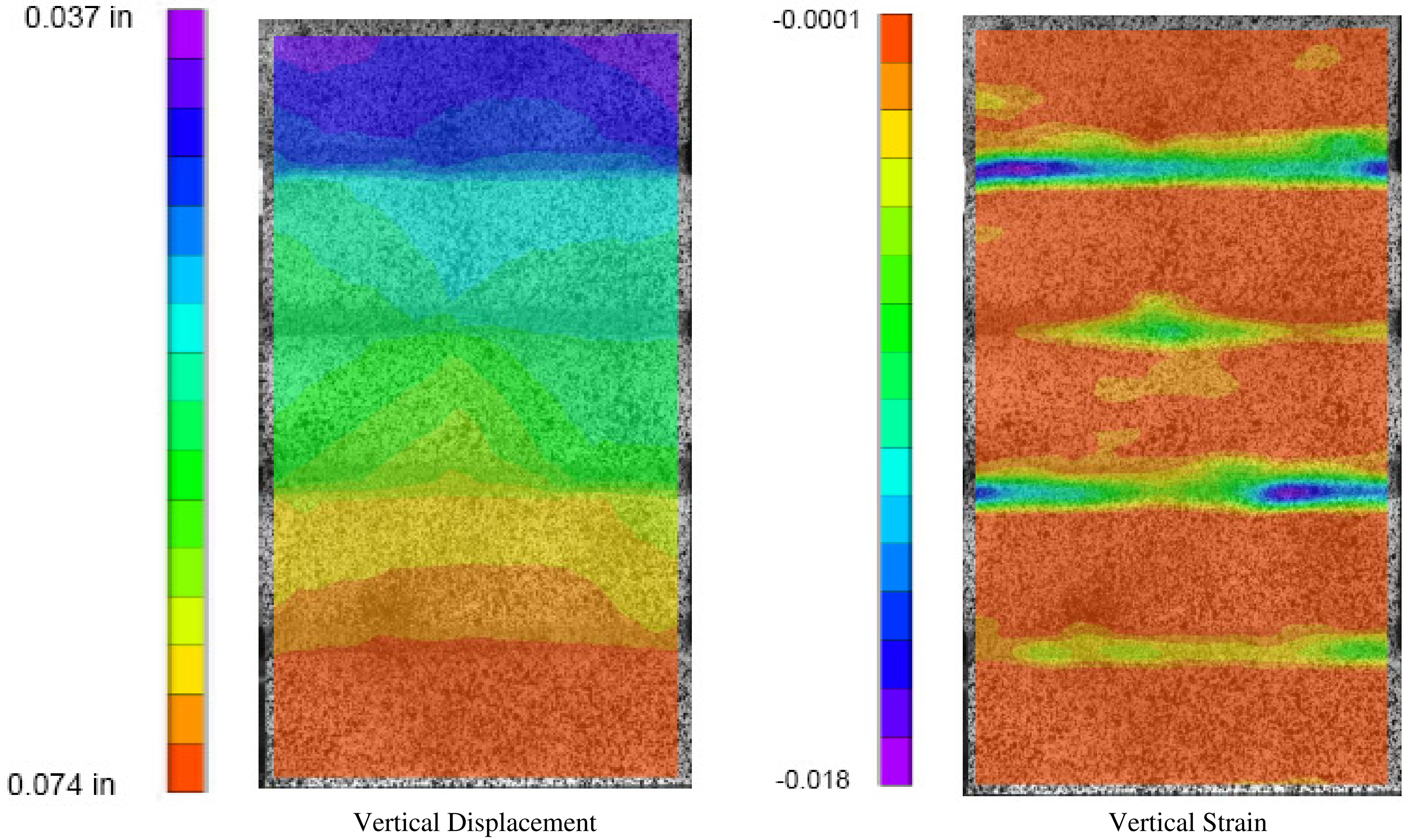

Figure 3.9: Vic-2D Images of Prism at Peak

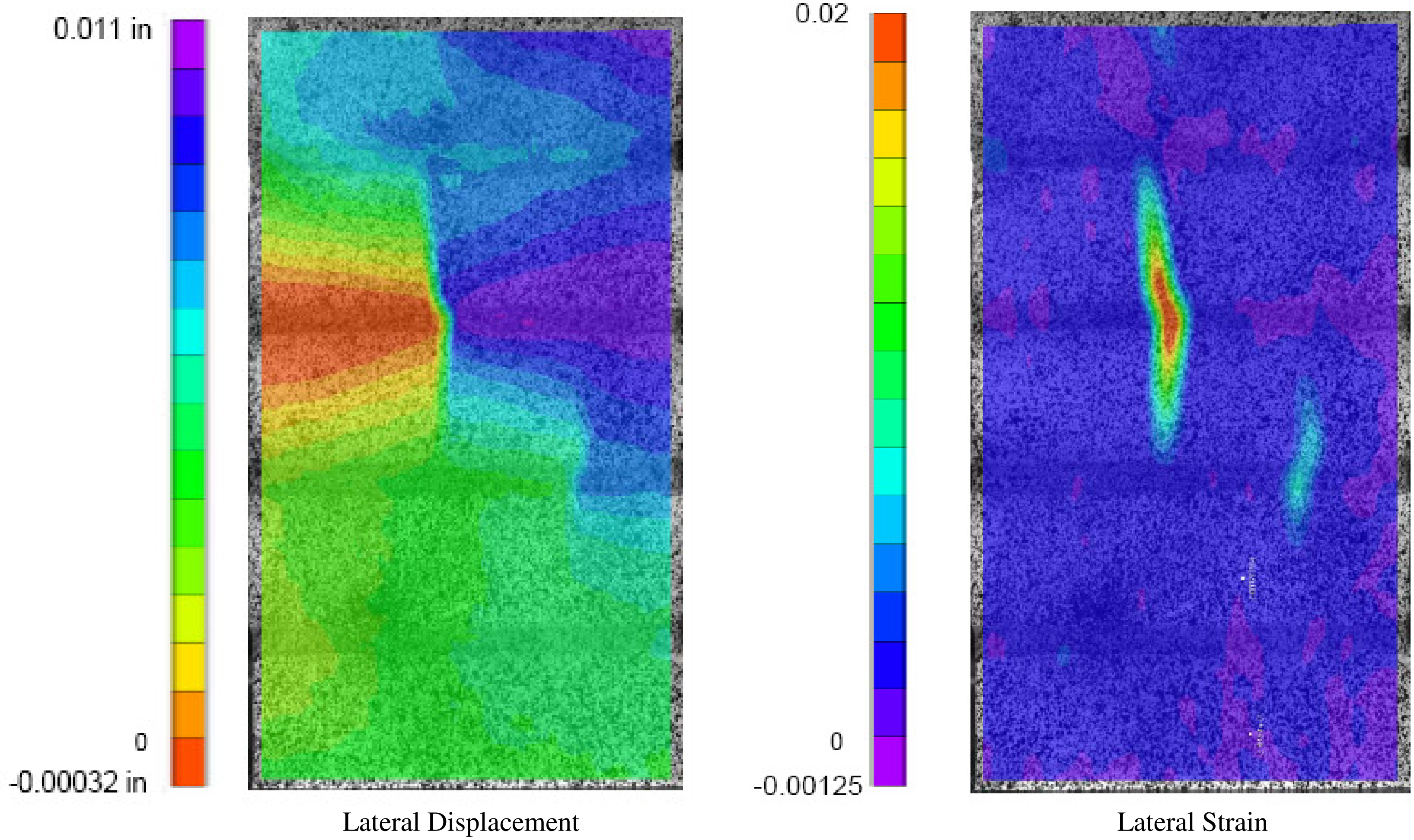

Figure 3.10: Vic-2D Images of Prism at Peak

Chapter 4: CU infilled RC Frames

This chapter is concerned with aspects common to all test frames. Included are details and descriptions of the RC frame, reinforcing, instrumentation, loading, and materials. Subsequent chapters address features related to individual test specimens and test results.

The prototype building is a three story 1920 era reinforced concrete frame with clay brick infill walls. The bay dimensions are 18′ by 22′ with an 11′ story height. Only the gravity loads were considered in the design of the building. The infill walls were not considered to be structural in the design.

The infilled RC frames tested at the University of Colorado were 2/3 scale of the prototype building. The infills consisted of two wythe clay brick walls with brick dimensions 7.75″×3.75″×2.25″ and 3/8″ mortar joints. The dimensions of the test frames are shown in figure 4.1. The reinforcing is shown in figure 4.2 with details in figure 4.3. Although not shown in the sketches, the rebar in the columns and top beam incorporated 180° hooks and extensions in accordance with ACI 318-08. There were no reinforcing splices in the columns. The beam stirrups and column ties included 90° bends and laps also in compliance with ACI 318-08. The cross ties in the columns were deigned to include 90° hooks, but these were increased to approximately 100° for construction convenience. The concrete clear cover was a minimum of 1" for all reinforcing.

Anchoring the frames to the strong floor consisted of six high strength steel threaded rods. Figures 4.4 and 4.5show the anchoring configuration. The interior four anchor points were embedded in the top of the base beam and covered with mortar with the masonry wall constructed above. This required pockets to be incorporated in the concrete pour, see figure 4.5. As a result of this geometry, these four rods are smaller with smaller plates and nuts. The result is a lower anchoring force than at the ends of the specimen. The two anchors at the ends were simply bearing on the top of the base beam with large plates, allowing a considerably higher anchoring force. These end anchor forces were reduced for frames 3, 5, and 6 to approximately 110 kips due to weaker concrete for these specimens. In order to create a high degree of sliding resistance a ¼″ layer of hydrostone was placed between the bottom of the frame and the strongfloor. This was accomplished by placing the frame on small styrofoam rings below the frame at the six locations where the threaded rods penetrate the specimen and strongfloor. The frame was then leveled and the rods modestly tightened. The liquid hydrostone was then forced under the frame with a system incorporating a high pressure tank and an air compressor. After a few days the hydrostone hardened and the steel rods were fully tightened.

The concrete strength was specified to be 3,000 psi. LaFarge mix RMXRE30DC5I was used for all five frames. The compressive strength varied considerably, as seen in table 4.1. The effect of this high variation in concrete strength is not completely clear.

The masonry walls consisted of solid clay bricks measuring 7.75″L × 3.75″D × 2.25″H. The mortar joints were all 3/8″ thick. A common running bond pattern was used with a header course at every sixth coursing. The walls were two wythes thick. The mortar was proportioned with a 1:1:5 cement:lime:sand mix for all walls. Each brick was soaked in water for a minimum of 30 seconds before installation in order to create a better bond in the brick/mortar interface.

Two solid walls, three walls with window openings, and one wall with a door opening were tested. Figure 4.6 shows sketches of the three specimen types. A reinforced ECC (engineered cementitious composite) was applied to one side of the wall for two of the specimens. Table 4.2 provides a list of the combinations of the six tests. Steel LL3×3×1/4 lintel double angles were used over each opening with a bearing length of approximately 2″ at each end. The components of the ECC are listed in table 4.3.

The vertical load was applied by two hydraulic cylinders controlled by a single electric pump, which is manually operated. The two hydraulic cylinders were mounted to the top of a W8×31 wide flange steel beam for the purpose of distributing the loads more uniformly to the top of the specimen. A diagram of the test setup is shown in figure 4.7. The reaction for the two vertical loads was supplied by two cross beams constructed from C12×20.7 steel channels. Each of these cross beams is kept in place by two steel rods that pass through the strongfloor. A photograph of one of the cross beams and one hydraulic cylinder appears in figure 4.8. Two small braces were used to help stabilize each cross beam laterally, see figure 4.8.

The horizontal loading was supplied by a 220 kip MTS actuator mounted at the west end of the specimen. A 3″ thick plate is attached to the actuator which makes a three point contact with the end of the top beam of the RC frame. The end of the actuator, along with the plate, were hung from a top W10×33 wide flange support beam, see figures 4.7 and 4.9. A similar 3″ plate was hung from the supporting wide flange beam at the opposite end of the RC frame (figure 4.9). The two end load plates were connected with four high strength steel rods, two on the front and two on the back of the specimen. The actuator was located at the right end of the specimen as viewed from the control room (the “front” side of the frame). A positive displacement is generated by the actuator pushing to the left, which makes direct contact with the specimen through the 3″ load plate. A negative displacement is accomplished by the actuator pulling to the right, which puts the four horizontal rods in tension causing the left end load plate to push the top beam of the RC frame to the right. Positive [half] cycles correspond to a displacement to the east (left), and negative half cycles to the west (right). For each cycle the positive cycle was applied first, followed by a negative cycle with the same magnitude and cycle number.

A lateral force resisting system was implemented in order to keep the specimens in line during testing. A plan view sketch of the lateral force resisting system is shown in figure 4.10. The system includes four steel triangular lateral braces attached to two C12×20.7 channels which spanned between end columns of the support structure. The braces also appear in figures 4.9 and 4.11. In addition, six cables deliver the forces from the C12×20.7 channels to the strongfloor rather than allowing the columns to take the lateral loads. Two of the cables are visible in the photograph in figure 4.11.

Strain gages were attached to the column reinforcing to determine the onset of plastic hinges. The strain gages used were Vishay model CEA-13-125UN-120/P2, with a strain limit of approximately 0.05 in/in. Figure 4.12 shows the locations of the strain gages. Figure 4.13 illustrates the results of tension tests of the same rebar. The average yield stress is approximately 68 ksi. Although not instrumented, column ties were tested for tensile strength as well. Figure 4.14 shows the results of the tests. The #2 column ties have a yield strength of approximately 55 ksi and an ultimate strength of 61 ksi.

Optical encoders were used to measure the relative story displacement. The encoders used were Heidenhain LS 629 with an accuracy of 10μm (0.00039 in). The locations of the encoders appear in figure 4.15. Two encoders were used for the top beam in order to cancel out any flexural rotations in the beam. As a result a story height of 80.75″ is used for the calculations, which is the distance from the top surface of the base beam to the mid-height of the top beam. It is understood that this is not the standard definition of story height, but for the encoder displacement this worked well.

Figure 4.16 illustrates the locations of the vertical and horizontal external strain gages. These gages were attached to high strength Dywidag threaded rods. The four vertical rods were used for the vertical load application. For test 1 the strain readings for these rods were used to determine the vertical load. A pressure transducer was used to collect vertical load data for tests 2 through 6. The horizontal Dywidags were used to transmit the actuator force to the east end of the specimen for displacements in the negative direction. The strain gages attached to these rods can be used to measure any longitudinal compression force that may build up in the top beam. For calibration purposes the force vs strain calibration for the Dywidag rods appears in figure 4.17.

Specimens 3 and 4 received ECC retrofit before testing. This consisted of welded wire fabric attached to the masonry wall and the ECC applied to one side of the masonry in a manner similar to the application of stucco. Each of specimens 3 and 4 received a different thickness of ECC and different WWF, as listed in table 4.2. Both of these specimens received the same ECC mix design, which is shown in table 4.3. Both of these specimens also had dowels installed in the top and bottom beams to supply a shear bond between the ECC layer and the frame. The dowels were #3 rebar approximately 10" long with 5″ embedded into the concrete. The spacing of the bars was approximately 6″ on both the top and bottom. A bonding agent called "weld-Crete" was applied to the surface of the wall for specimen 3. After this the 6×6 W1.4×W1.4 WWF was installed, with a minimum number of drywall anchors to keep it in place. The final stage was the application of the ECC, which was approximately 1/2″ thick for specimen 3. For the ECC application of specimen 4 the same #3 dowel arrangement was used. The ECC layer was increased to 1″. The WWF was increased to 4×4 W4.0×W4.0. No Weld-Crete was used, instead 1/2″ diameter expansion anchors were inserted in the masonry at a spacing of 12″ in each direction. The WWF was secured to these anchors at a distance of 1/2″ from the surface of the wall. The 1″ thick ECC layer was then applied. Details for the retrofit are illustrated in figure 4.18.

Several LVDTs were attached to each frame and infill wall in order to measure displacements within the test specimens. The specific locations of these instruments varied from one test to another. These locations can be seen in chapters 5 through 10 with further information regarding the individual specimens and test results. The LVDTs were made by Macro Sensors, with a variety of strokes ranging from ±1/4” to ±3” with an accuracy of 0.5% of full stroke.

Table 4.1: LaFarge Mix RMXRE30DC5I Compressive Strength

Frame	Pour Date	Age (days)	Compressive Strength (ksi)
1	7/31/07	28	4.3
		66	4.3 (1 day before the frame test)
2	11/08/07	28	2.2
		119	2.8 (1 day before the frame test)
3	6/05/08	28	2.3
		95	2.3 (1 day before the frame test)
4	8/19/08	28	3.2
		136	4.0 (1 day before the frame test)
5	5/02/08	28	1.8
		300	2.2 (1 day before the frame test)
6	4/21/09	7	1.7
		28	2.4
		48	2.4 (1 day before the frame test)

Table 4.2: CU Infilled Frame Test Specimens

Frame	Opening	Retrofit	Retrofit Reinforcing
1	no opening	no retrofit	
2	window opening	no retrofit	
3	window opening	½″ ECC	6×6 W1.4×W1.4
4	no opening	1″ ECC	4×4 W4.0×W4.0
5	door opening	no retrofit	
6	large window opening	no retrofit	

Table 4.3: ECC Mix Design (per 100 lb patch)

Component	Quantity
Type I/II Portland Cement	36.6 lb
Calcium Aluminate Cement	1.9 lb
F-110 Silica Sand	30.8 lb
Fly Ash	11.6 lb
Methylcellulose (Viscous Agent)	0.024 lb
Adva Cast 530 (Superplasticiser)	32.75 mL
Polyvinyl Alcohol Fibers	1.23 lb
Water	17.7 lb

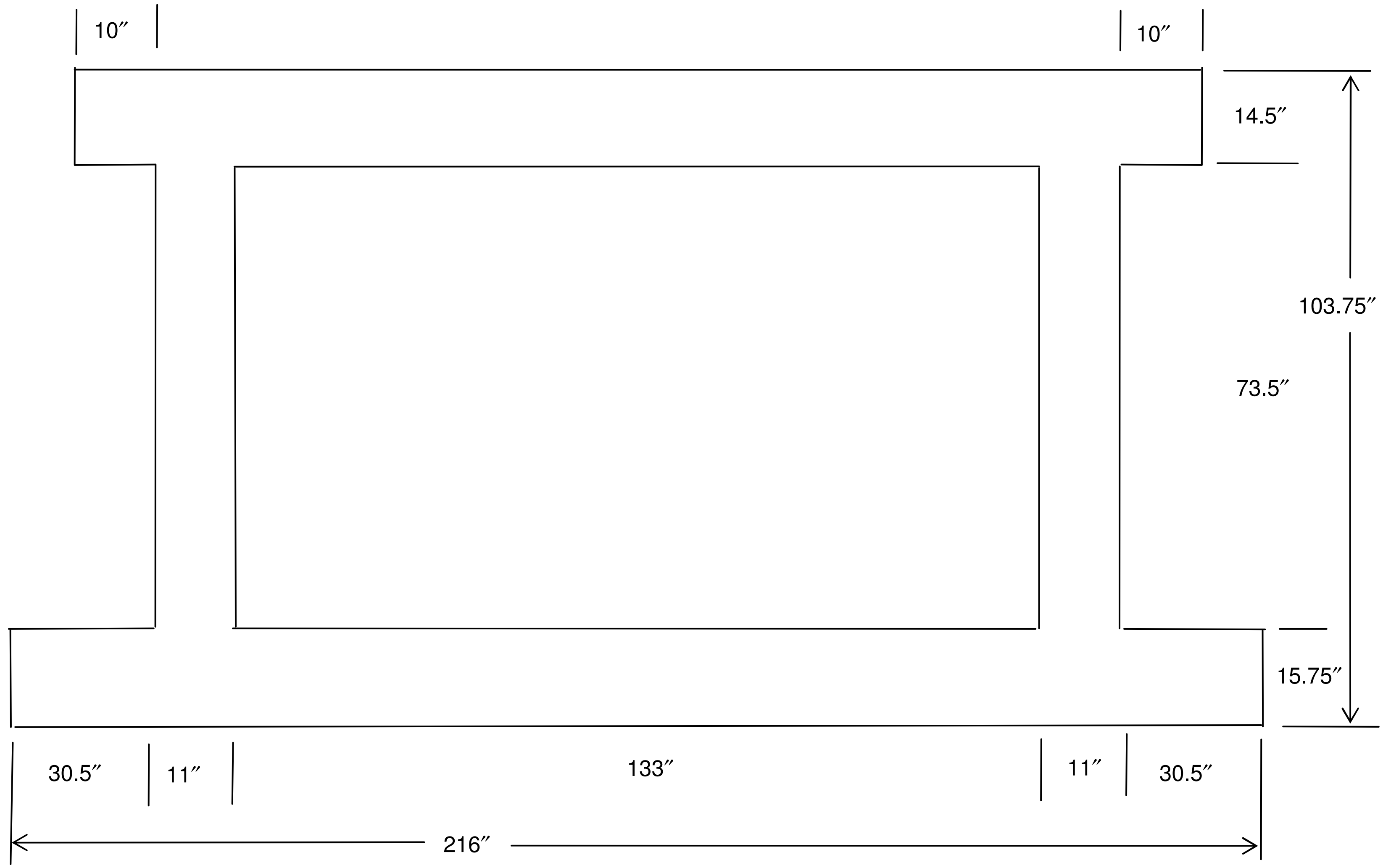

Figure 4.1: RC Frame Dimensions

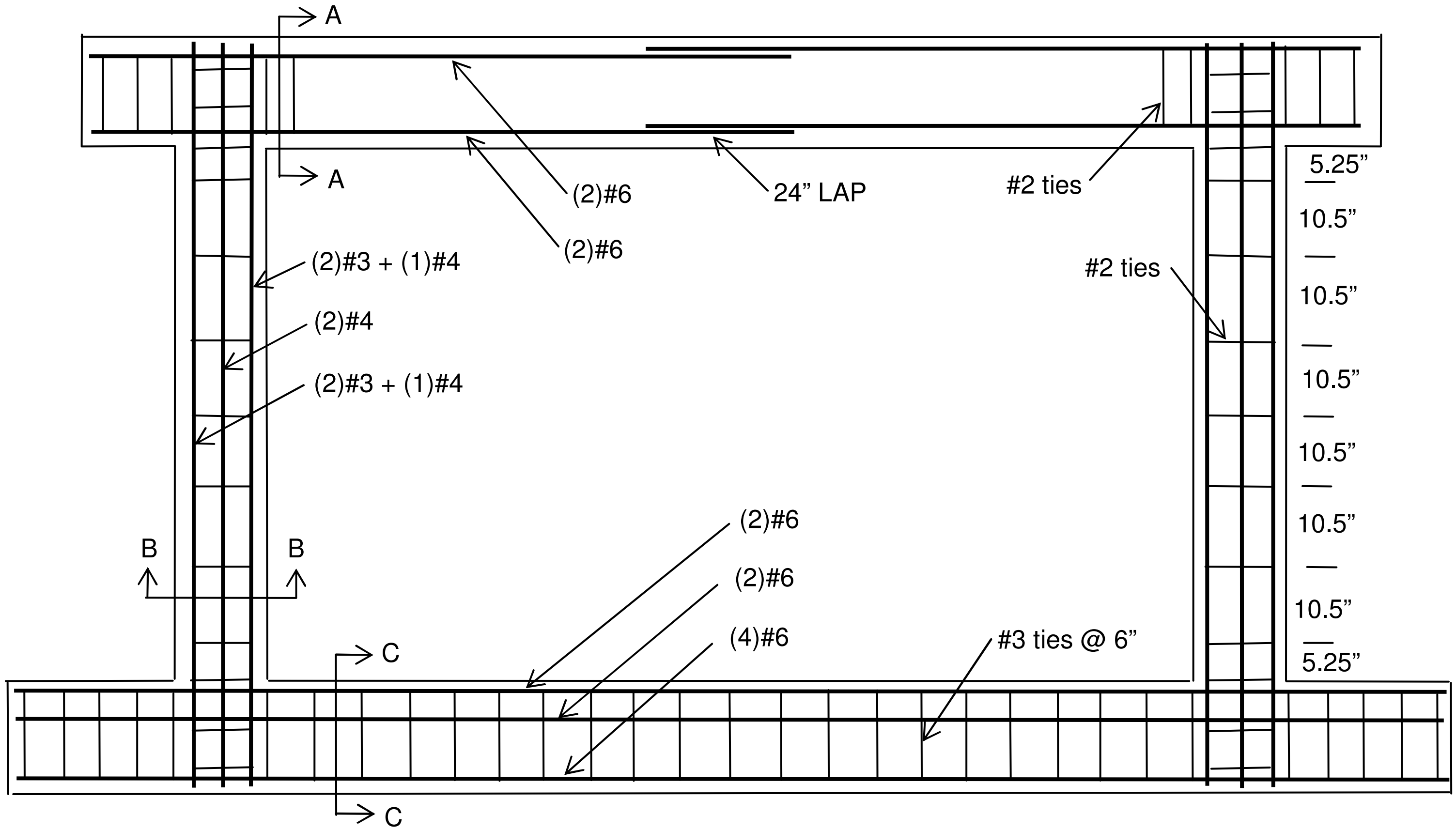

Figure 4.2: RC Frame Reinforcing

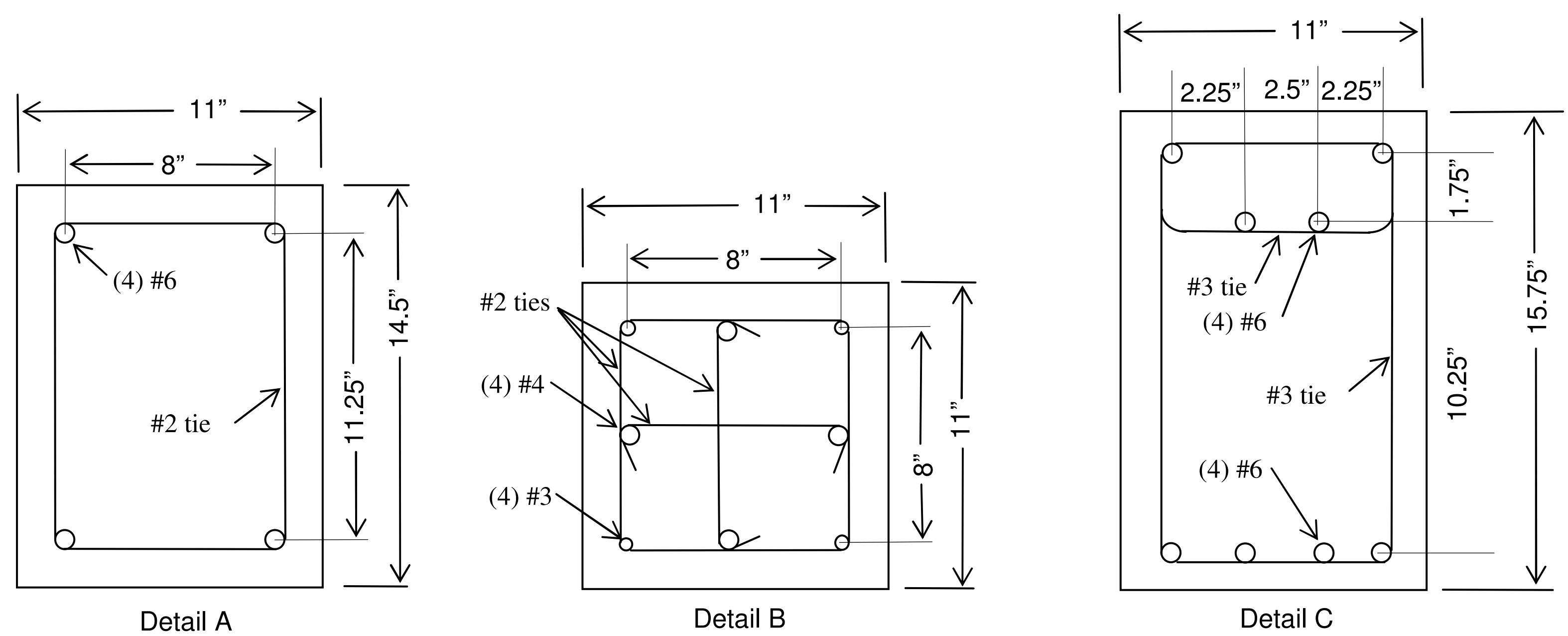

Figure 4.3: Reinforcing Details

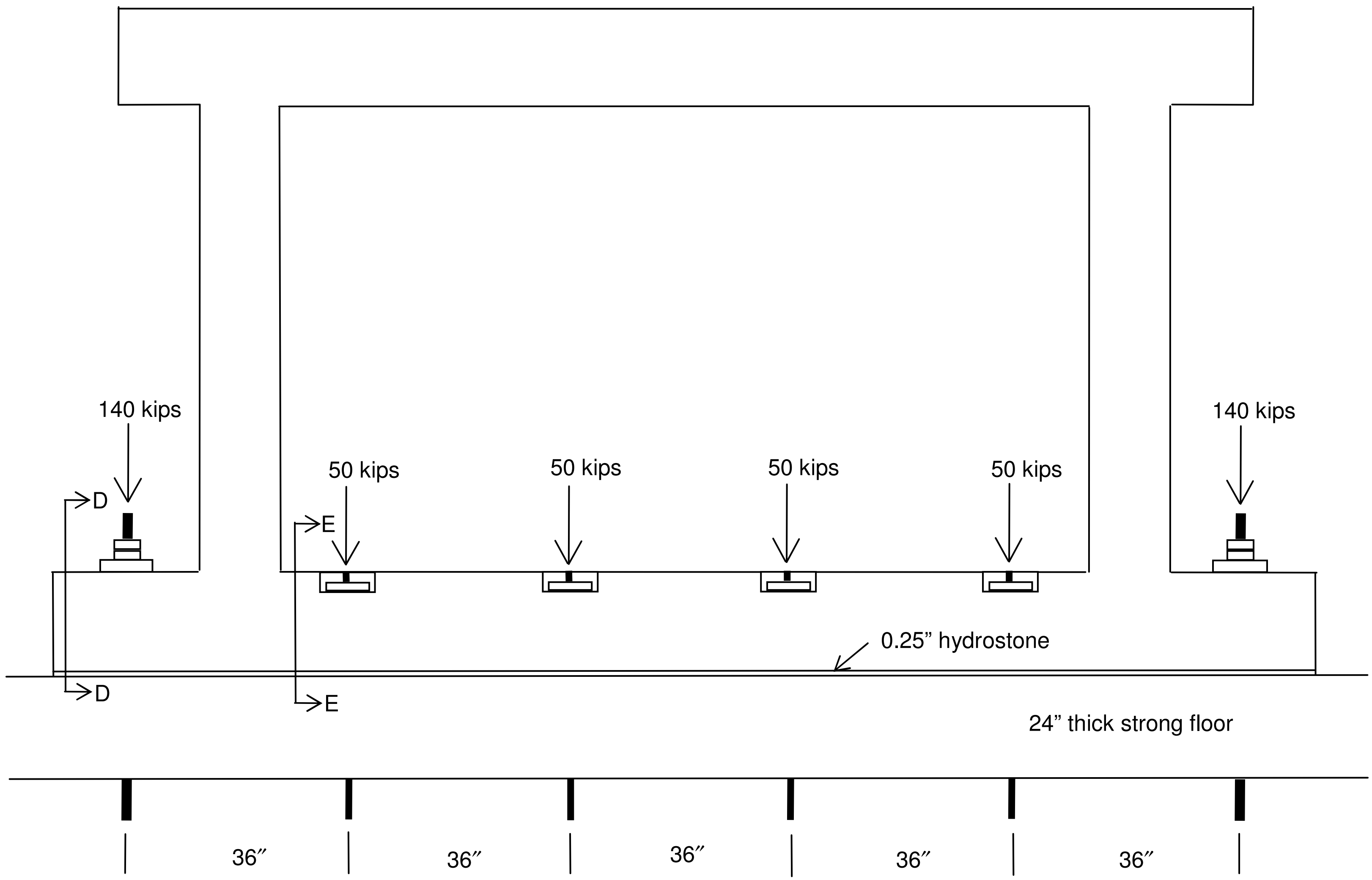

Figure 4.4: Frame Anchorage

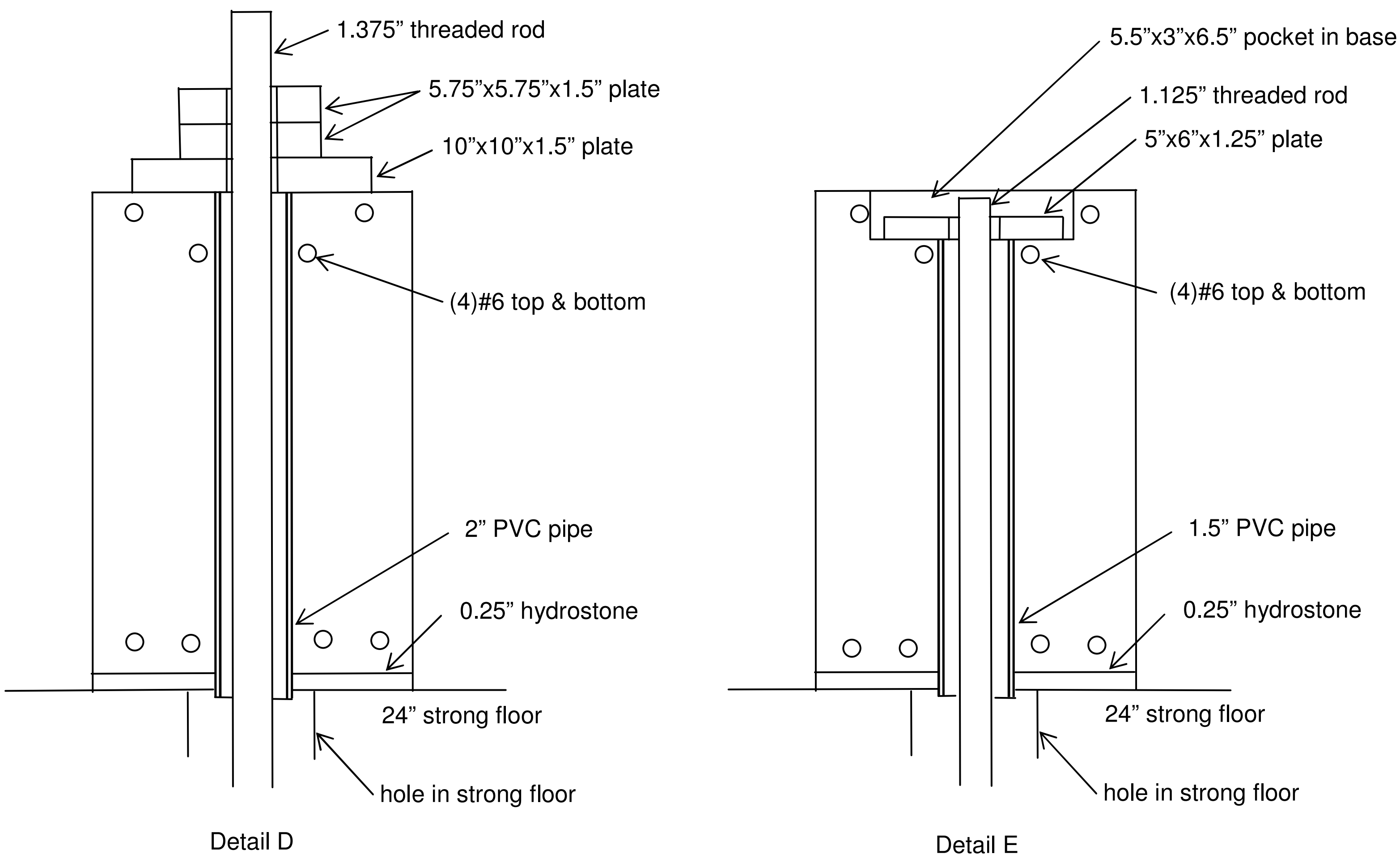

Figure 4.5: Anchorage Details

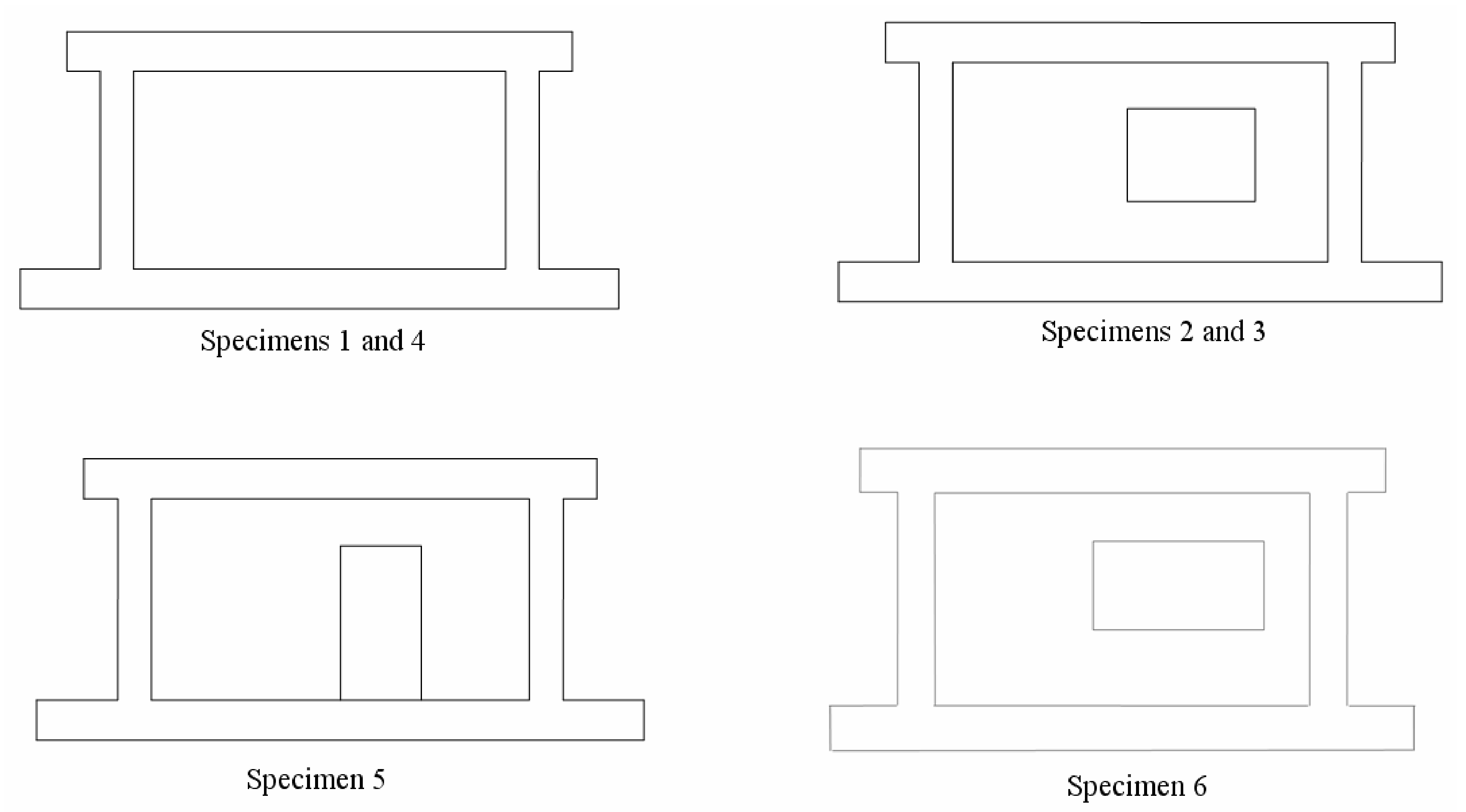

Figure 4.6: Schematic of the Six Test Specimens

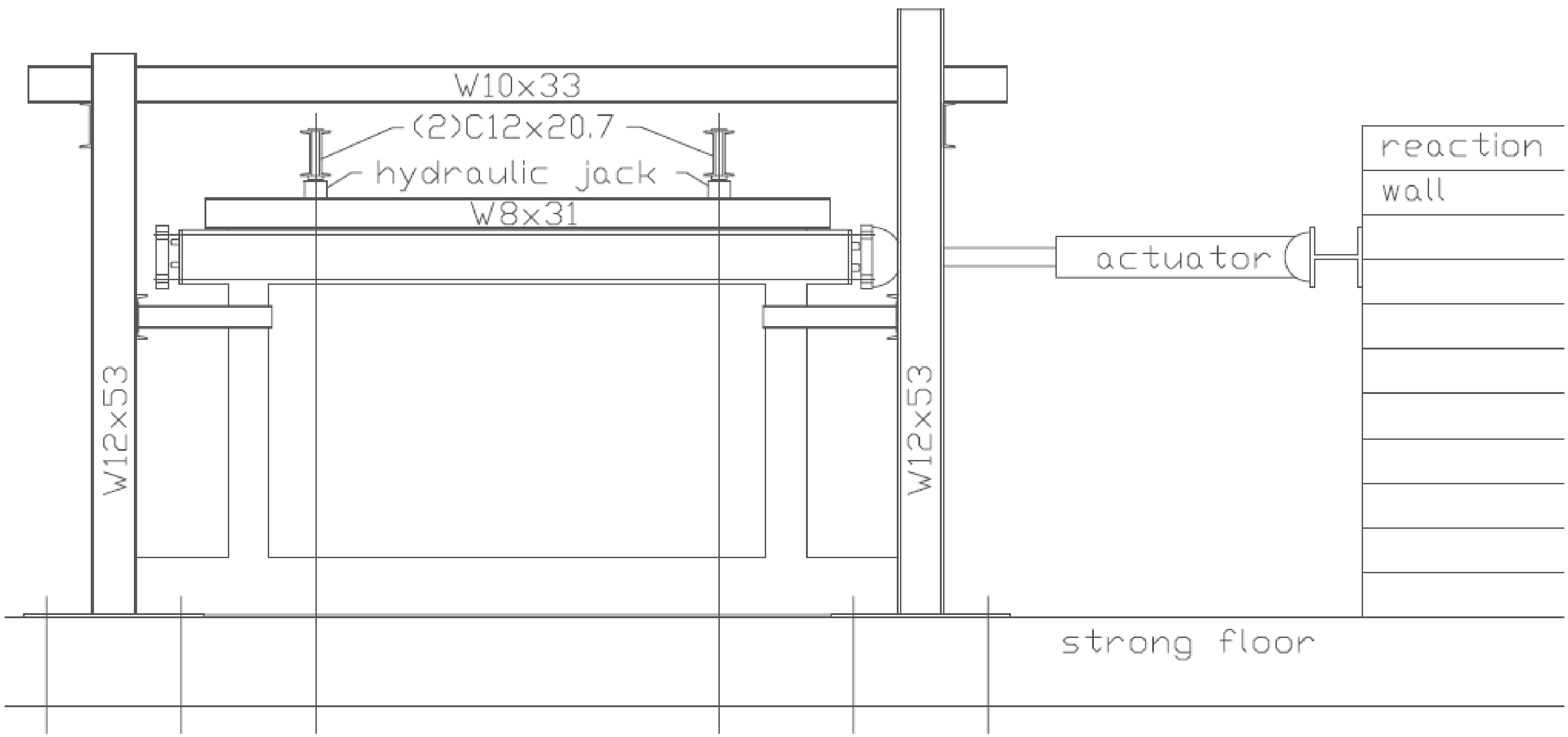

Figure 4.7: Test Setup

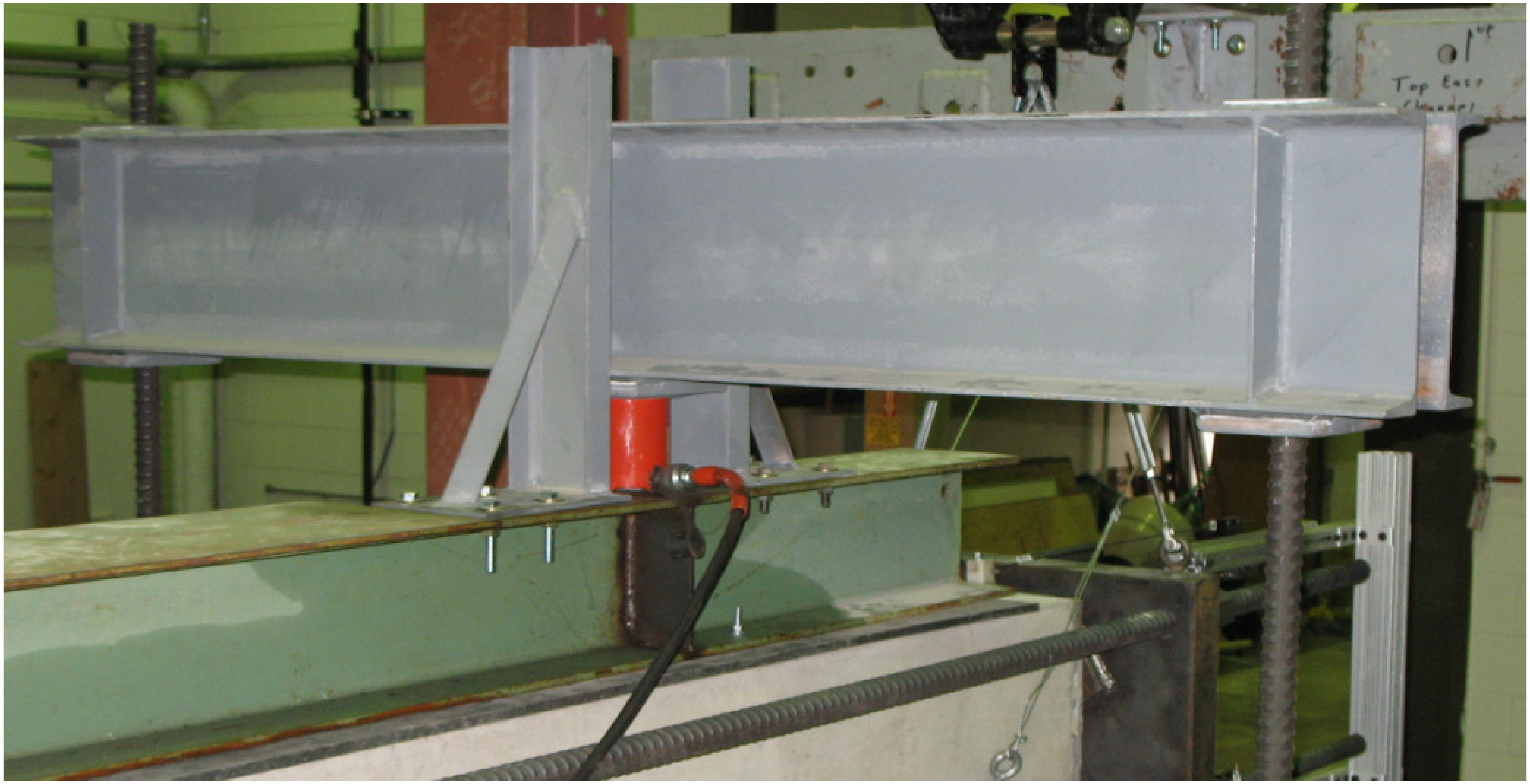

Figure 4.8: Vertical Load Apparatus

East End

West End

Figure 4.9: Horizontal Loading Apparatus

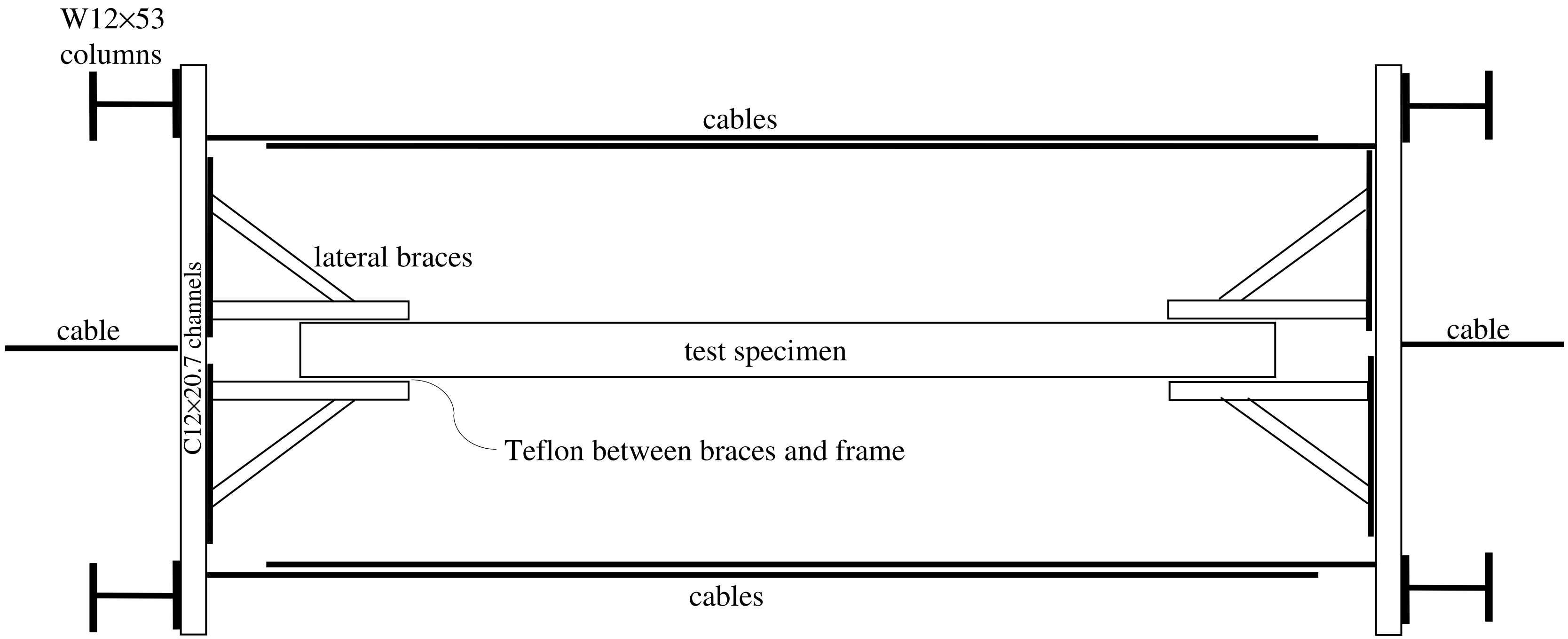

Figure 4.10: Plan View of Lateral Force Resisting System

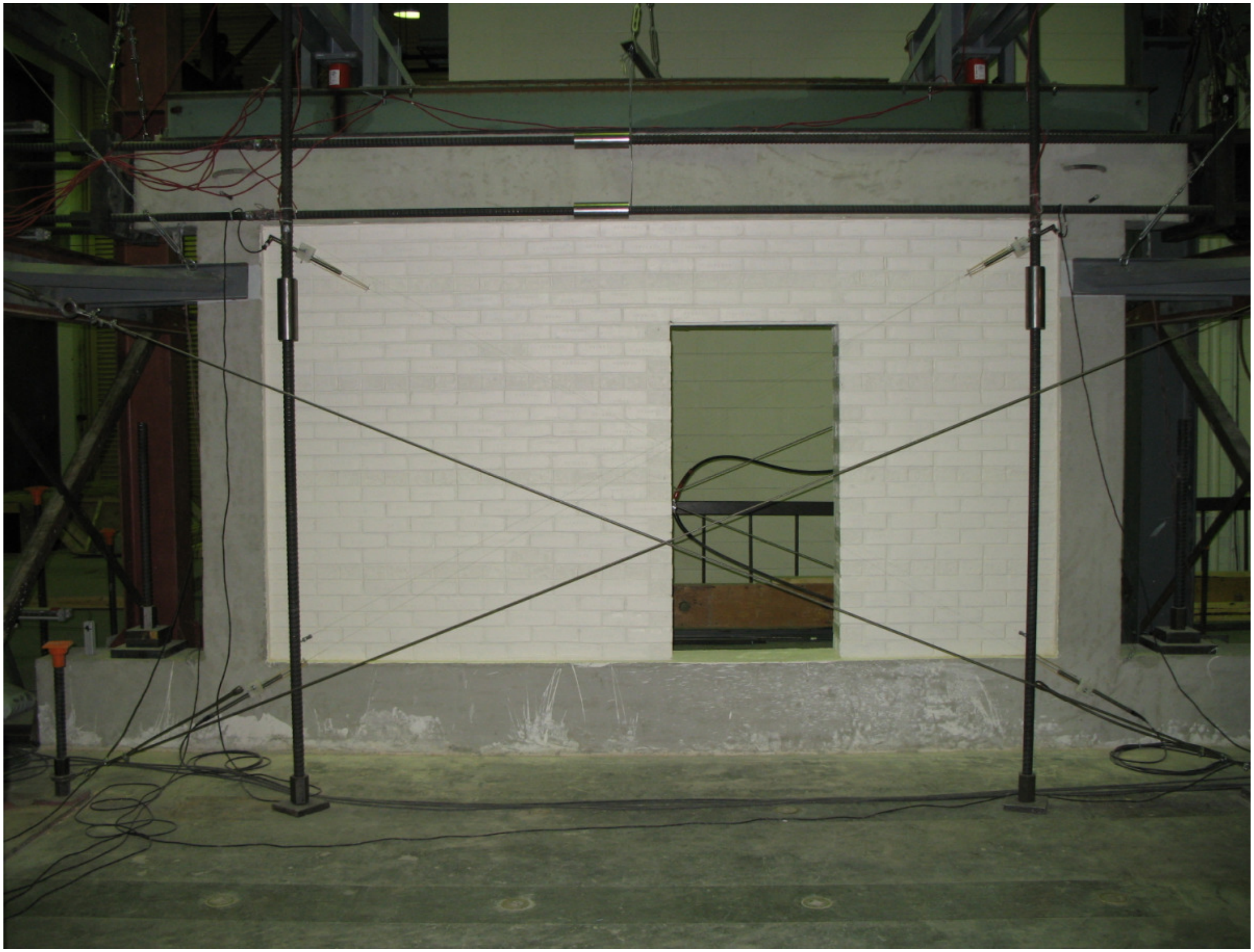

Figure 4.11: Typical Infilled Frame Ready For Testing

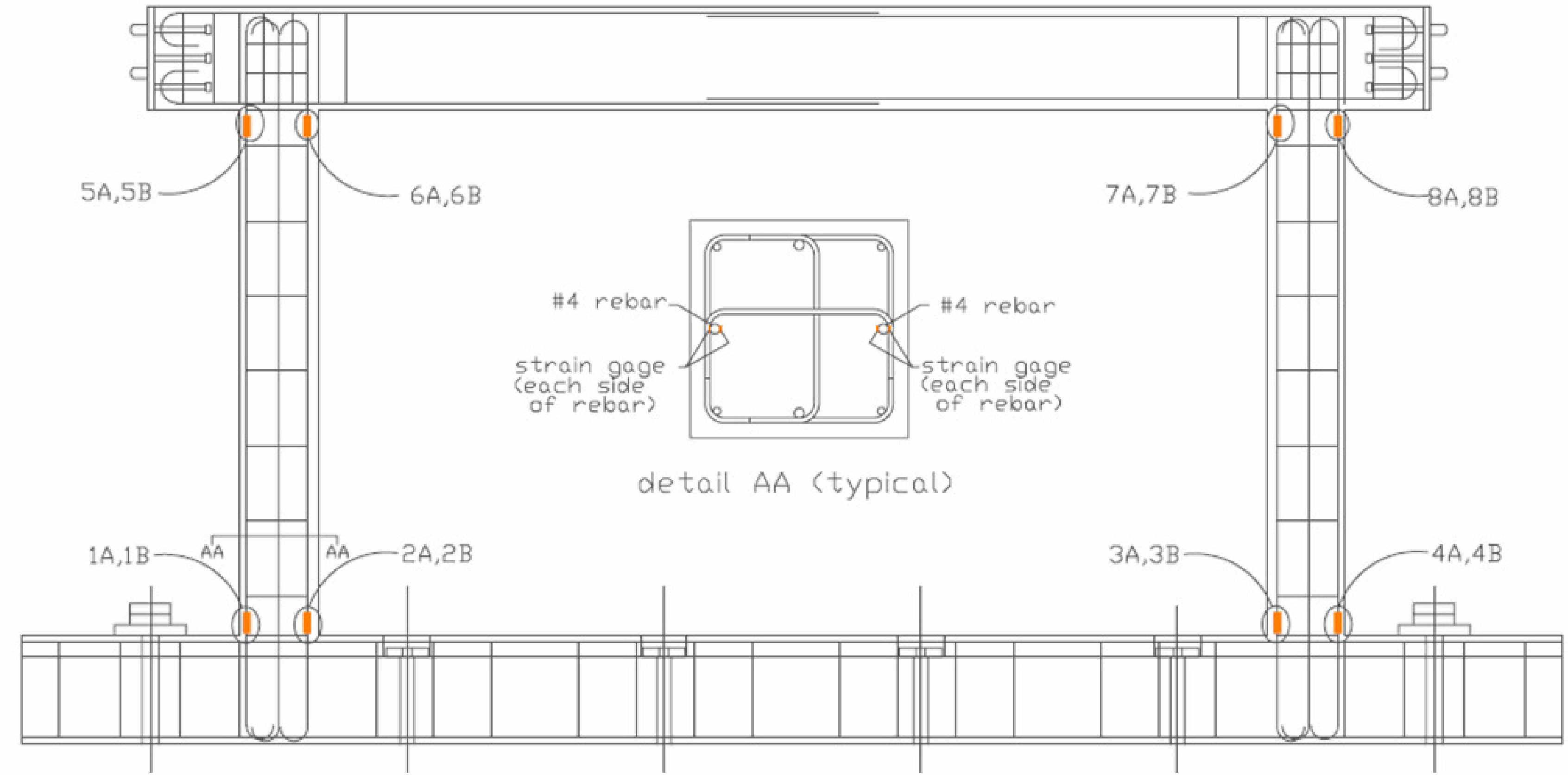

Figure 4.12: Strain Gages Attached To Rebar

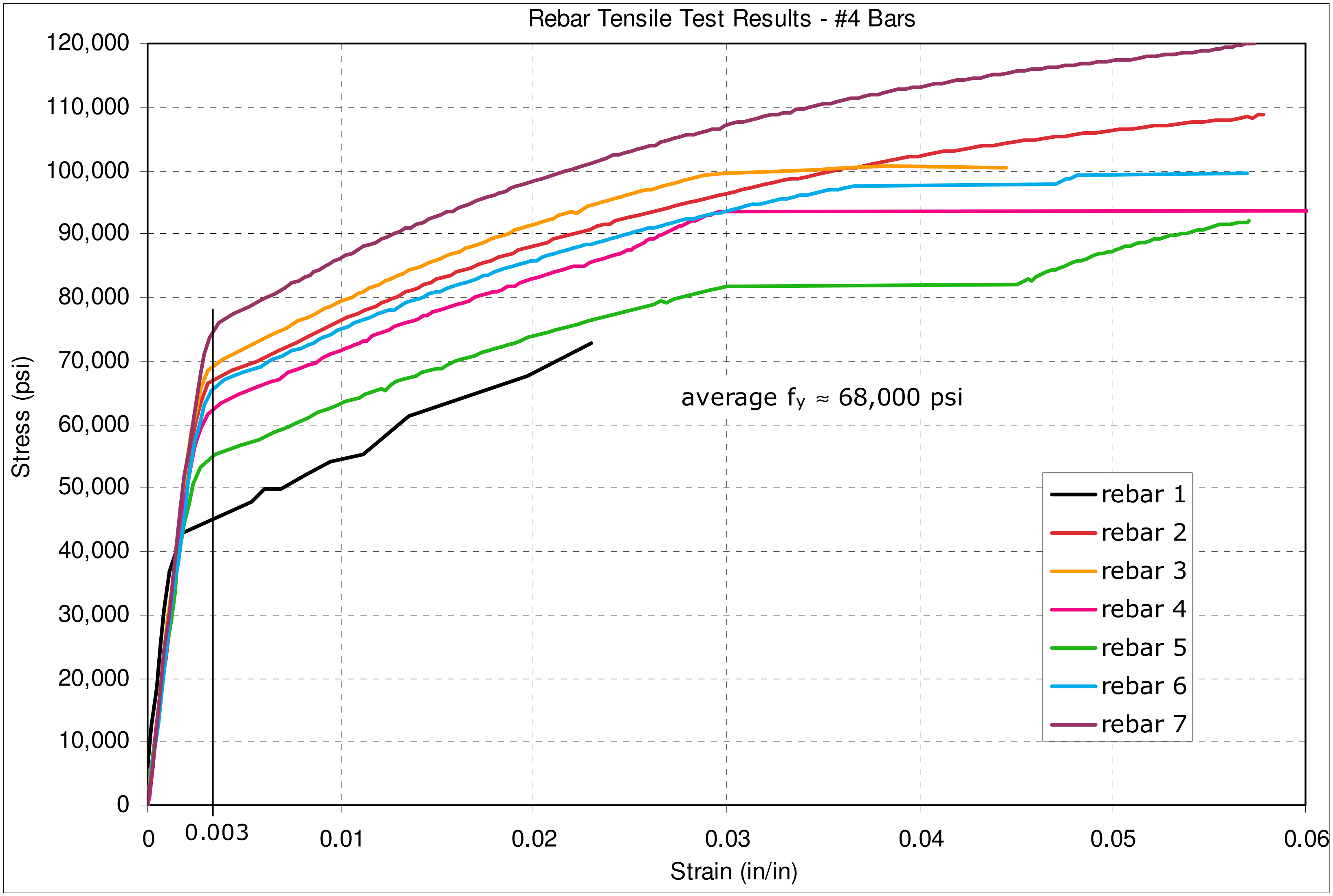

Figure 4.13: Rebar Tension Test Results

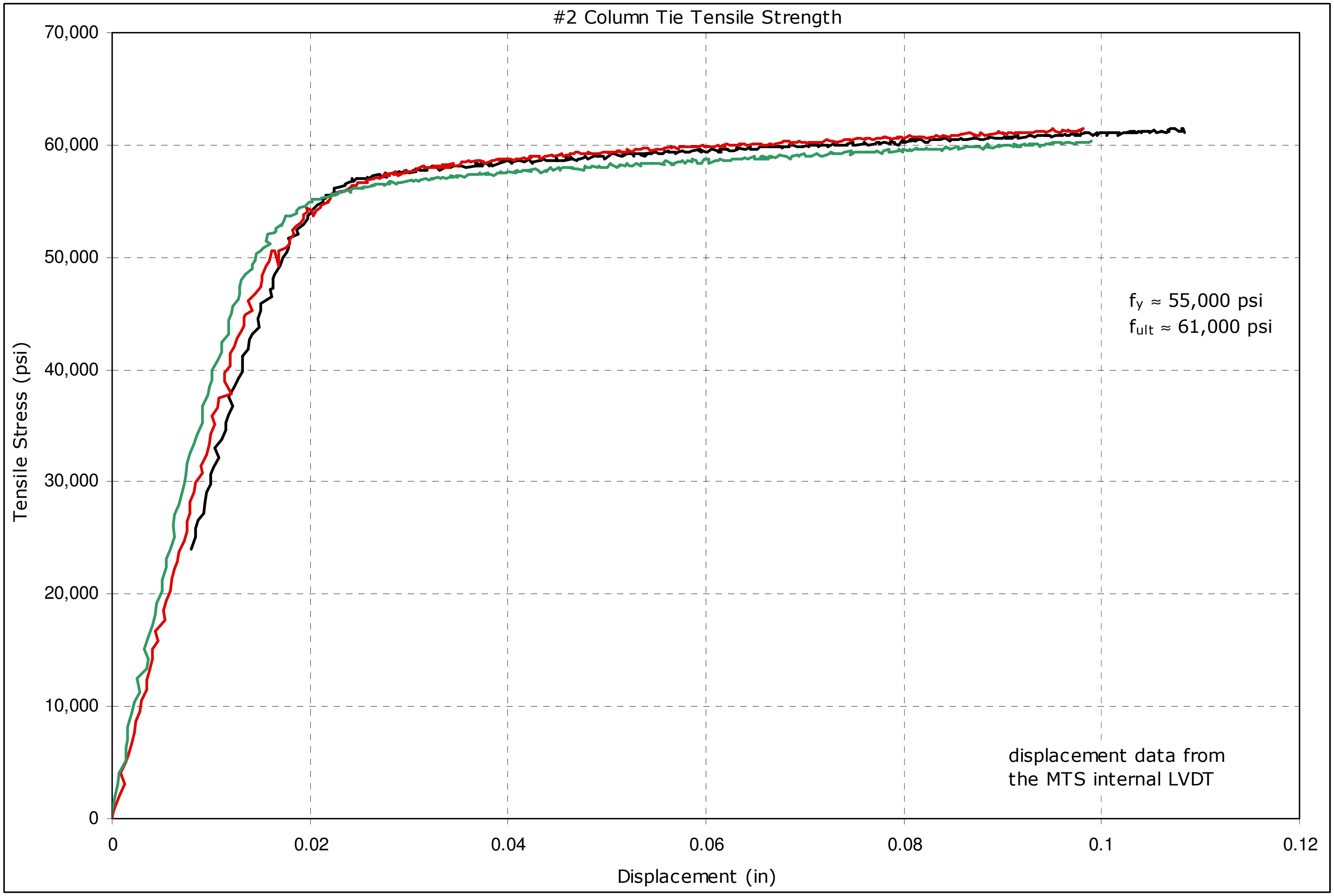

Figure 4.14: Column Tie Tension Test Results

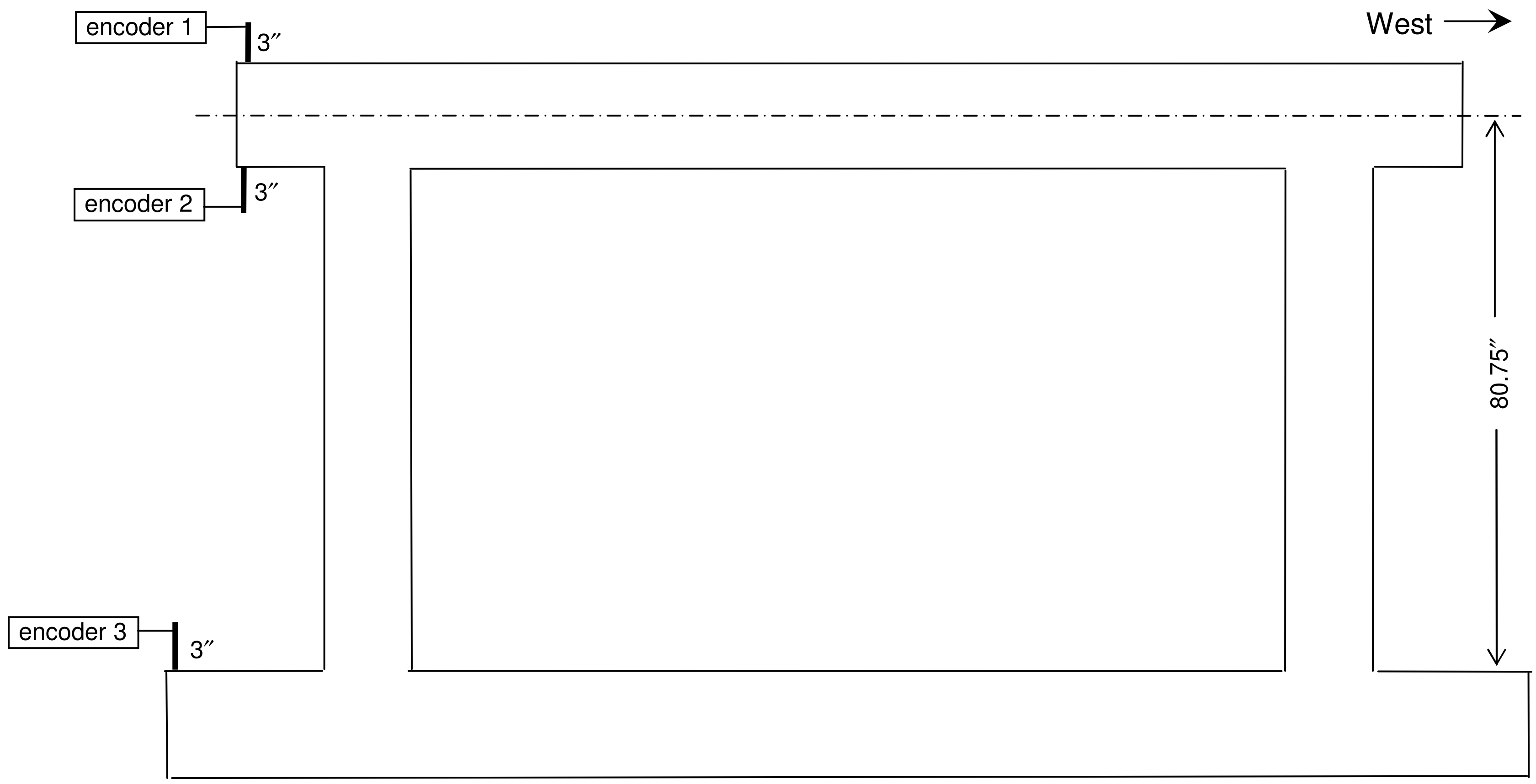

Figure 4.15: Optical Encoder Placement

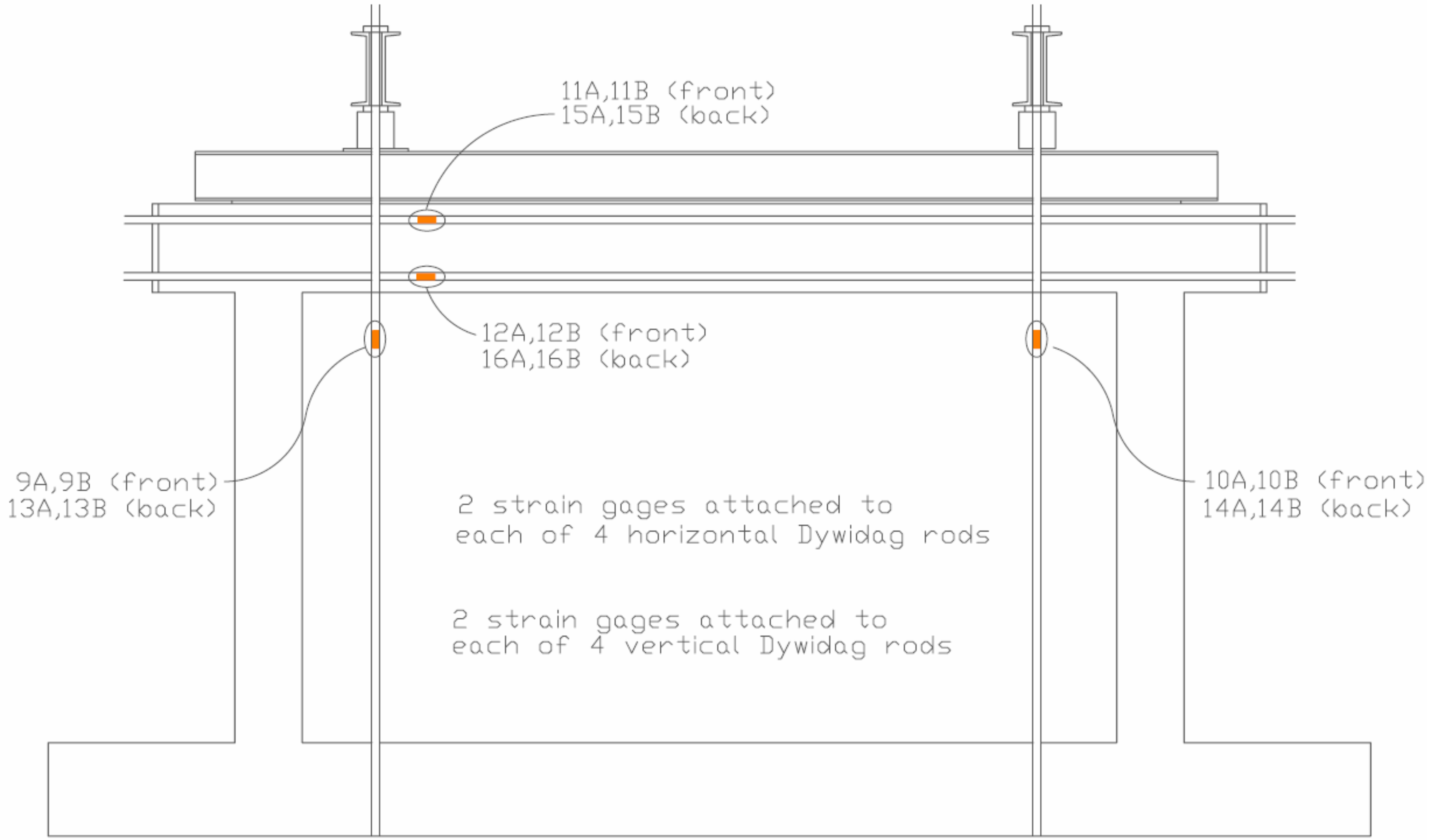

Figure 4.16: External Strain Gages

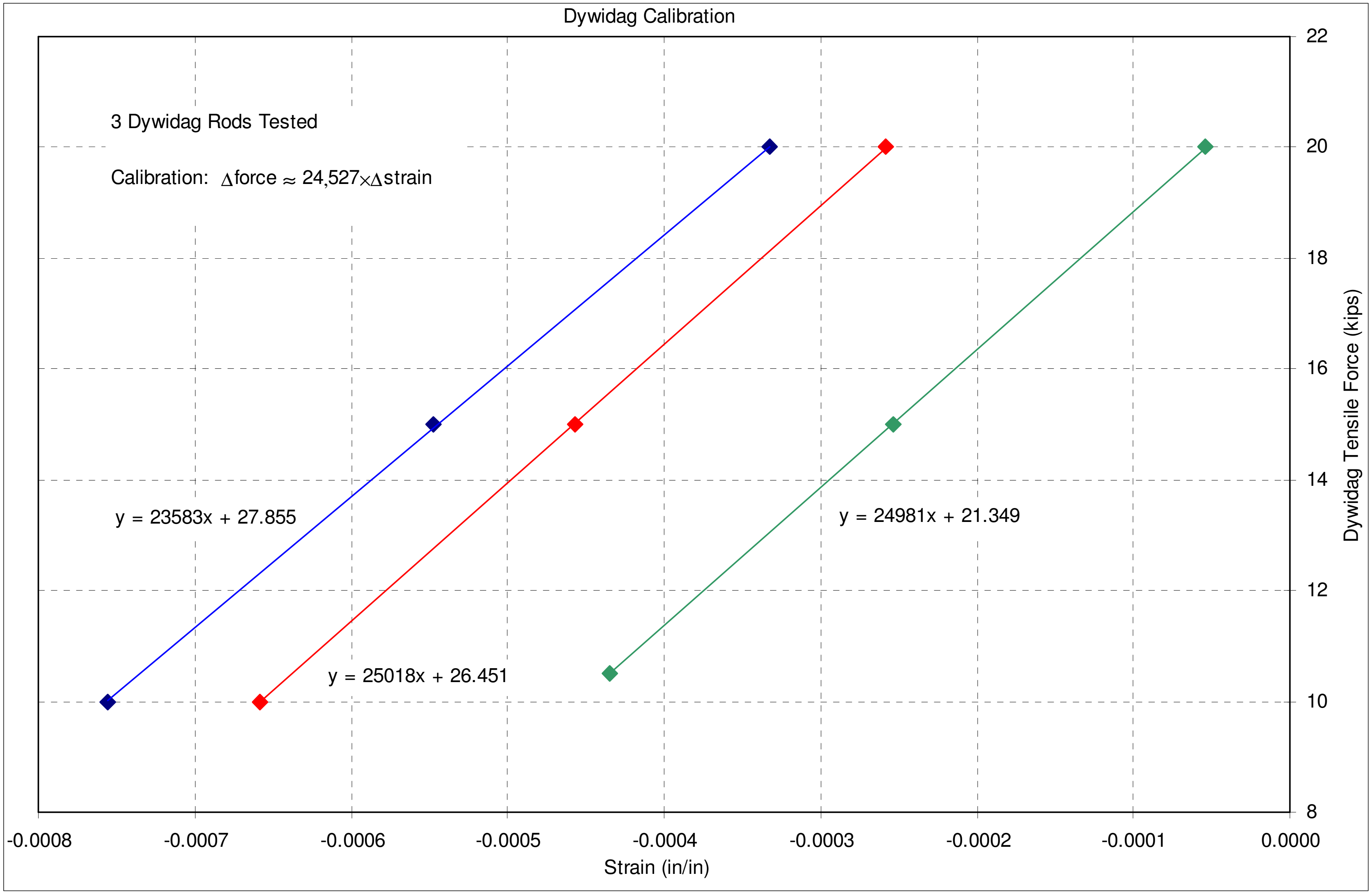

Figure 4.17: Dywidag Force vs Strain Calibration

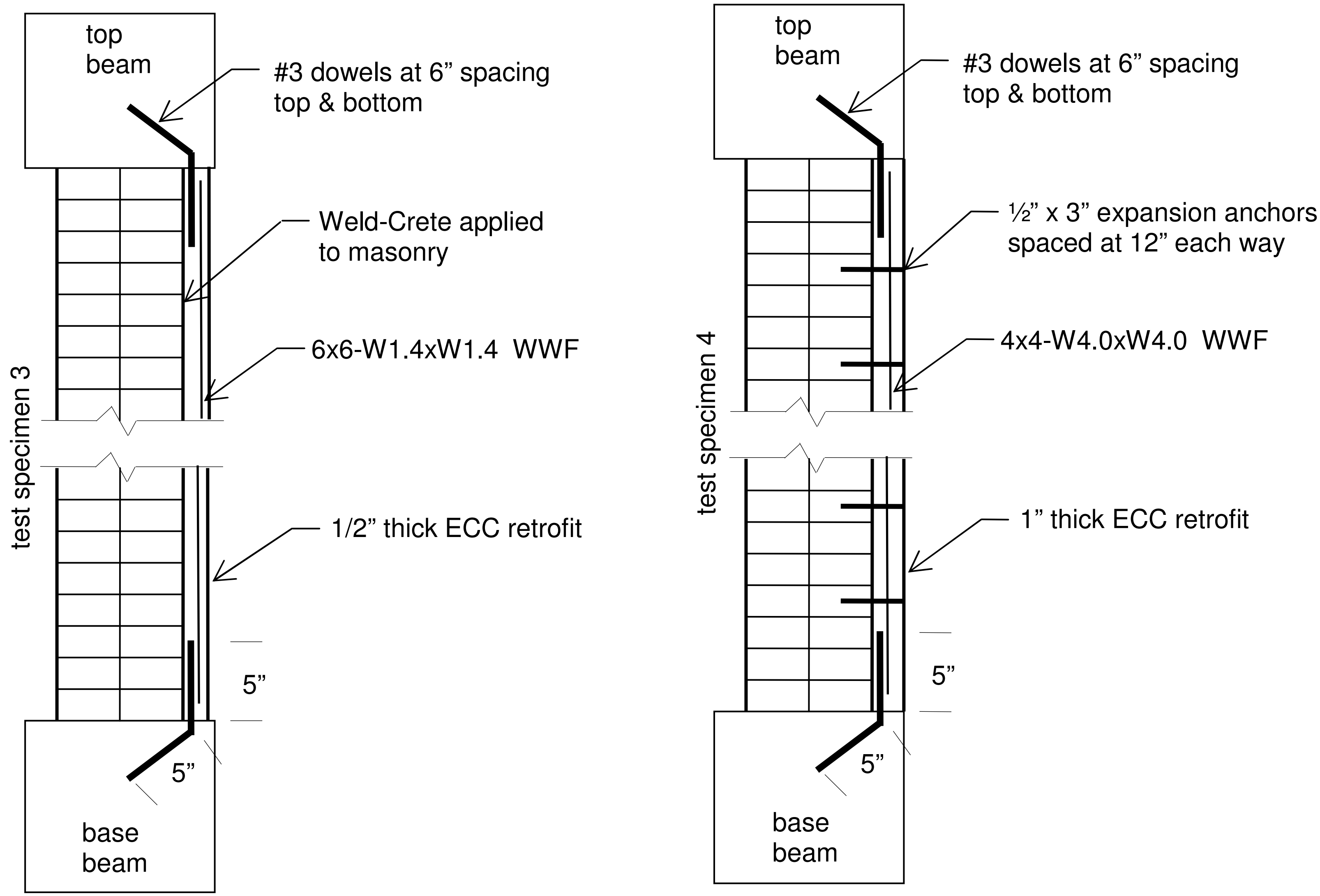

Figure 4.18: ECC Retrofit Details

Chapter 5: Infilled Frame Test 1

The first test specimen consisted of a solid infilled RC frame with no retrofit. The dimensions for the frame and reinforcing details can be seen in figures 4.1, 4.2, and 4.3. The material properties pertinent to this test are listed in table 5.1. As can be seen, the concrete compression strength is considerably higher than the 3,000 psi specified. Photographs of the finished specimen appear in figures 5.1 and 5.2. The LVDT instrumentation for the frame and wall can be seen in figures 5.3 and 5.4.

After a few load control cycles to establish the initial stiffness of the infilled frame, displacement cycles 5 through 20 were applied. The magnitudes of the displacement cycles are ploted in figure 5.5. Cycles 5 through 19 had a “normal” range of magnitude and essentially constitute the test of the structure. After these were completed, one large cycle was applied (cycle 20), simply to push the equipment and specimen to an extreme. This last cycle was also beneficial for the demolition of the specimen. Figure 5.6 shows the total hysteresis plot for the force vs displacement. Figure 5.7 shows the response for the main portion of the test. The figures show four regions of the behavior. The initial elastic range is followed by softening to a peak plateau, which is followed by further softening and then a residual state. This pattern is more apparent in the positive cycles than the negative cycles. The residual hardening of cycle 20 seen in figure 5.6 is likely due to plastic bending of the column rebar that occurred during the extreme positive half of cycle 20. Figure 5.11 is a photograph of the top left column taken after the test. The extreme opening of this column shear crack occurred during cycle 20. The top right column showed similar distress.

Figure 5.8 shows the force-displacement response with key events indicated. Minor cracks in the wall and frame, along with separation between the masonry and concrete, cause softening early in the test. Cracks gradually develop in the wall and frame during the plateau. The drop in strength in the negative direction coincides with a completion of a diagonal wall crack during cycle N10. In the positive direction a more abrupt drop occurs that coincides with the shearing at the top of the west column. The residual shear strength of the structure is approximately 80 kips in both directions. This residual is thought to be predominately from the bed joint sliding of the wall.

Figure 5.9 indicates that plasticity in the reinforcing started late in the test. The exception to this observation is with gage 2, which is at the lower end of the east column.

The final crack pattern is shown in figure 5.10. The classic “H” pattern of wall cracks is clear. Both columns experienced shear failure at the top. Only the west column sheared at the bottom. The top left column shear is shown in figure 5.11. It is interesting to note that the #2 stirrup did not rupture, even with the extreme shear opening of the column.

Table 5.1: Test 1 Material Properties

Concrete Compressive Strength	4,360 psi
Mortar Compressive Strength	1,340 psi
Masonry Prism Compressive Strength	3,530 psi
Reinforcing Tensile Yield Strength	68,000 psi
Column Tie Yield Strength	55,000 psi

Figure 5.1: Test 1 Specimen

Figure 5.2: Test 1 Specimen With Support Frame

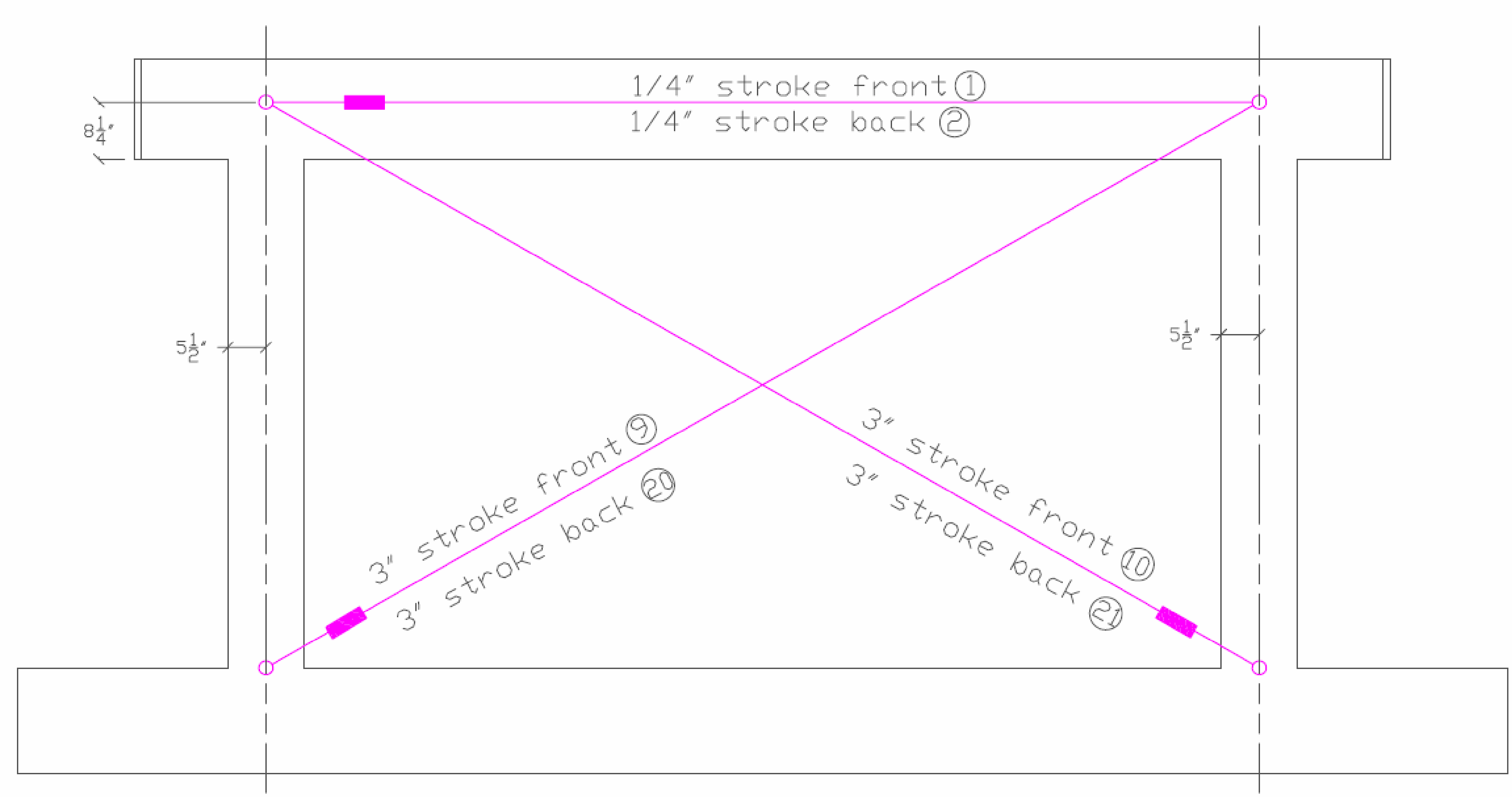

Figure 5.3: Test 1 Frame Mounted LVDT Placement

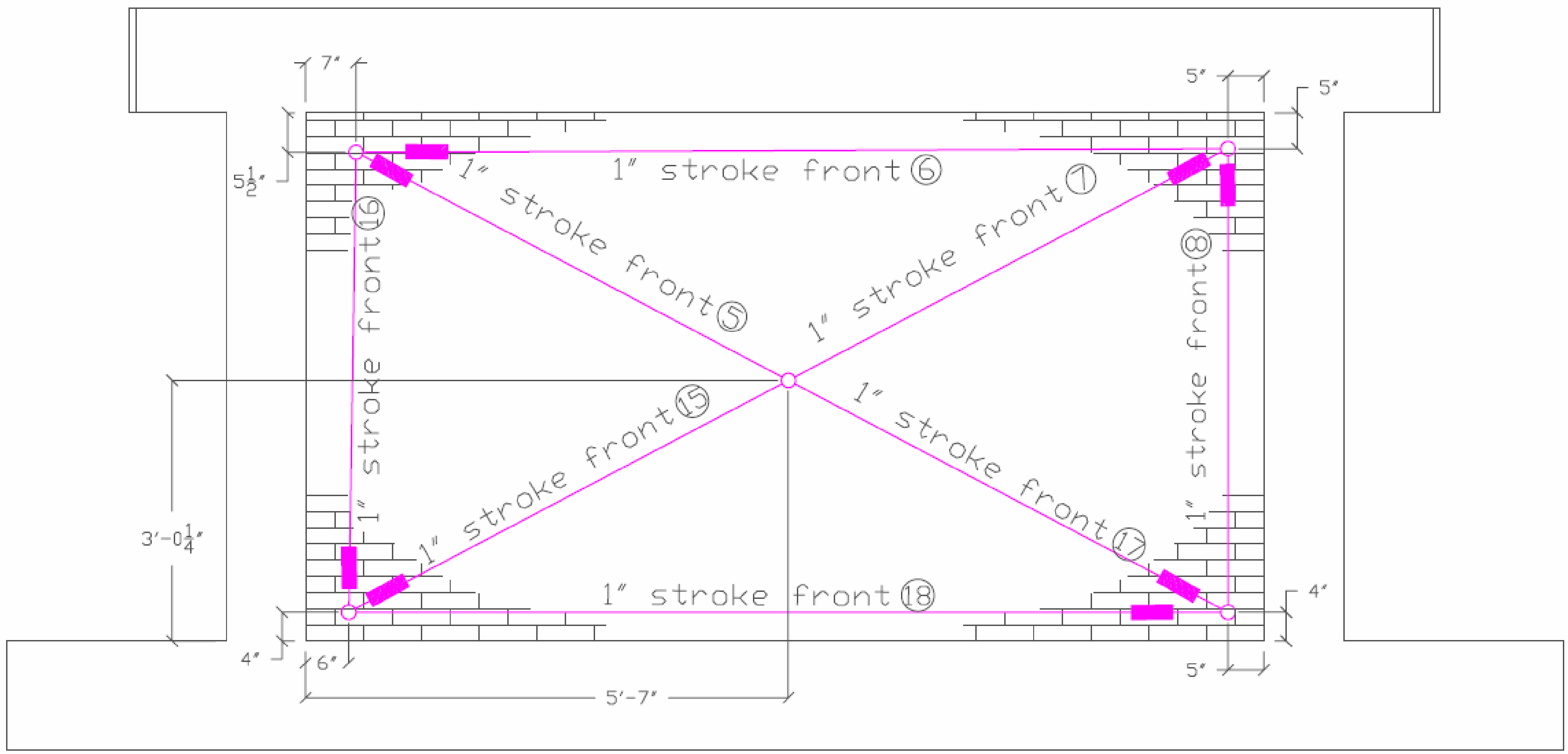

Figure 5.4: Test 1 Wall Mounted LVDT Placement

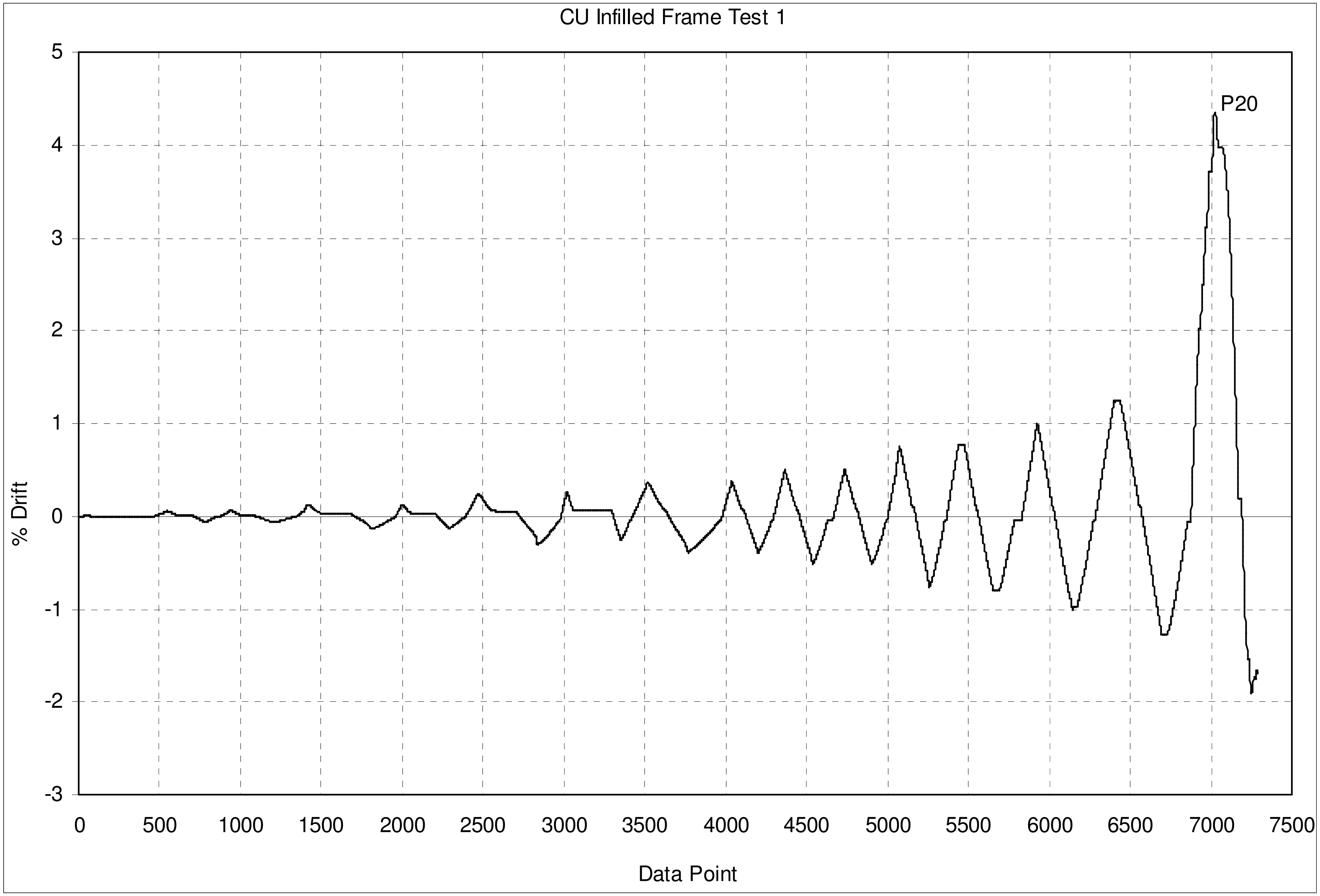

Figure 5.5: Test 1 Applied Displacement Cycles

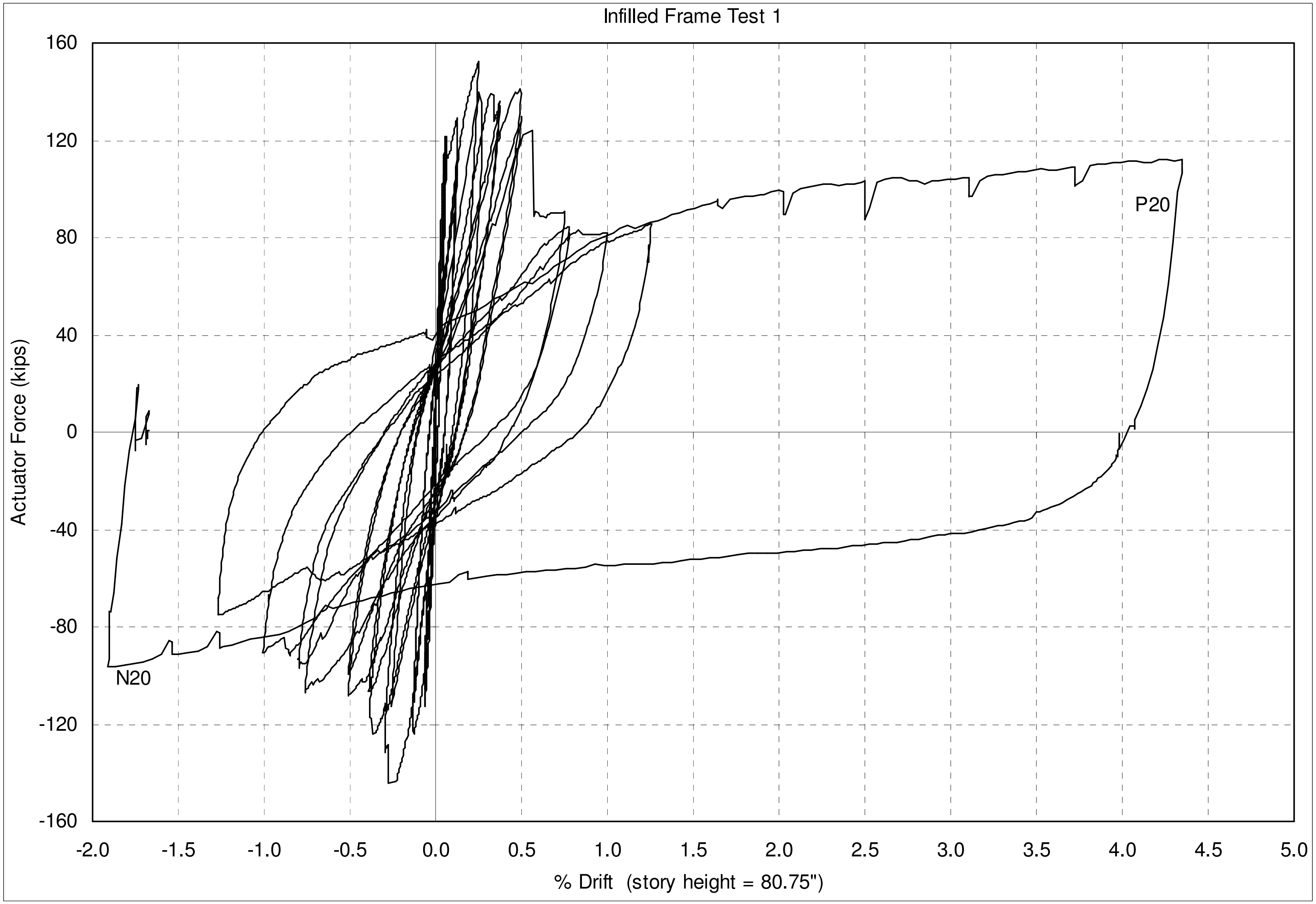

Figure 5.6: Test 1 Force vs Displacement

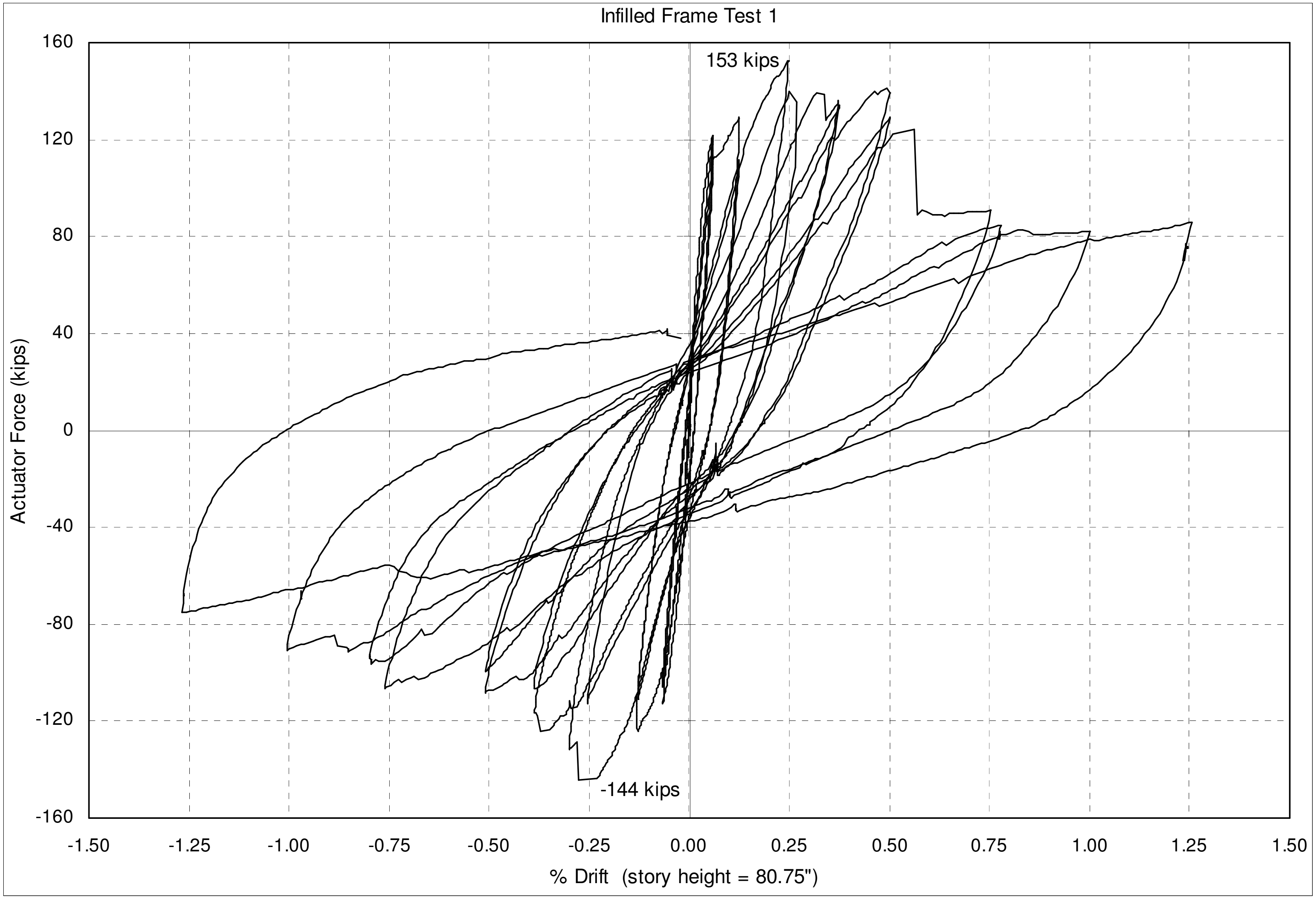

Figure 5.7: Test 1 Force vs Displacement

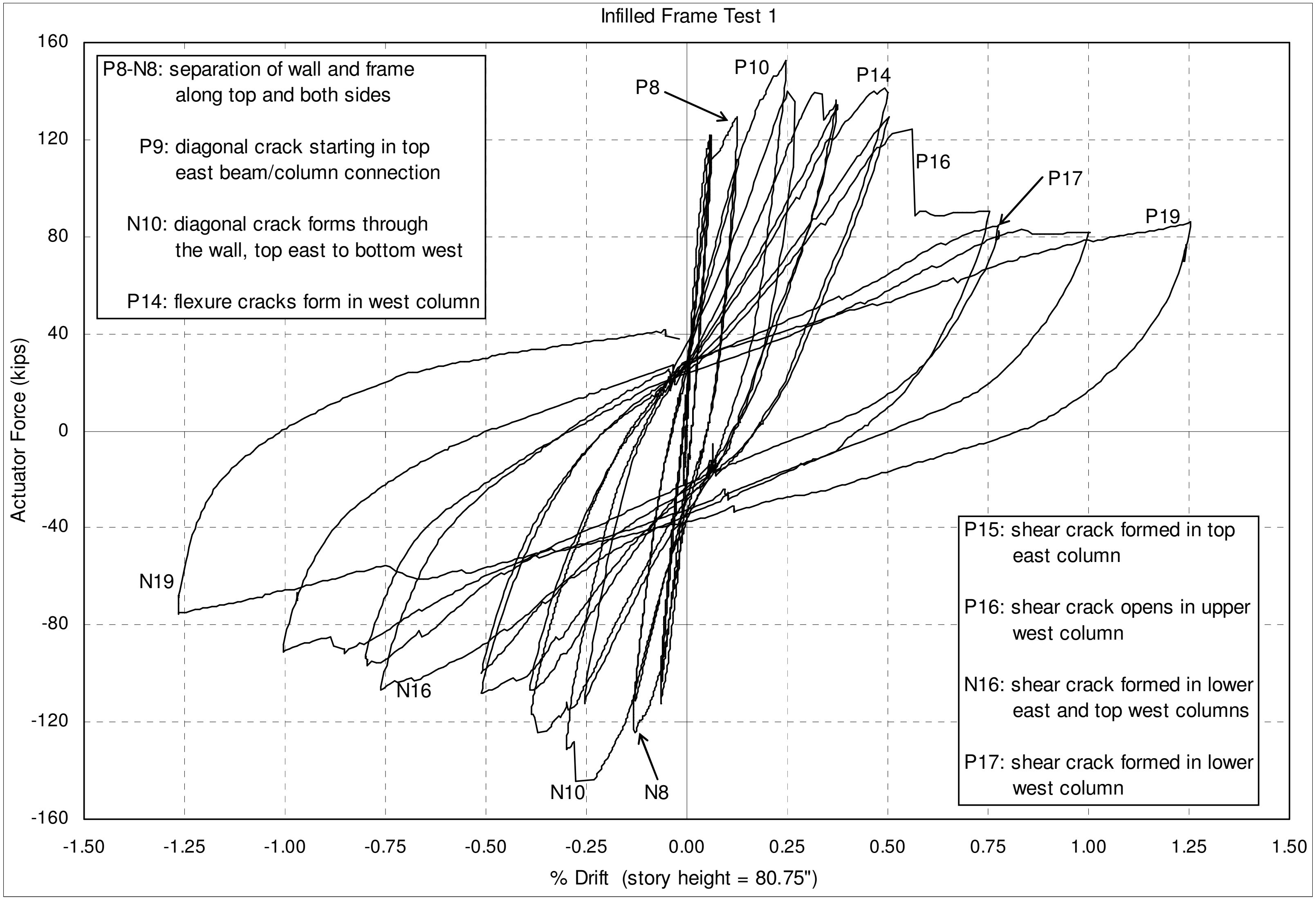

Figure 5.8: Test 1 Force vs Displacement

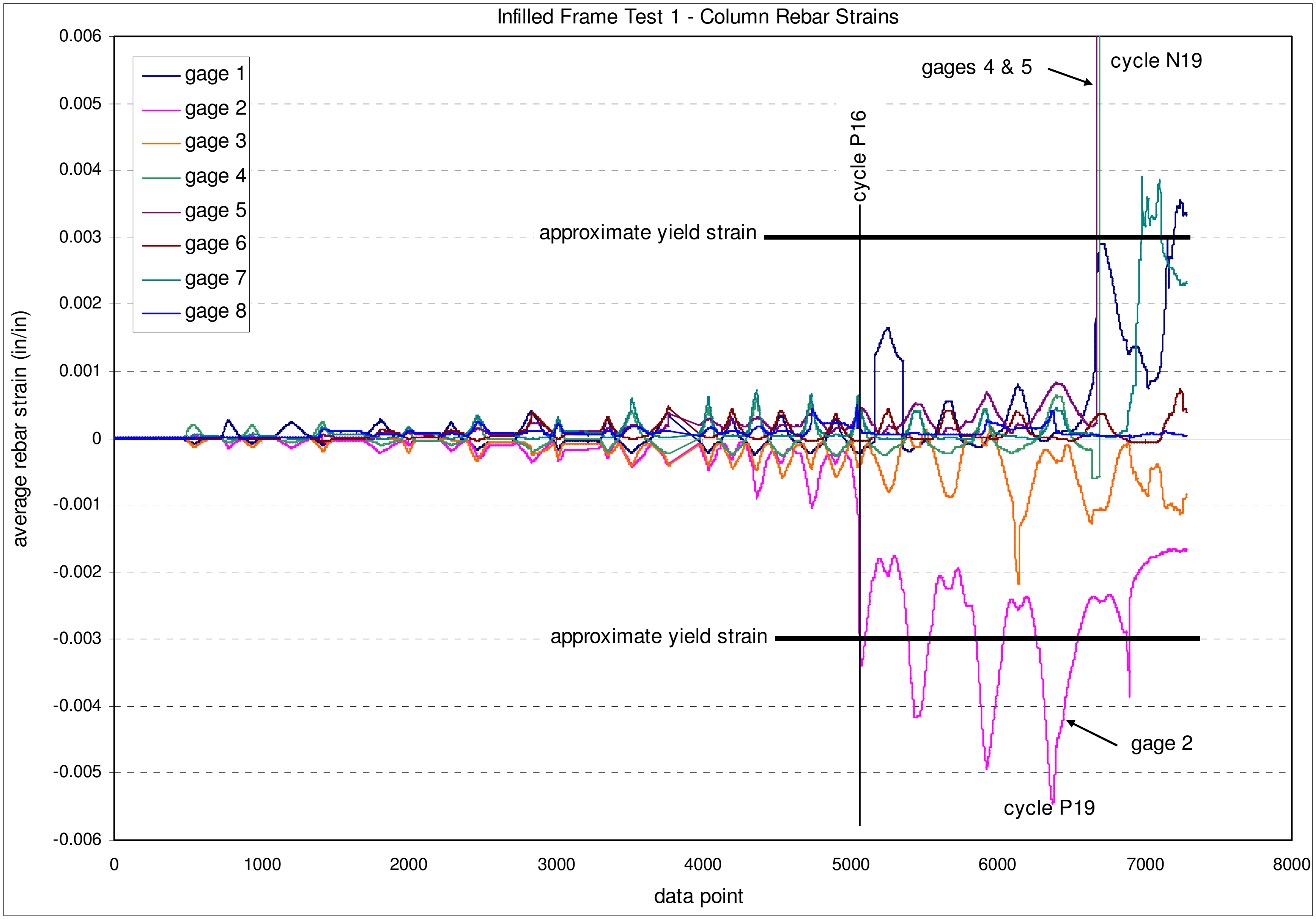

Figure 5.9: Column Rebar Strains

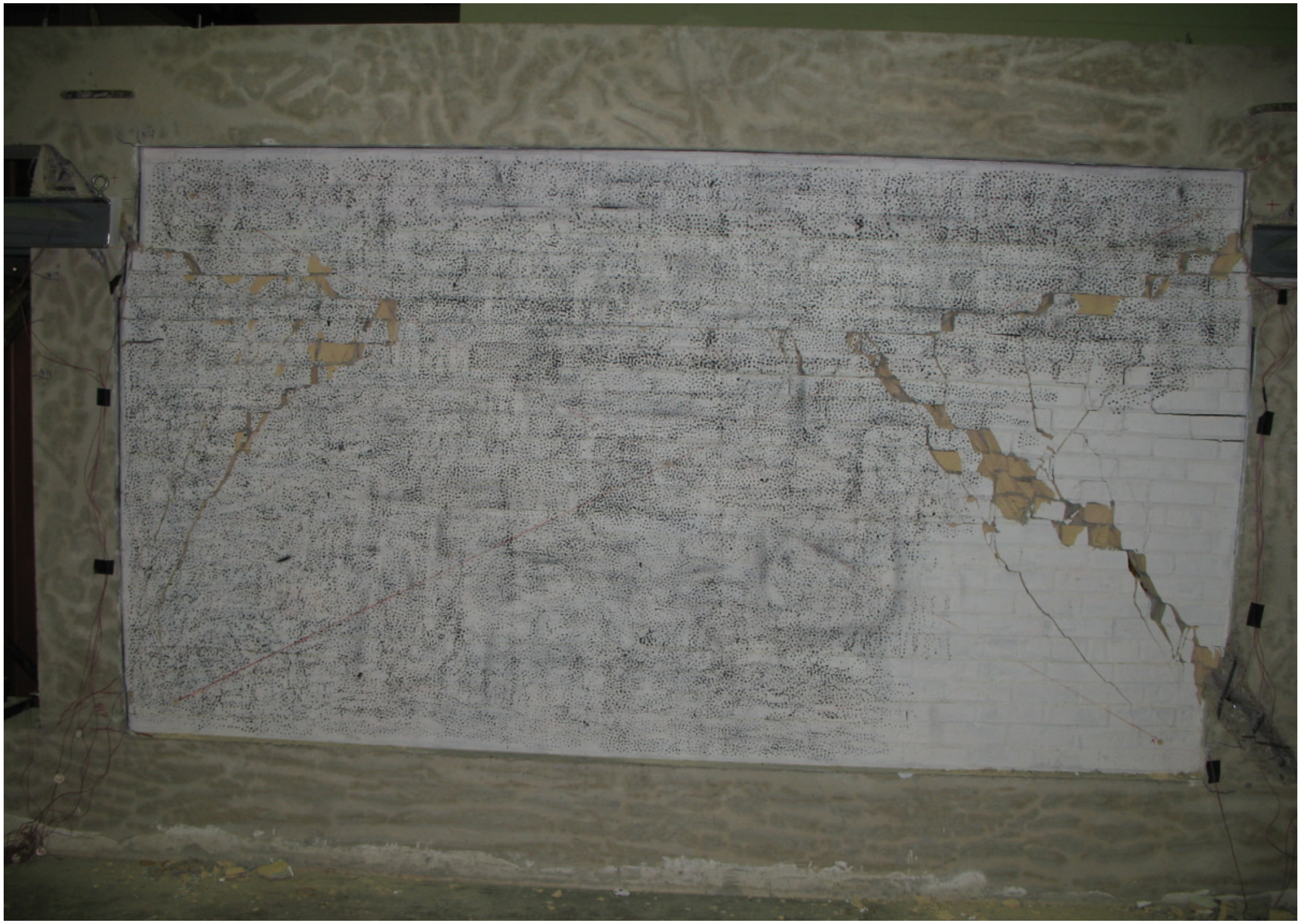
Figure 5.10: Final Crack Pattern

Figure 5.11: Top Left Column After the Test

Chapter 6: Infilled Frame Test 2

The second test consisted of an infilled frame with the same dimensions as the first test specimen. The modification for test 2 was the addition of a window opening. Frame, wall and opening dimensions are shown in figure 6.1. The reinforcing details are the same as those of the first frame, see figures 4.2 and 4.3. An LL3×3×1/4 steel double angle was used for the window lintel. Figure 6.2 is a photograph of the specimen with the vertical and horizontal load apparatus installed. LVDT instrumentation of the wall and frame are shown in figures 6.3 and 6.4. The applied vertical load is shown in figure 6.5. Table 6.1 shows the relevant material properties. The concrete strength was below the 3,000 psi specified, and considerably lower than the 4,360 psi for the first test.

After a few load controlled cycles, the displacement cycles started with cycle number 4. The applied cycles for test 2 appear in figure 6.6. One additional cycle (P22-N22) was applied after the core test cycles in order to facilitate demolition. The complete force vs displacement response is shown in figure 6.7. Figure 6.8 shows the main cycles that constitute test 2. The two directions show a noticeable difference in the response. The elastic regime is followed by softening caused by minor cracks in the wall and frame, as well as separation of the wall from the frame. After brittle drops in the structure strength plateaus were reached in both directions.

Figure 6.9 shows the force vs displacement response along with details of critical occurrences in the test. The negative direction showed a higher peak than the positive direction. In the negative direction there was no plateau as seen in the positive direction. After peak a brittle drop occurred coinciding with a large diagonal crack in the wall east of the window opening. This crack opened abruptly with an audible “bang”. The crack is shown in figure 6.11 immediately after it occurred. As can be seen in figures 6.8 and 6.9, this crack was responsible for an sudden 33% decrease in strength in the negative direction. In the positive direction a long plateau developed keeping a high strength past 1% drift. The quick drop in strength at cycle P18 was caused by the left column shearing near mid-height. This can be seen in figures 6.12 and 6.13.

The rebar strain gage readings are shown in figure 6.10. Yielding of a few of the column reinforcing bars occurred sooner than for test 1. The rebar in the upper west column, in particular gage 7, showed signs of yielding by N13, with a drift of approximately 0.4%. Gage 6A (top east column) shows considerable plastic strain starts at cycle N16.

Table 6.1: Test 2 Material Properties

Concrete Compressive Strength	2,570 psi
Mortar Compressive Strength	unreliable test results
Masonry Prism Compressive Strength	unreliable test results
Reinforcing Tensile Yield Strength	68,000 psi
Column Tie Yield Strength	55,000 psi

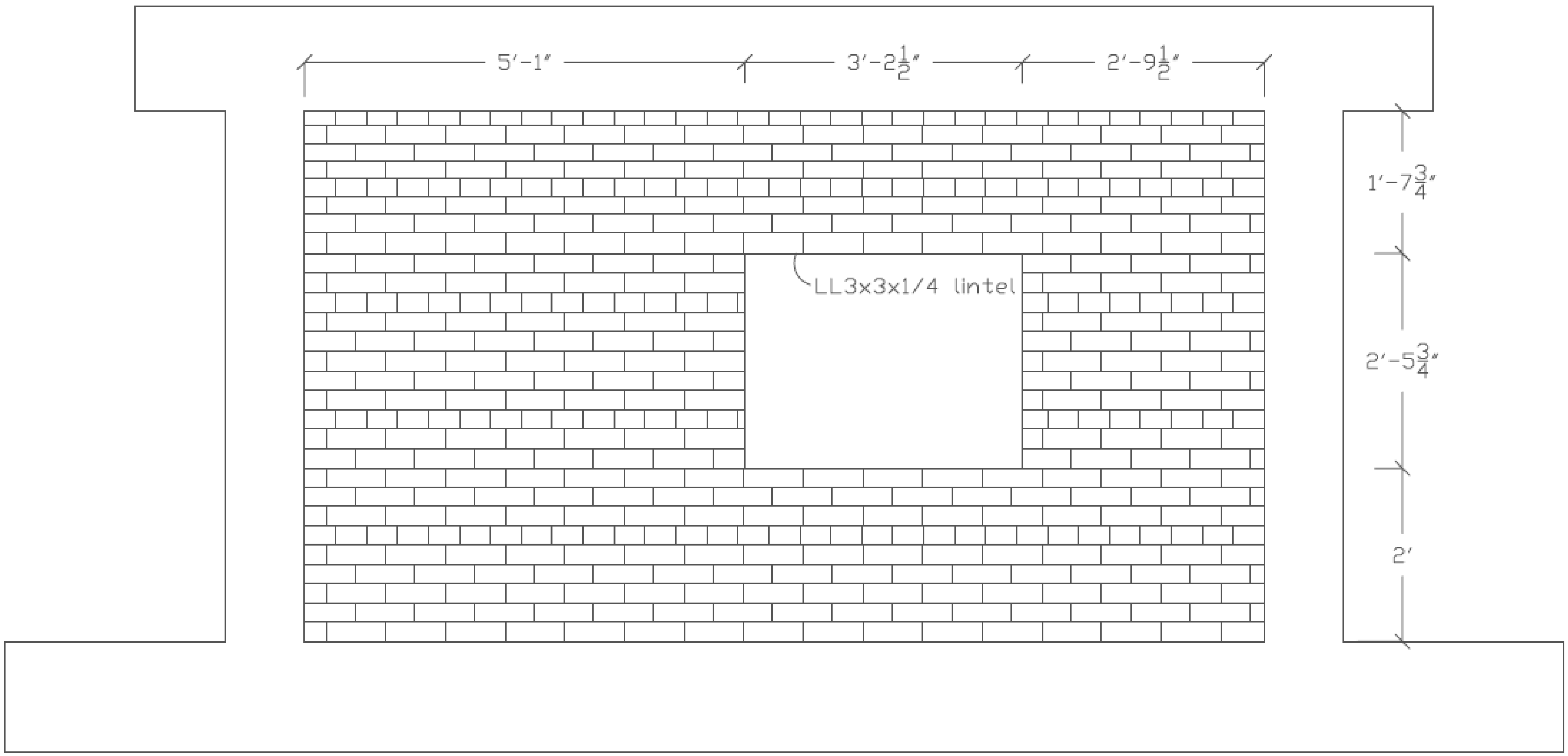

Figure 6.1: Test 2 Specimen

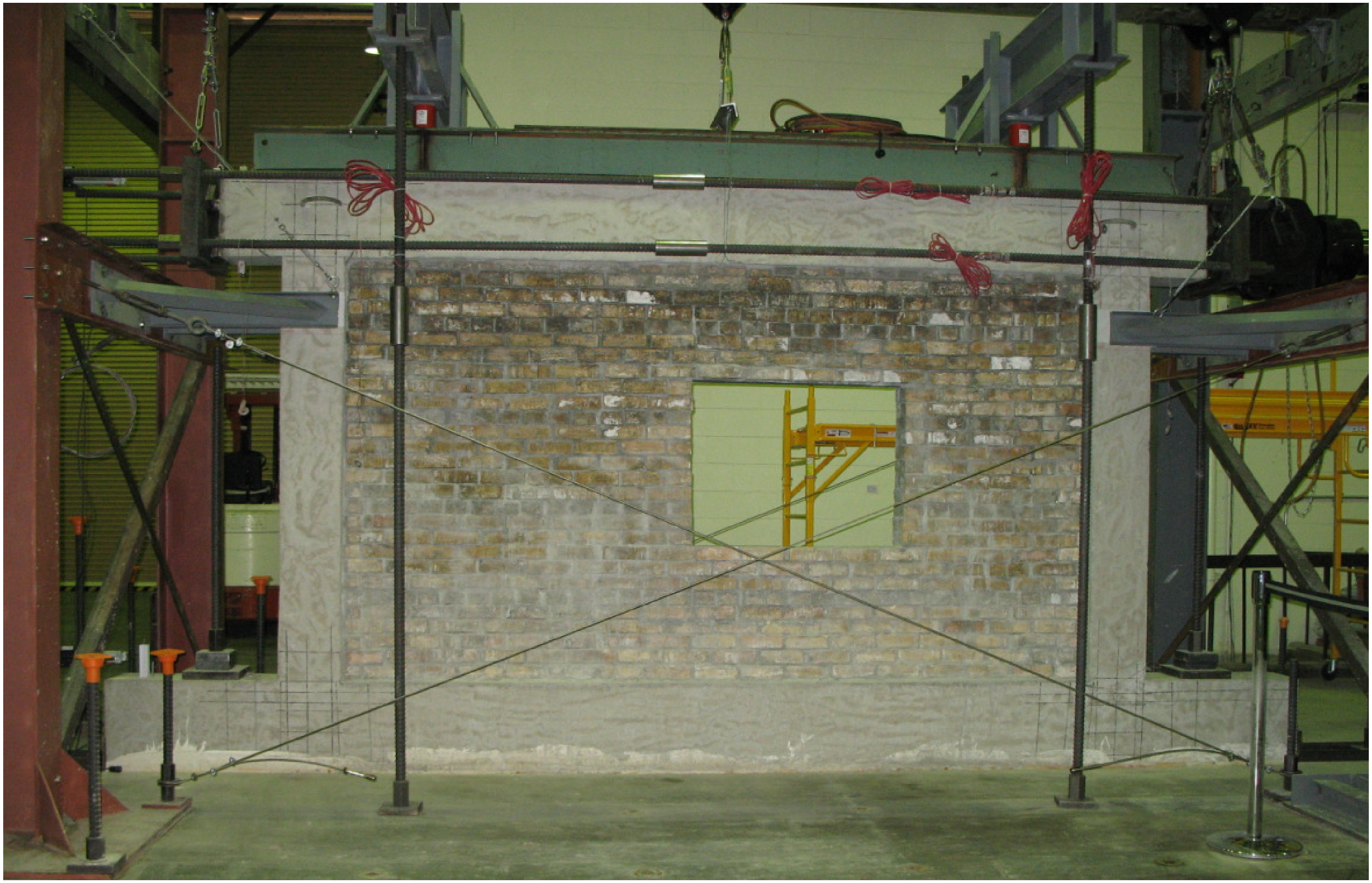

Figure 6.2: Test 2 Specimen

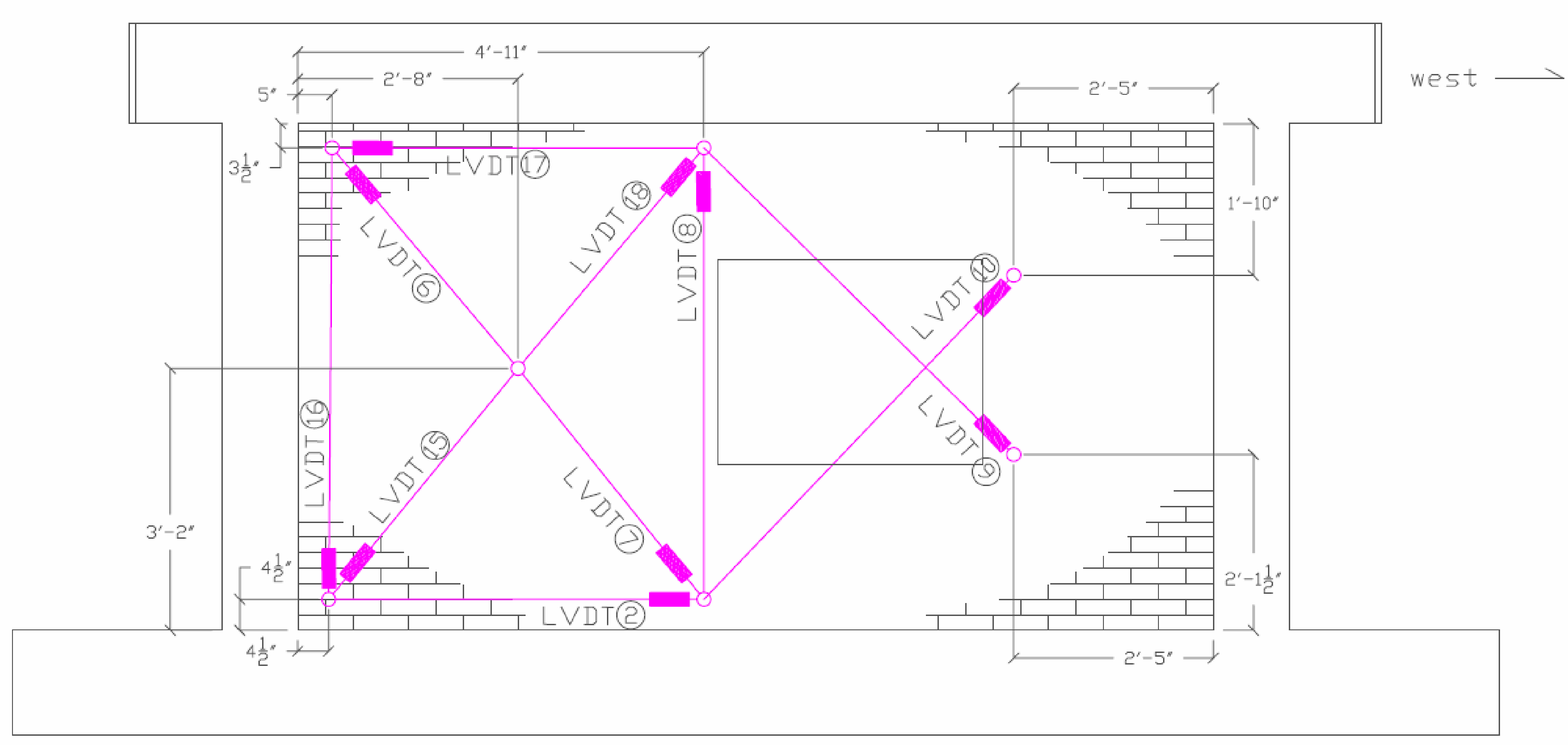

Figure 6.3: Test 2 LVDT Placement - Front

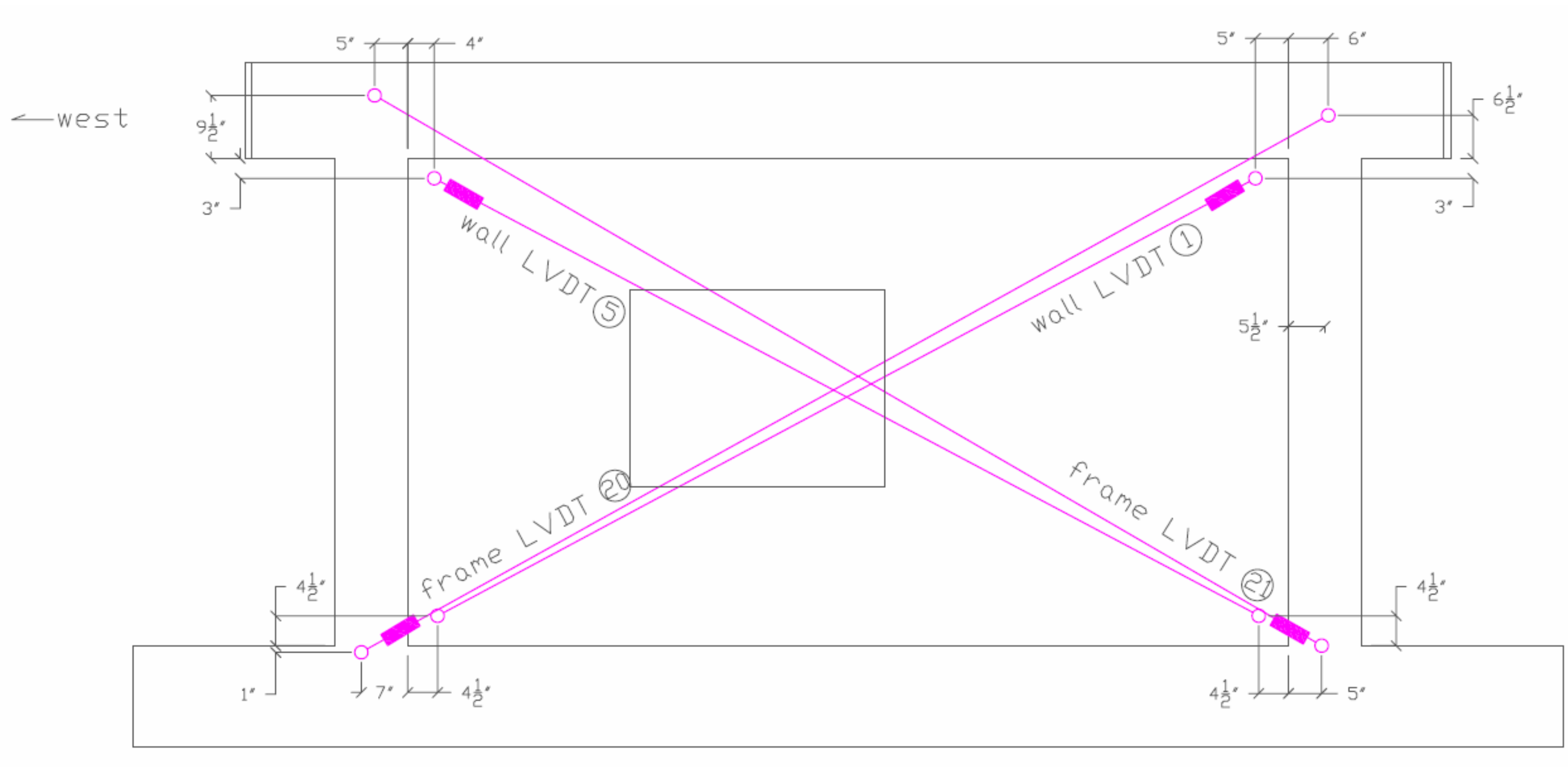

Figure 6.4: Test 2 LVDT Placement - Back

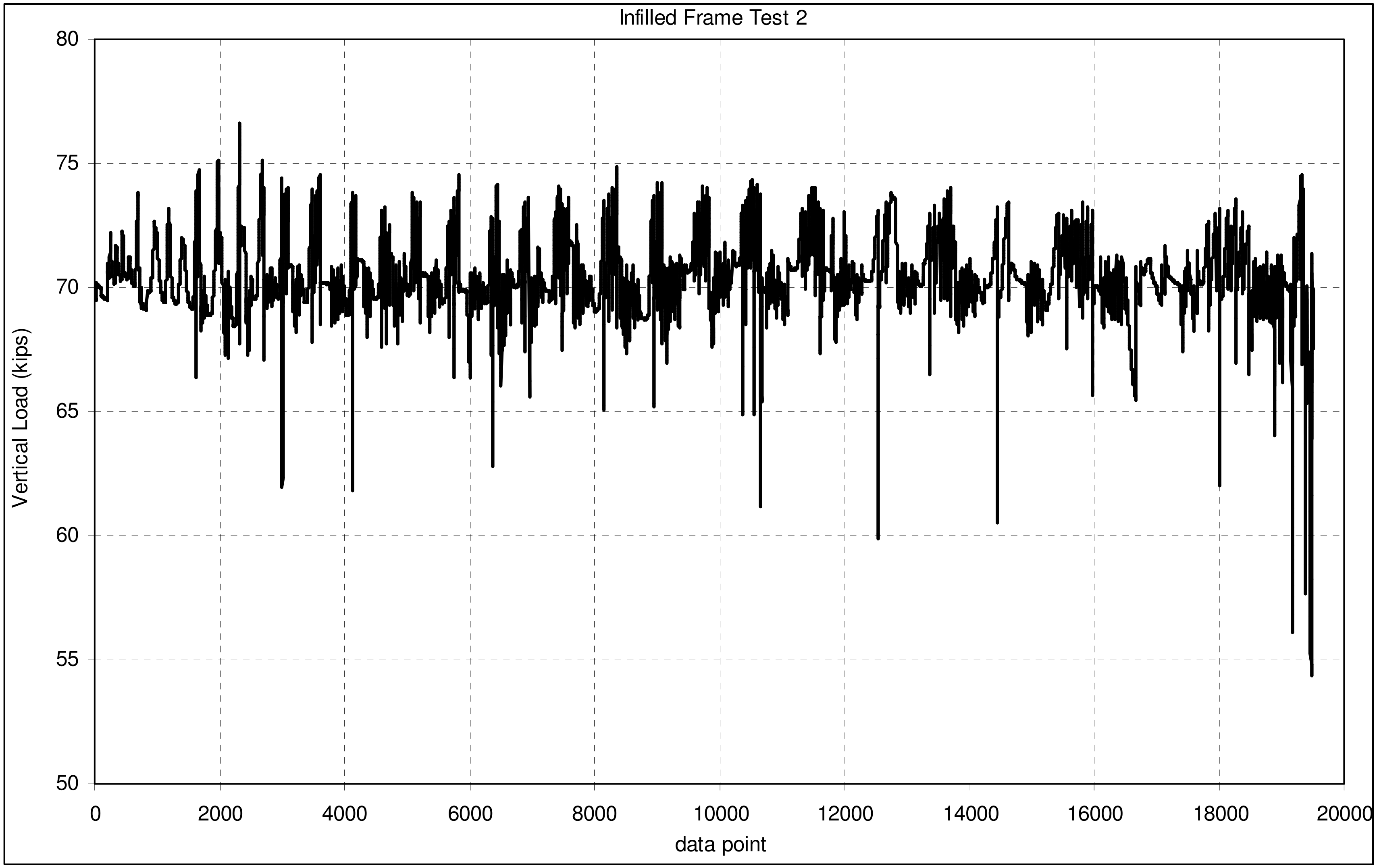

Figure 6.5: Vertical Load

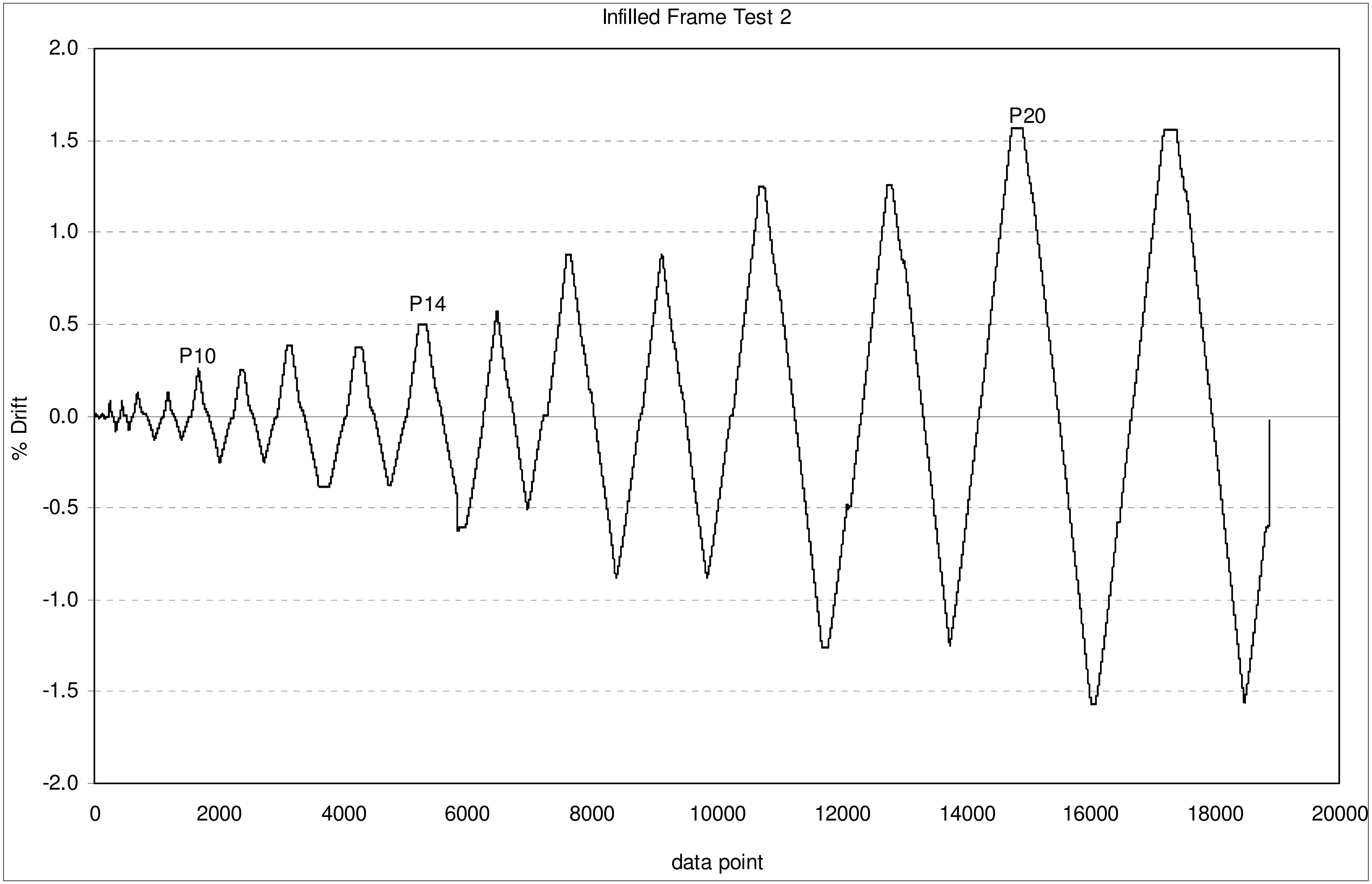

Figure 6.6: Test 2 Applied Displacement Cycles

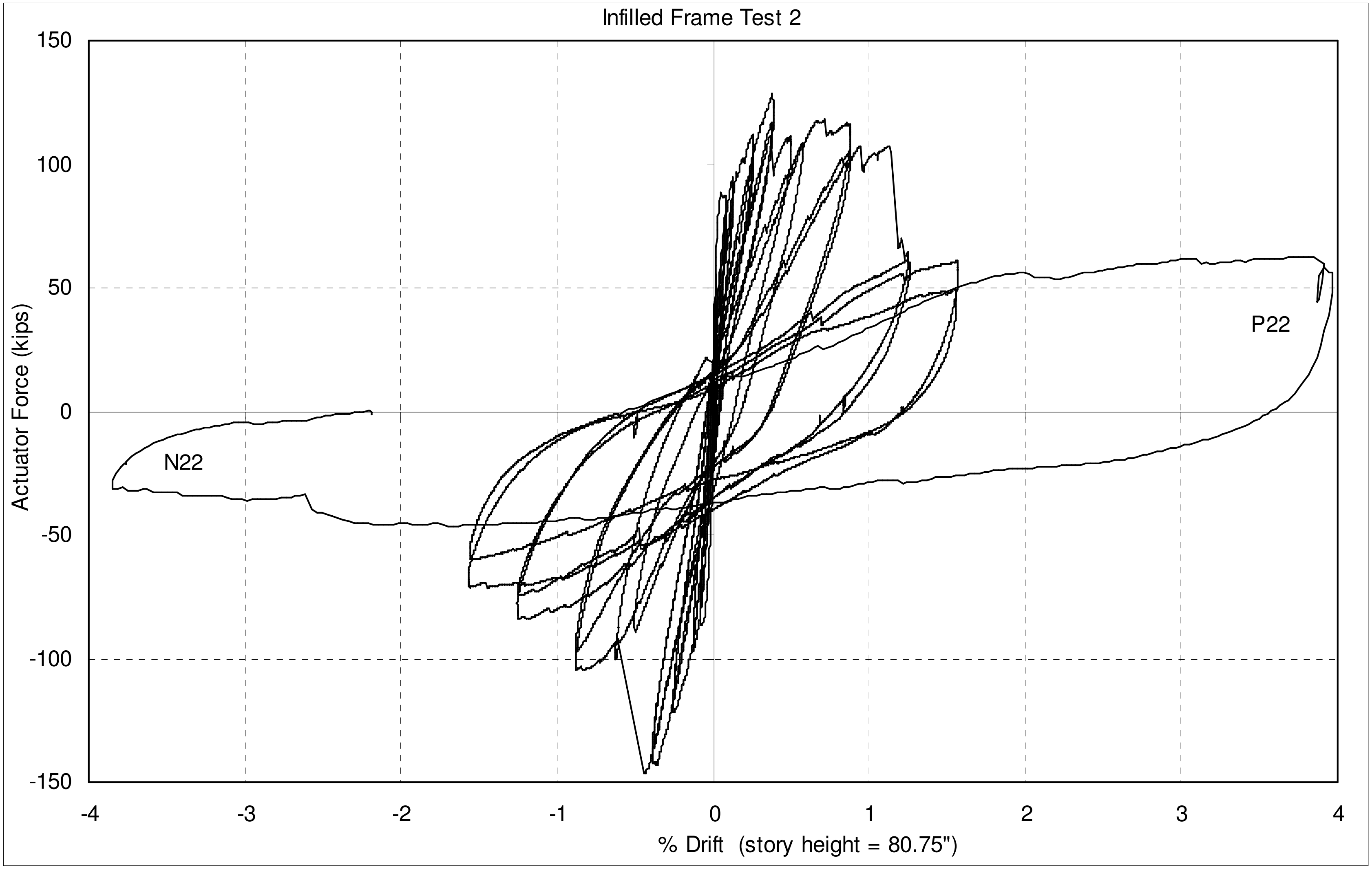

Figure 6.7: Test 2 Force-Displacement Response

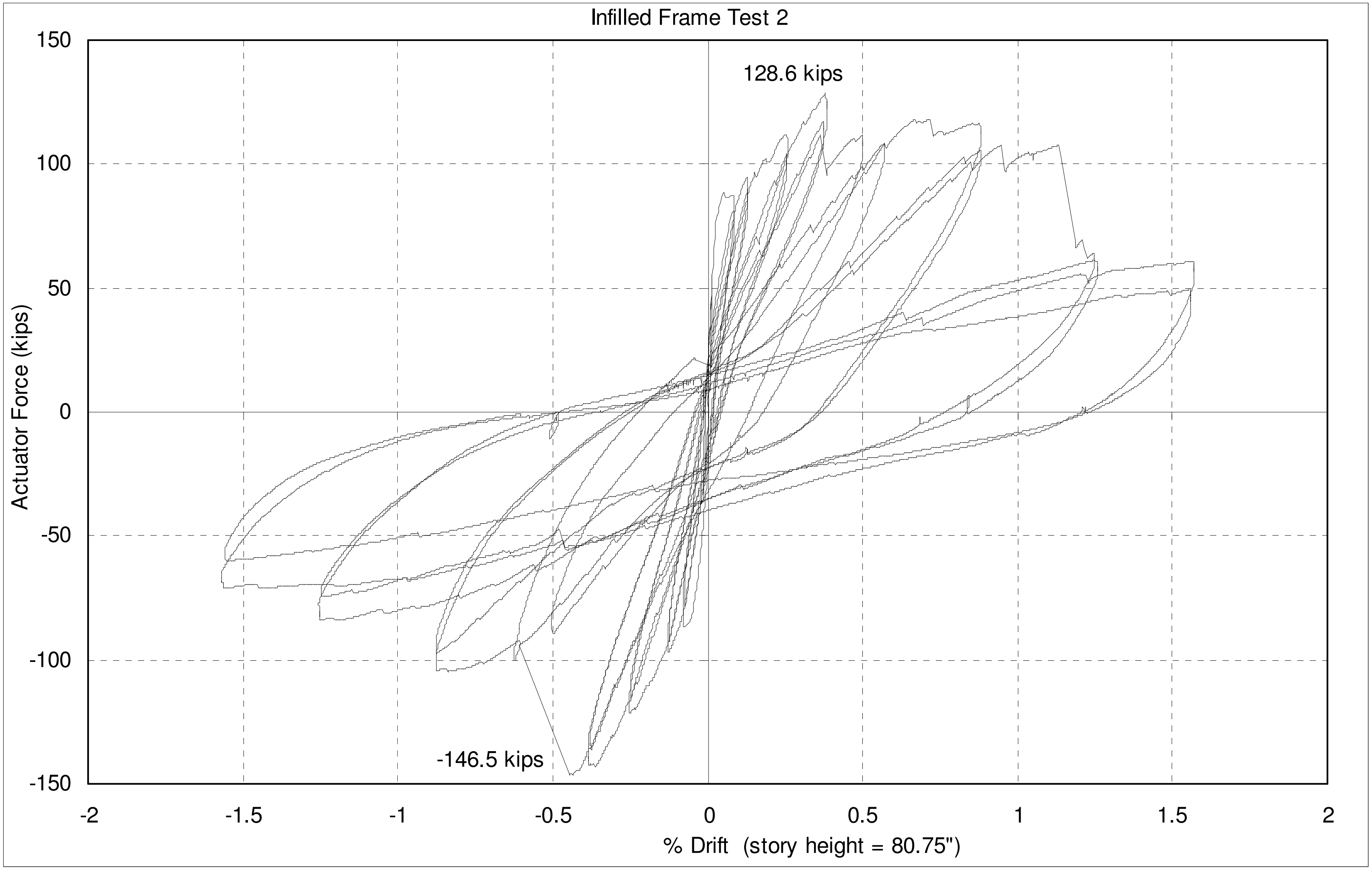

Figure 6.8: Test 2 Force-Displacement Response

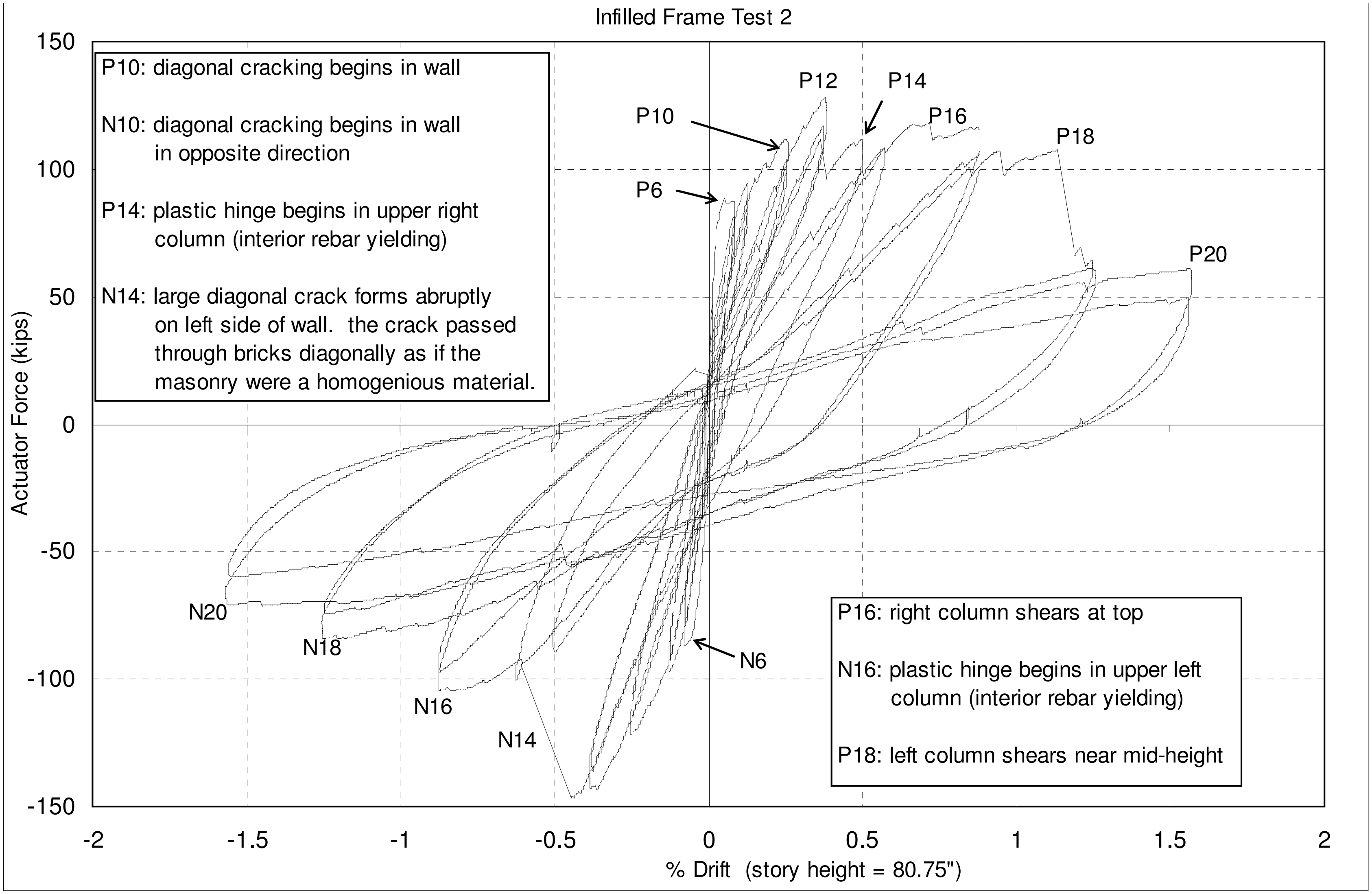

Figure 6.9: Test 2 Force-Displacement Response

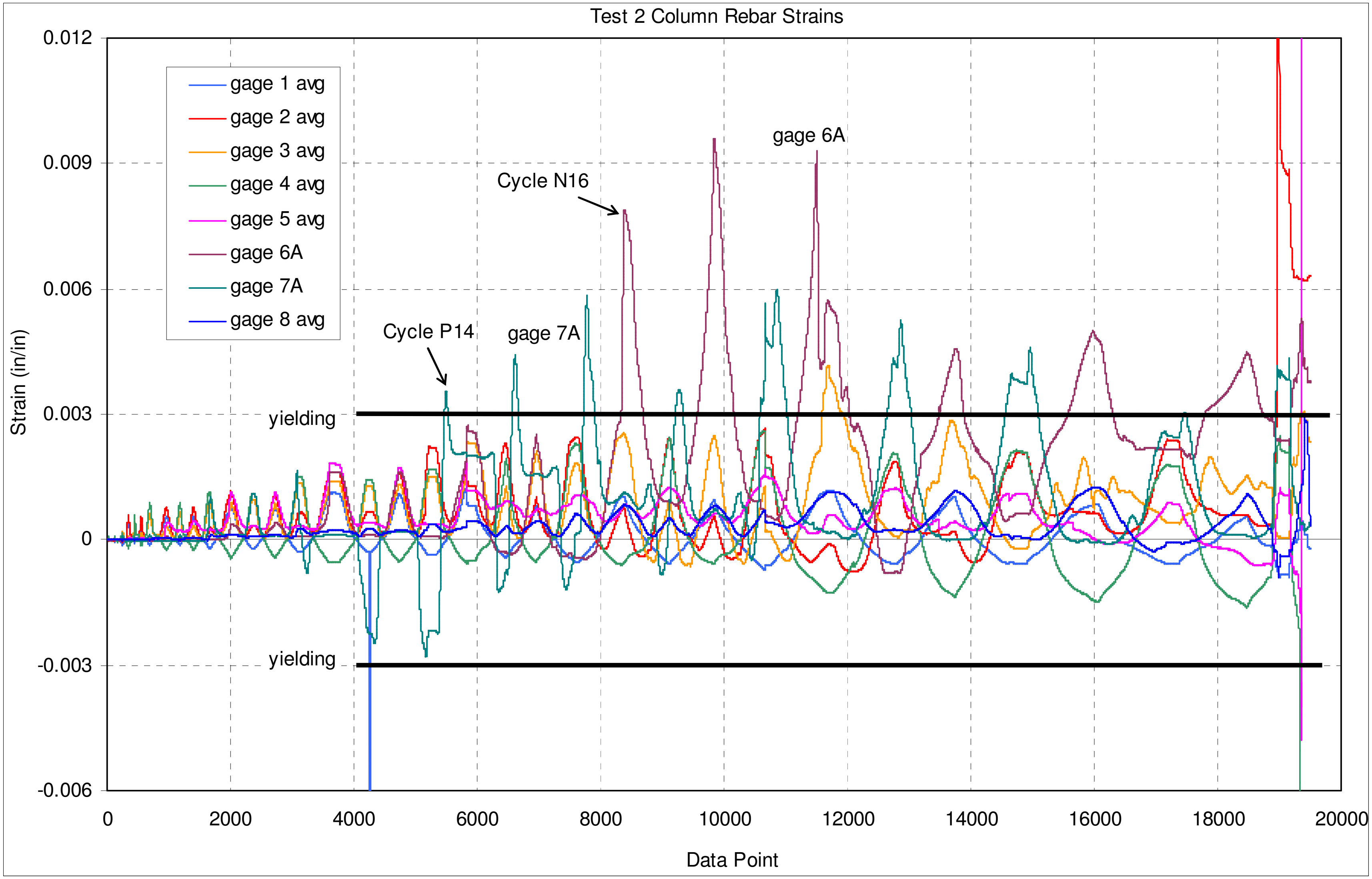

Figure 6.10: Column Rebar Strains

Figure 6.11: Large Diagonal Crack At Cycle N14

Figure 6.12: Test 2 Final Crack Pattern

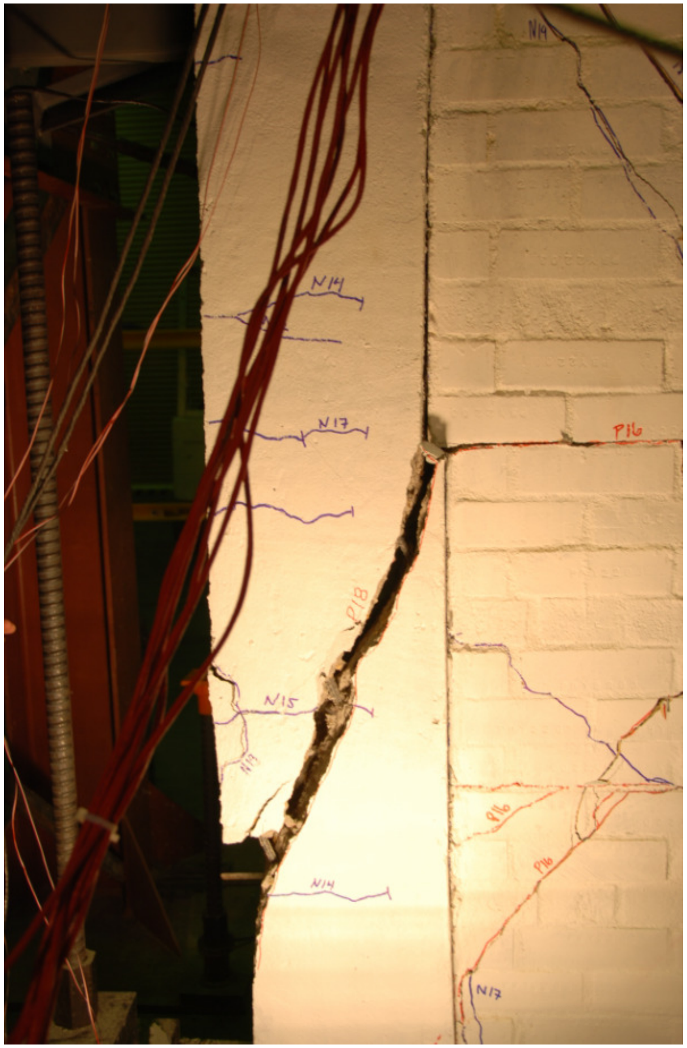

Middle Left Column

Upper Right Column

Figure 6.13: Test 2 Column Shear

Chapter 7: Infilled Frame Test 3

Test 3 was comprised of the same wall and window opening of the test 2 specimen. The same reinforcing details apply to this test (figures 4.2 and 4.3). The current specimen incorporated a layer of ECC (engineered cementitious composite) retrofit on each side of the window opening, see figure 7.1. The details of the layer of ECC are shown in figure 4.18. Table 7.1 shows the material properties for test specimen 3.

Figures 7.2 and 7.3 show the specimen with #3 dowels, WWF, and Weld-Crete installed, with no ECC applied. The blue Weld-Crete was used to enhance the bond between the ECC and the masonry. The bond showed to be questionable, thus no Weld-Crete was used for the next retrofitted wall. The #3 dowels were intended to provide a shear connection between the retrofit layer and the frame. At the bottom beam the dowels were wrapped in duct tape and coated with grease in order to reduce or eliminate any axial bond between the dowels and the ECC. No dowels were installed in the columns. Figure 7.4 shows the test specimen after the ECC was applied. Table 7.2 gives the mix proportions for the ECC. LVDT placement on the specimen is shown in figures 7.5 and 7.6.

Figure 7.7 shows the applied vertical load. After a few load cycles were applied, the test procedure shifted to displacement control starting with cycle P4. The applied displacement cycles are shown in figure 7.8.

The force vs displacement plots are shown in figures 7.9 and 7.10. As with the previous tests, the significant brittle behavior coincides with column shear. One new phenomenon not seen in the previous tests was a delamination of the two wythes of bricks. This occurred on the west (right) side of the window opening, as can be seen in figures 7.13 and 7.14.

Table 7.1: Test 3 Material Properties

Concrete Compressive Strength	2,500 psi
Mortar Compressive Strength	1,400 psi
Masonry Prism Compressive Strength	2,900 psi
Reinforcing Tensile Yield Strength	68,000 psi
Column Tie Tensile Yield Strength	55,000 psi
ECC Compression Strength	6,000 psi
WWF Tensile Yield Strength (6x6 W1.4xW1.4)	120,000 psi

Table 7.2: ECC mix design (100 lb of ECC)

Portland Cement	36.6 lb
Silica Sand	30.8 lb
Fly Ash	11.6 lb
Fibers (Polyvinyl Alcohol)	1.2 lb
Viscous Agent (Methylcellulose)	10.8 grams
Superplasticiser (Adva Cast 530)	32.7 mL
Calcium Aluminate Cement (Secar 51)	1.9 lb
Water	17.7 lb

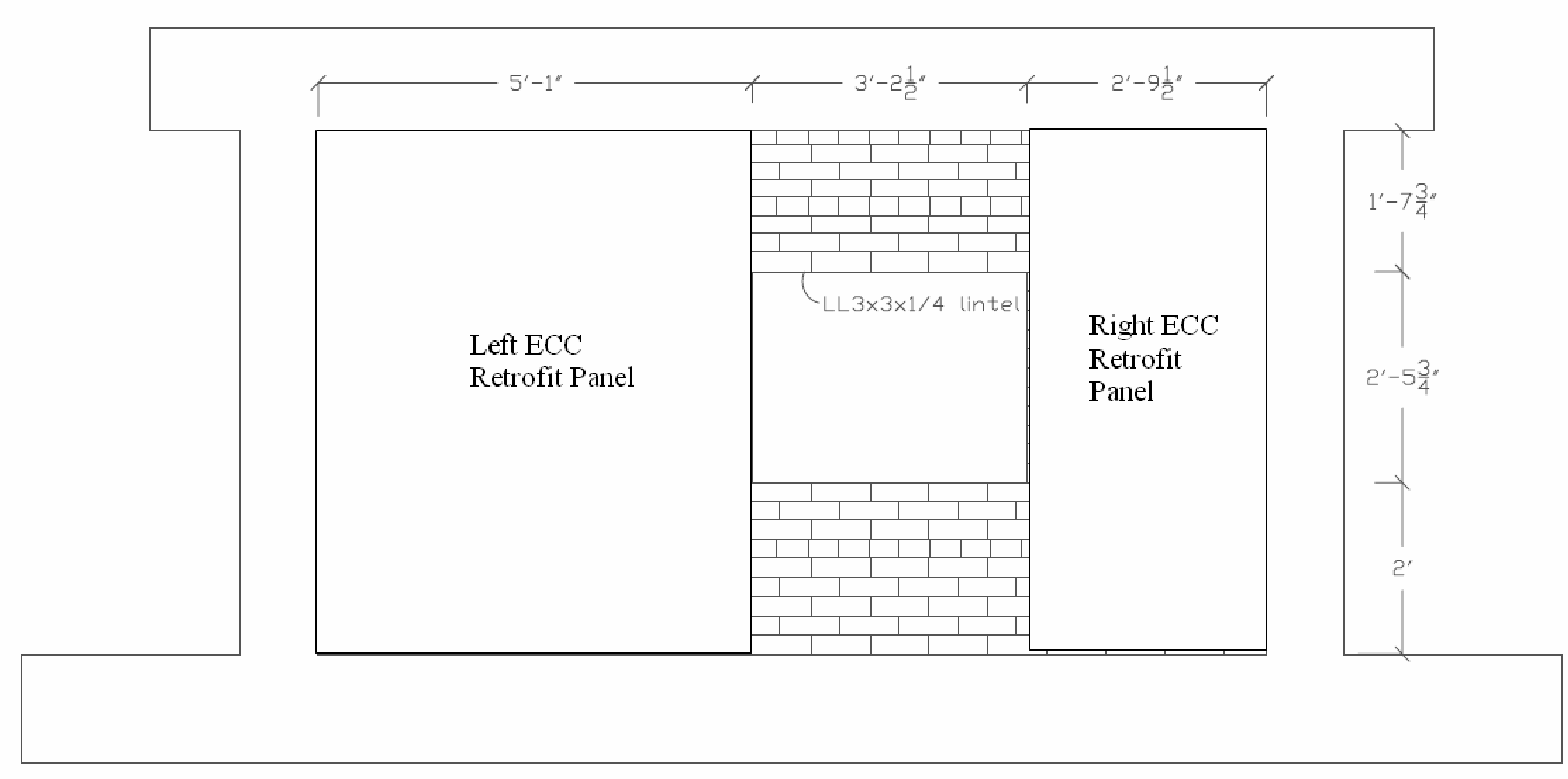

Figure 7.1: Test 3 Specimen Dimensions

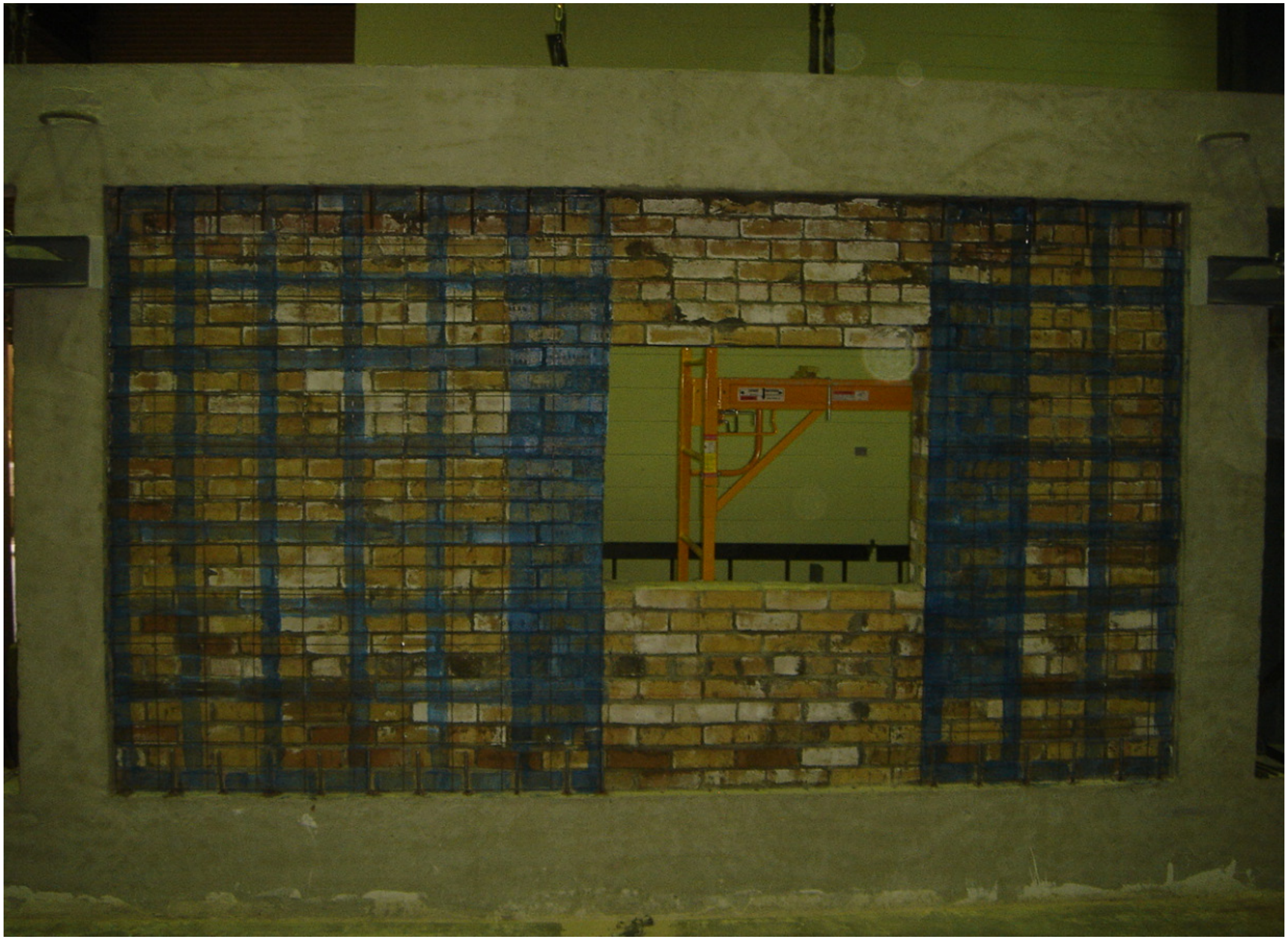

Figure 7.2: Test 3 Specimen With Bonding Agent and WWF

Figure 7.3: Test 3 Specimen Retrofit Details


Figure 7.4: Test 3 Specimen With Retrofit

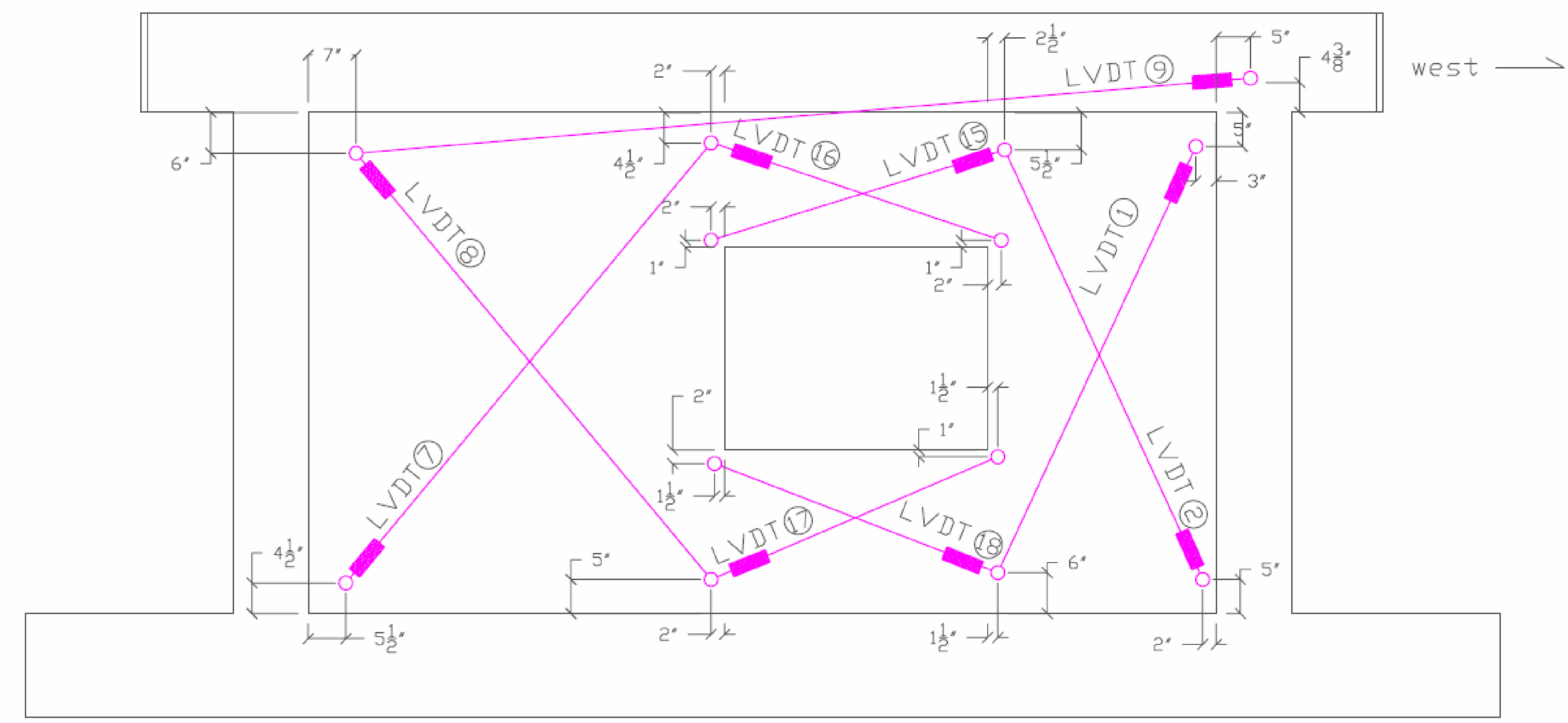

Figure 7.5: Test 3 LVDT Placement - Front

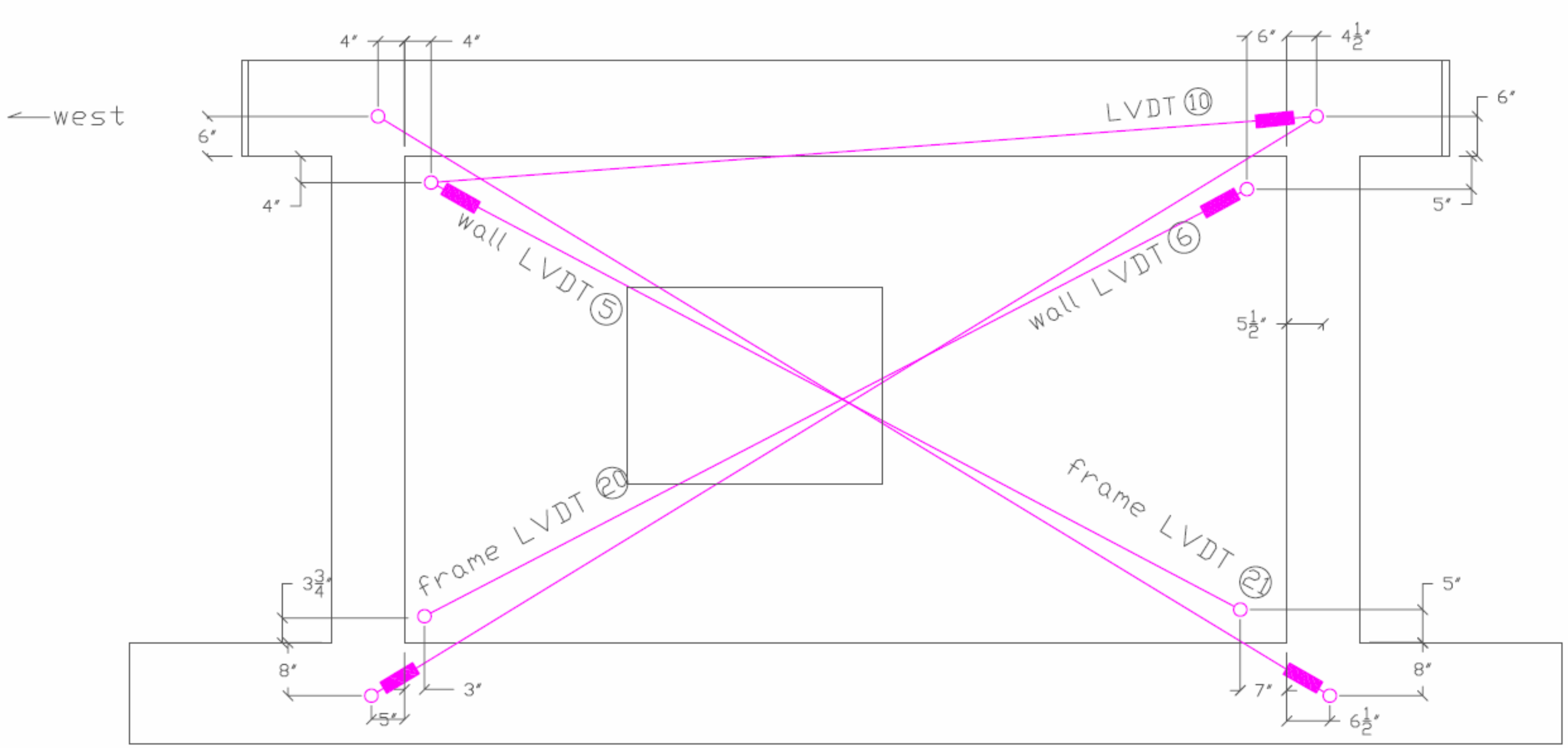

Figure 7.6: Test 3 LVDT Placement - Back

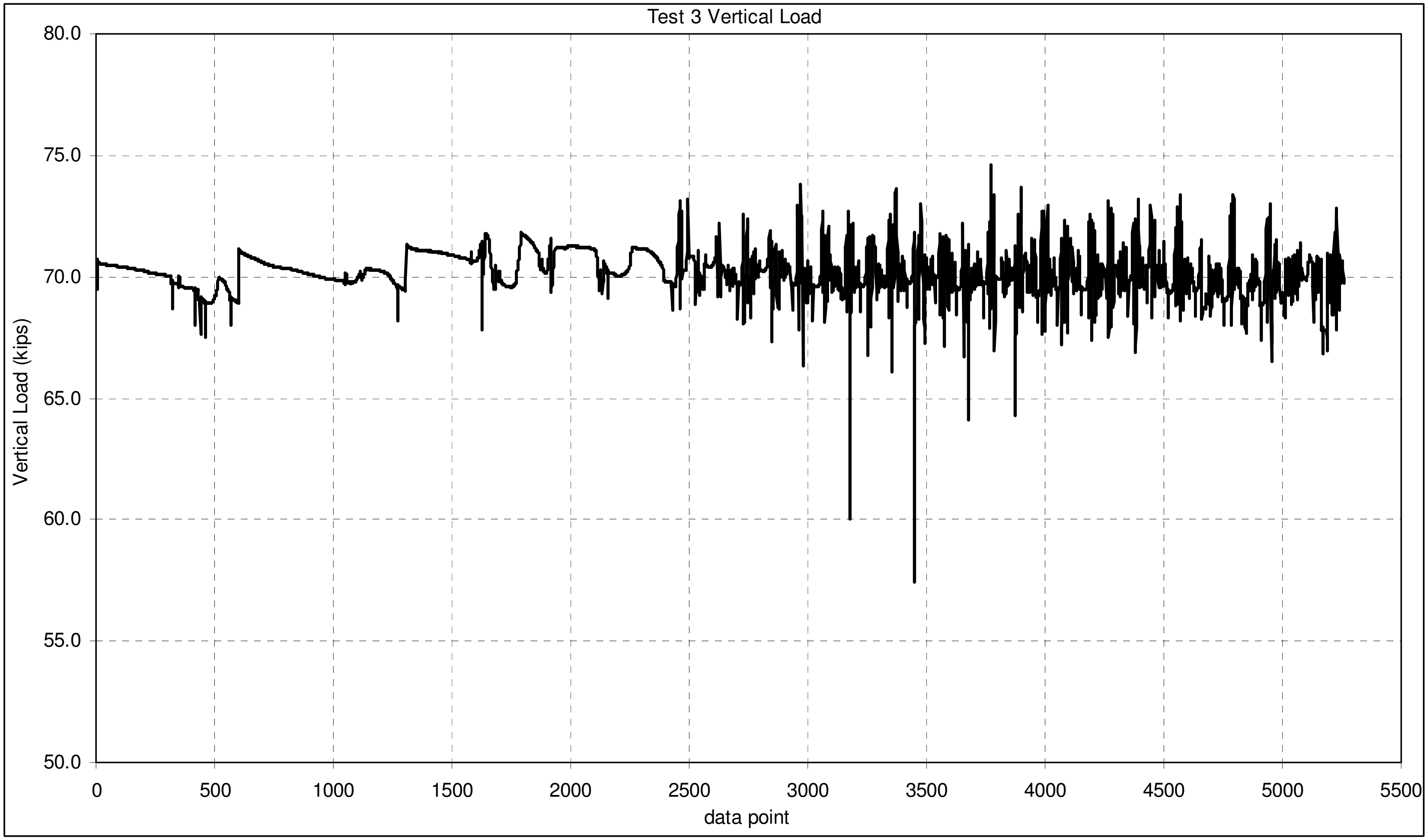

Figure 7.7: Test 3 Vertical Load

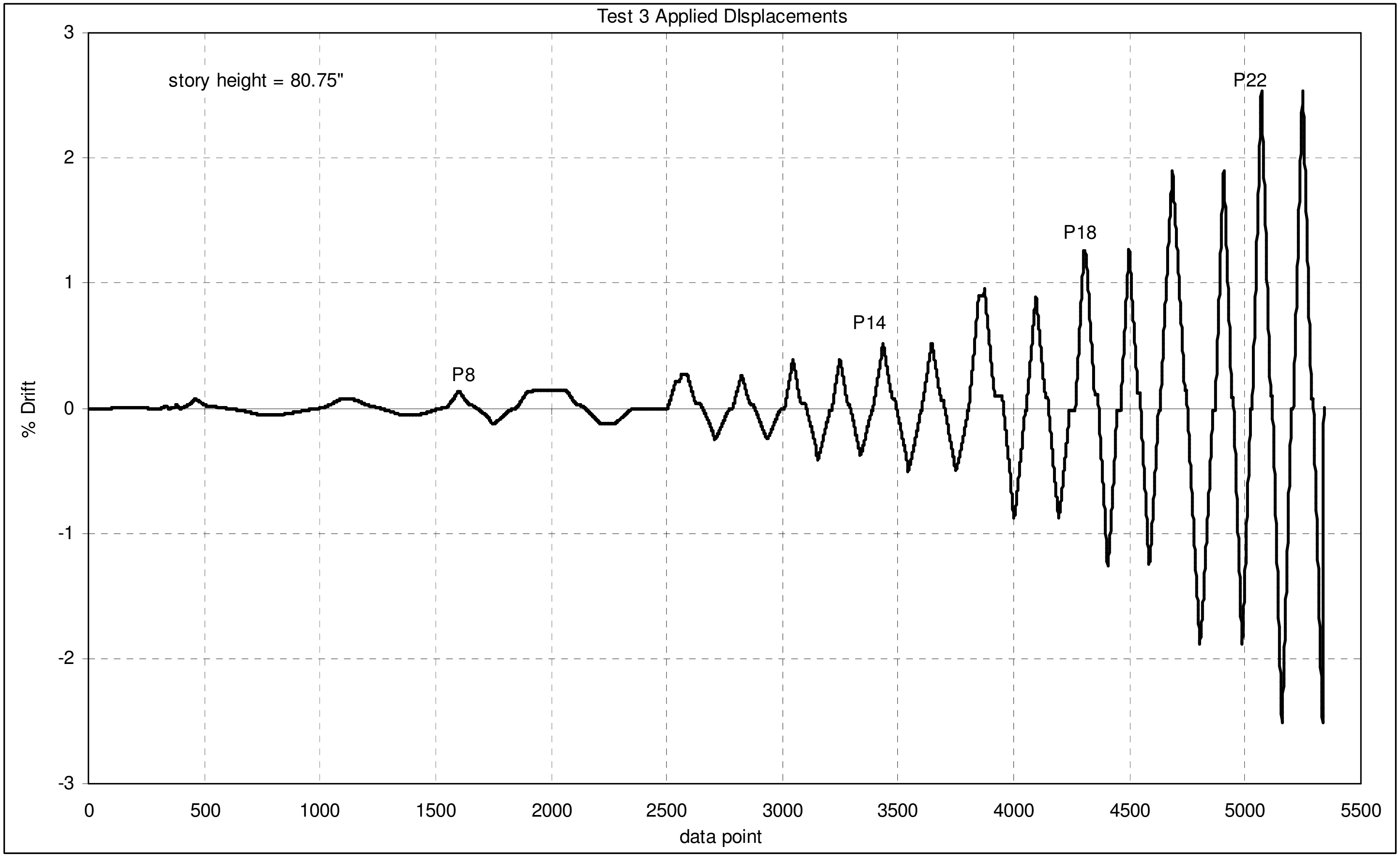

Figure 7.8: Test 3 Applied Displacement Cycles

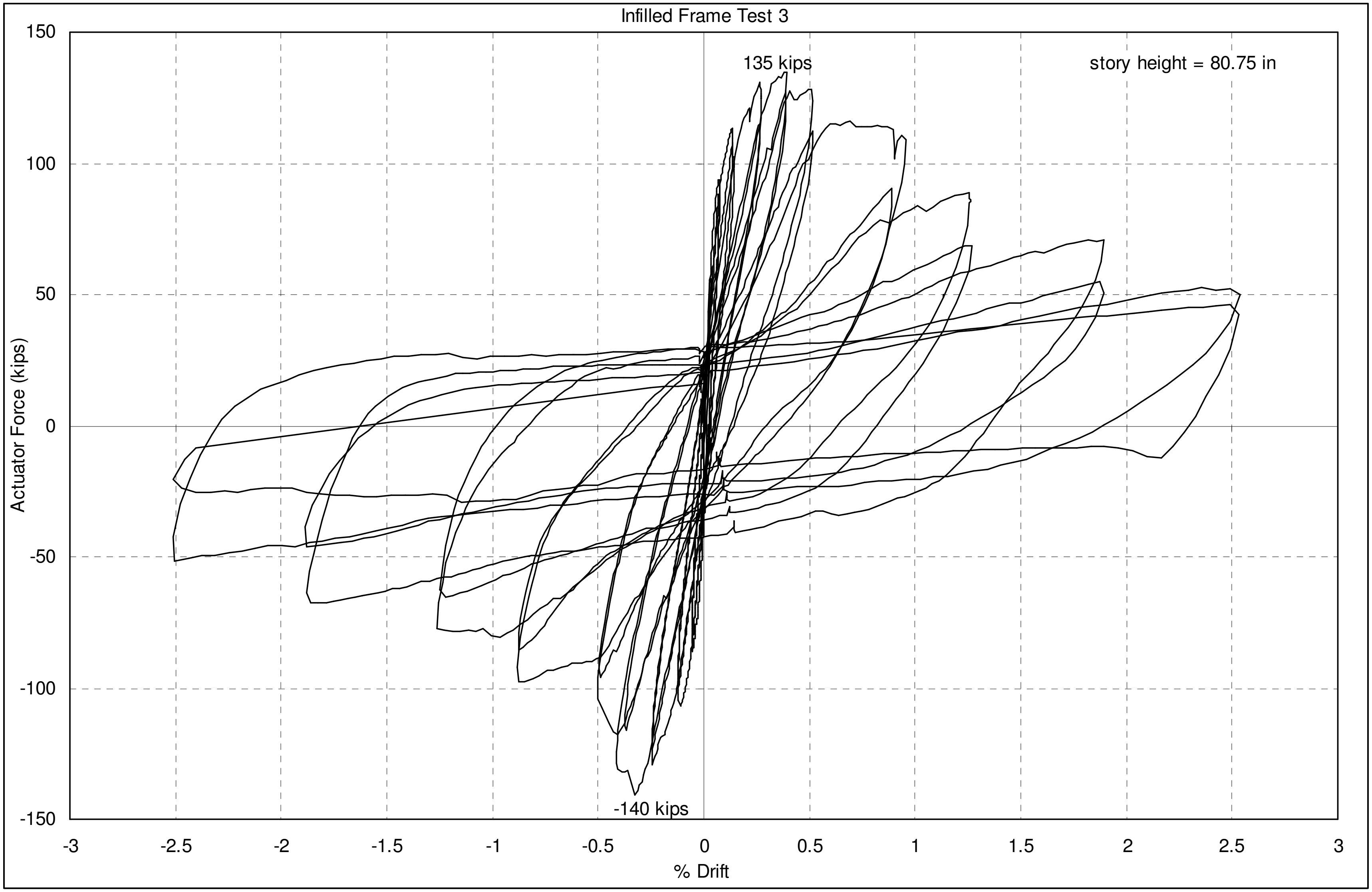

Figure 7.9: Test 3 Force-Displacement Response

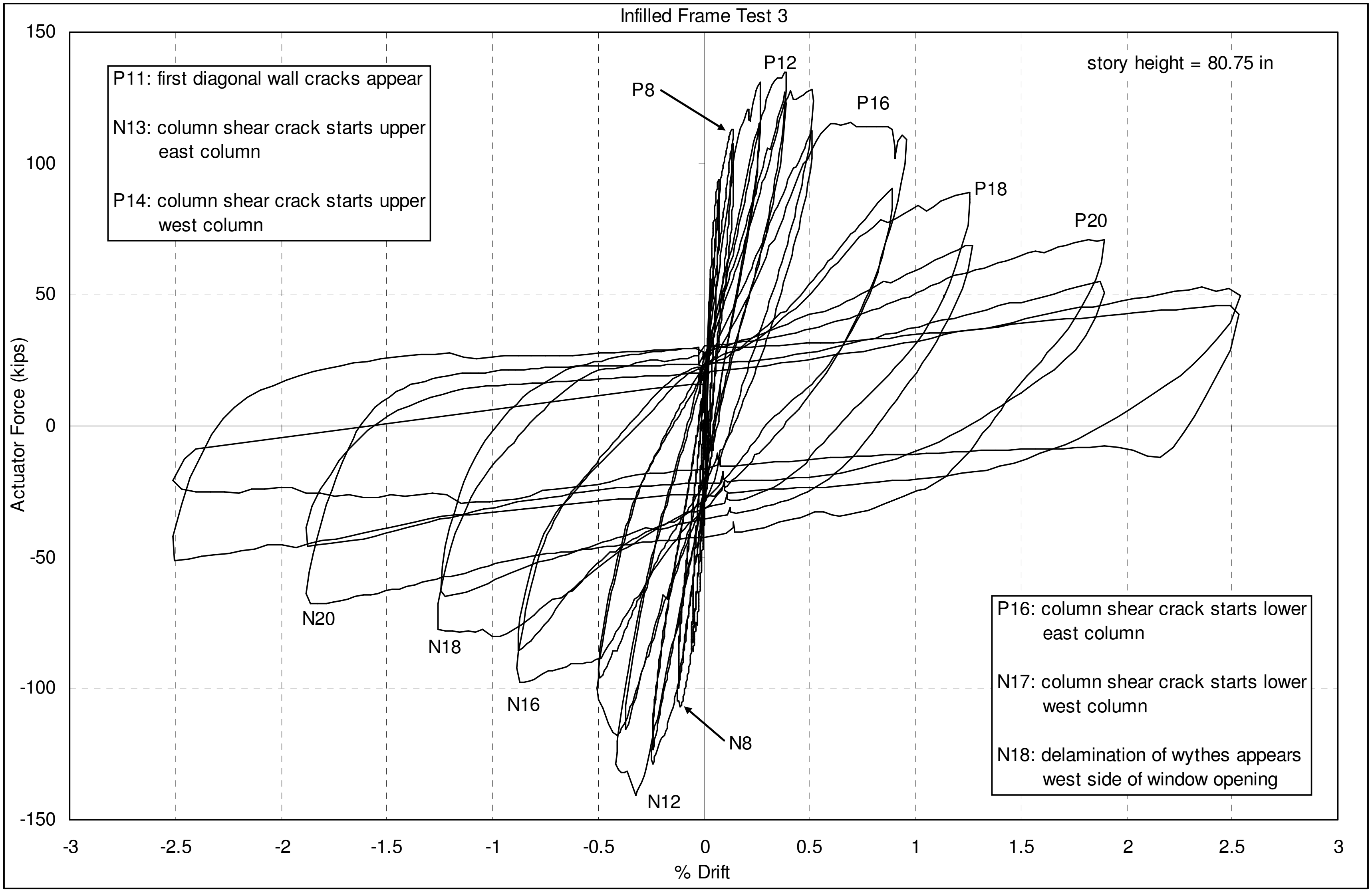

Figure 7.10: Test 3 Force-Displacement Response

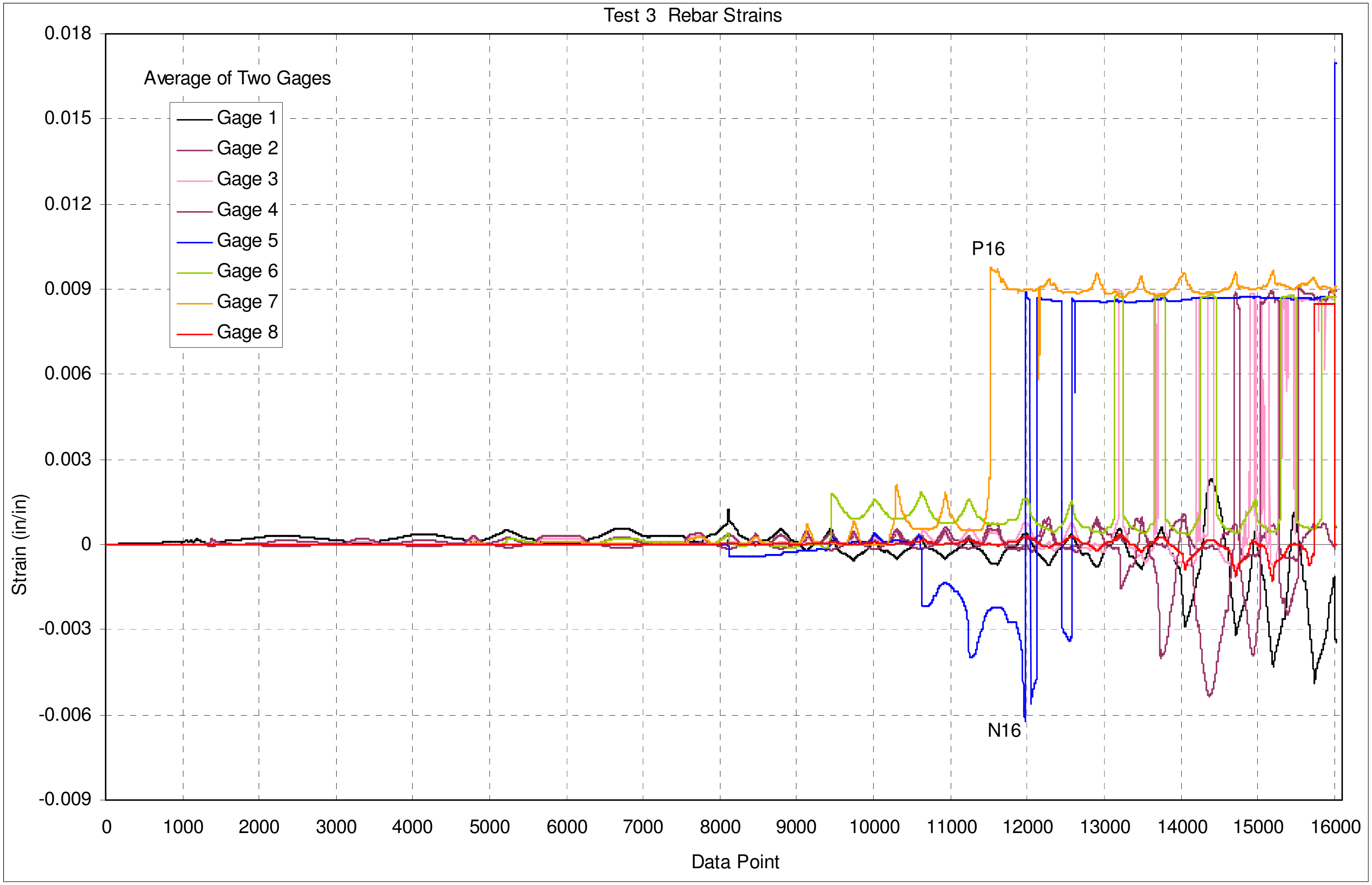

Figure 7.11: Test 3 Rebar Strain Gages

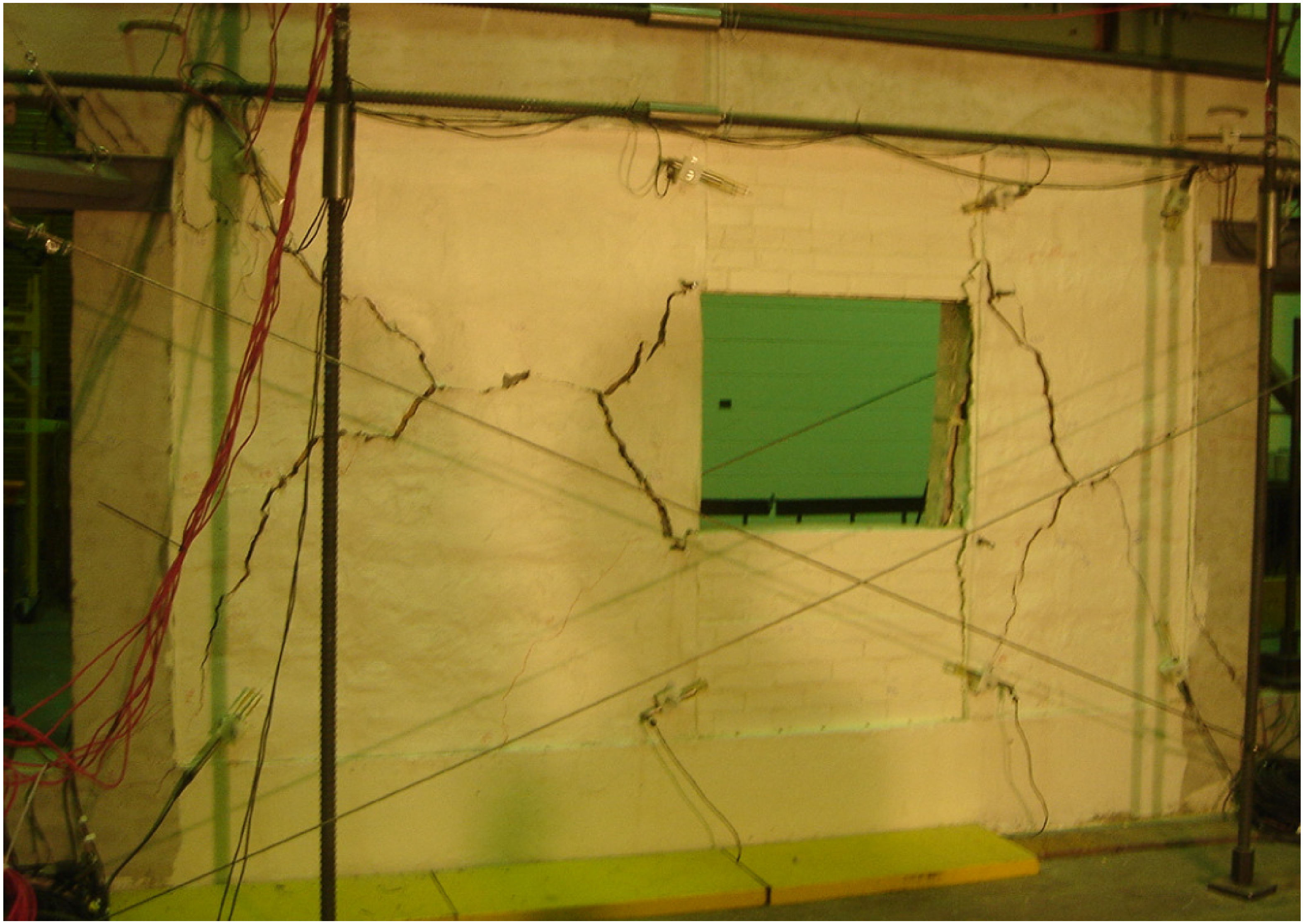

Figure 7.12: Test 3 Crack Pattern

Figure 7.13: Test 3 Wall Delamination

Figure 7.14: Test 3 Wall Delamination

Chapter 8: Infilled Frame Test 4

The fourth test specimen was a solid wall with 1″ of ECC retrofit. The same frame and wall dimensions as test 1 were used, see figures 4.1 – 4.3. Material properties relevant to this test are shown in table 8.1. Figure 8.1 shows the test specimen with the retrofit dowels embedded in the top and bottom beams, along with the WWF ready to be installed. A detail photograph of the WWF anchorage to the wall can be seen in figure 8.2. The 3″ × ½″ diameter sleeve anchors were inserted into the bricks to a depth of 2″, leaving 1″ extending out of the wall. The WWF was attached to the anchors a distance of ½″ from the surface, placing it at the center of the 1″ thick ECC retrofit. The spacing for the anchors was 12" each way. As with the test 3 specimen, the #3 dowels at the bottom of the wall were wrapped with duct tape and coated with grease to prevent axial bonding. Unlike test 3, no Weld-Crete was used for this specimen. Table 7.2 displays the ECC mix design for both specimen 3 and specimen 4 retrofits. Figure 8.3 shows the wall with the ECC retrofit applied. Figure 8.4 shows the front view of the specimen with instrumentation and load apparatus installed. Figures 8.5 and 8.6 give the locations of the LVDT placement.

The vertical load for test 4 is shown in figure 8.7. The large drop at the end of the test was caused by the inability of the structure to support the vertical load during the last two cycles. The applied displacement cycles are shown in figure 8.8.

Figure 8.9 shows the full set of force vs displacement cycles. The response of this test specimen is clearly more symmetrical than that of the first test. As with previous tests, the final cycle was more to facilitate demolition than to collect meaningful data. Figure 8.10 shows the response along with key events. Two significant occurrences are the drop in strength at cycles P15 and N16. These coincide with the column shear at the lower ends of both columns.

Soon after the column shear, the ECC layer began to peel away from the RC frame, pulling the brick wall with it. The masonry remained attached to the ECC layer. The bottom of the retrofit pulled away from the dowels embedded in the lower beam. The bottom three courses of masonry remained attached to the RC frame, but the rest of the wall moved forward, remaining well anchored to the retrofit layer. Figures 8.13 – 8.16 show this separation. The fact that less than a full brick width was left in contact in the wall appears to be the reason for the lower residual strength, comparing figure 8.9 with figure 5.6 for specimen 1. In test 1 the wall bed joints slide along the length of the specimen, but were not removed from the shearing as with the current specimen. Thus a much lower residual for this test than test 1.

For this test the ECC showed only a few insignificant cracks near the center of the wall. The retrofit panel was fully in tact at the end of the test, and most of the wall was attached to it. The wall itself did experience the classic H pattern of cracks, as can be seen on the back of the wall shown in figure 8.12.

Table 8.1: Test 4 Material Properties

Concrete Compressive Strength	4,000 psi
Mortar Compressive Strength	970 psi
Masonry Prism Compressive Strength	2,600 psi
Reinforcing Tensile Yield Strength	68,000 psi
Column Tie Yield Strength	55,000 psi
ECC Compression Strength	7,300 psi
WWF Tensile Yield Strength (4x4 W4.0xW4.0)	88,000 psi

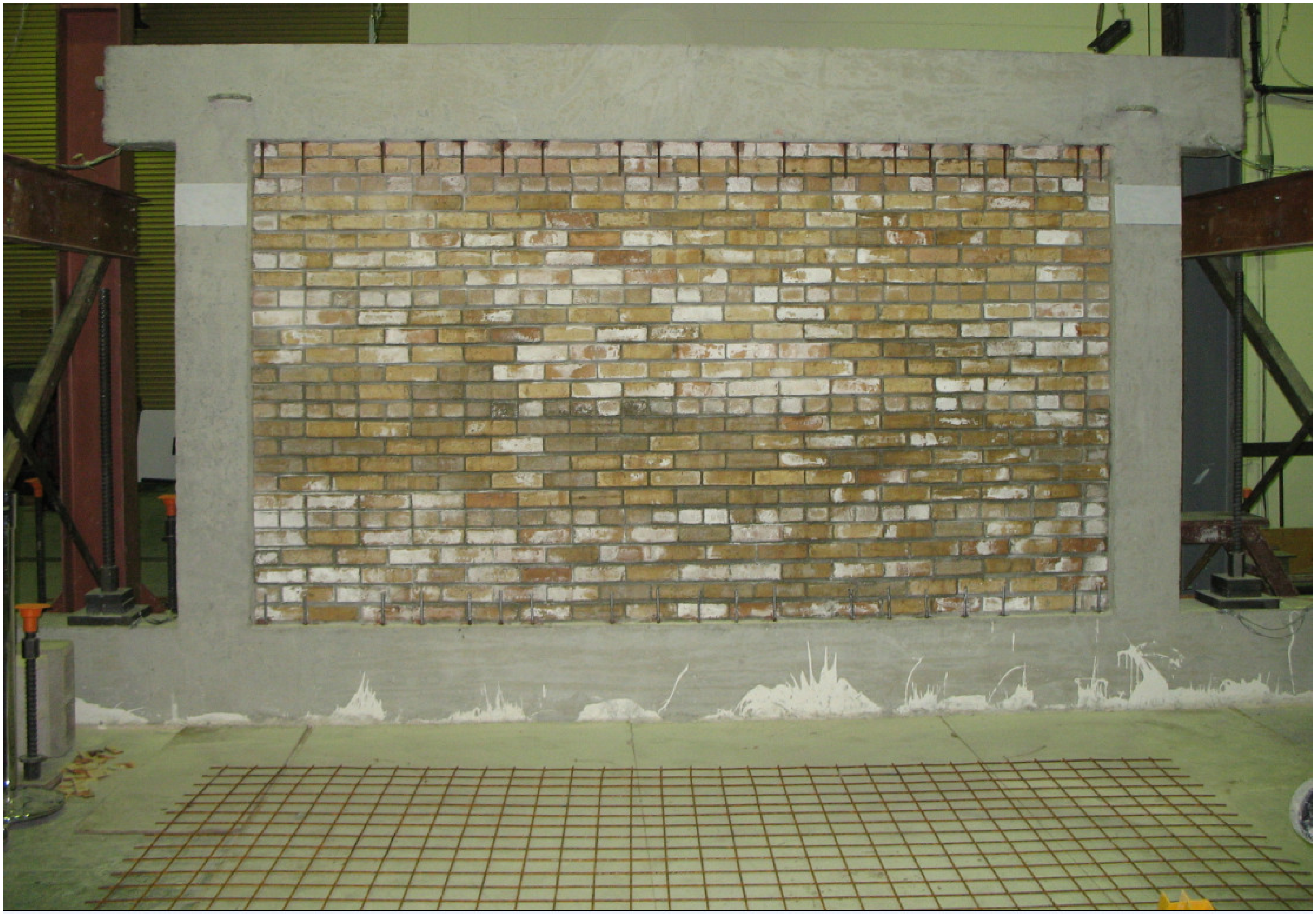

Figure 8.1: Test 4 Specimen Before ECC Retrofit Was Applied

Figure 8.2: Retrofit Anchoring Detail


Figure 8.3: Test 4 Specimen After ECC Retrofit Was Applied

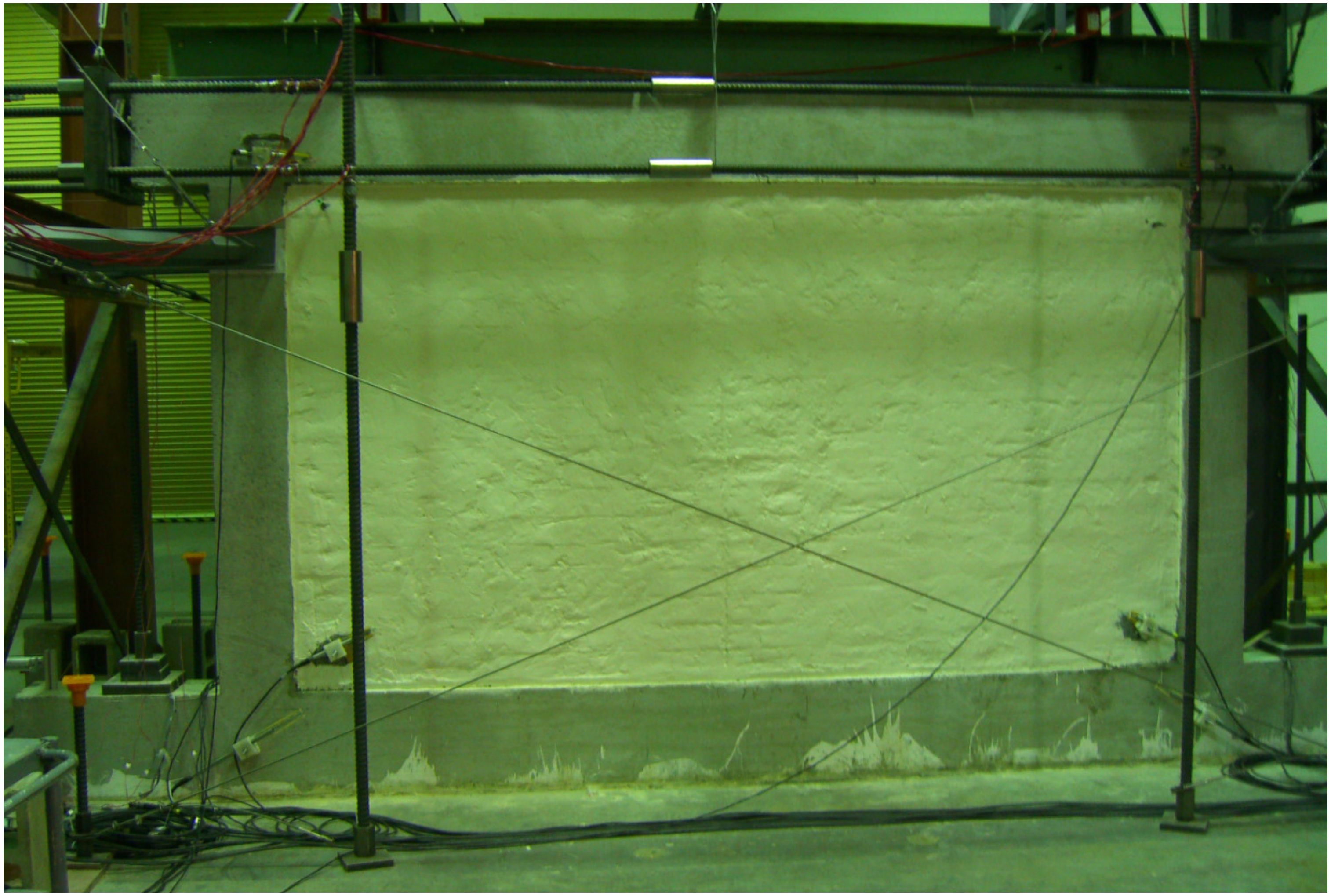

Figure 8.4: Test 4 Specimen With Instrumentation Installed

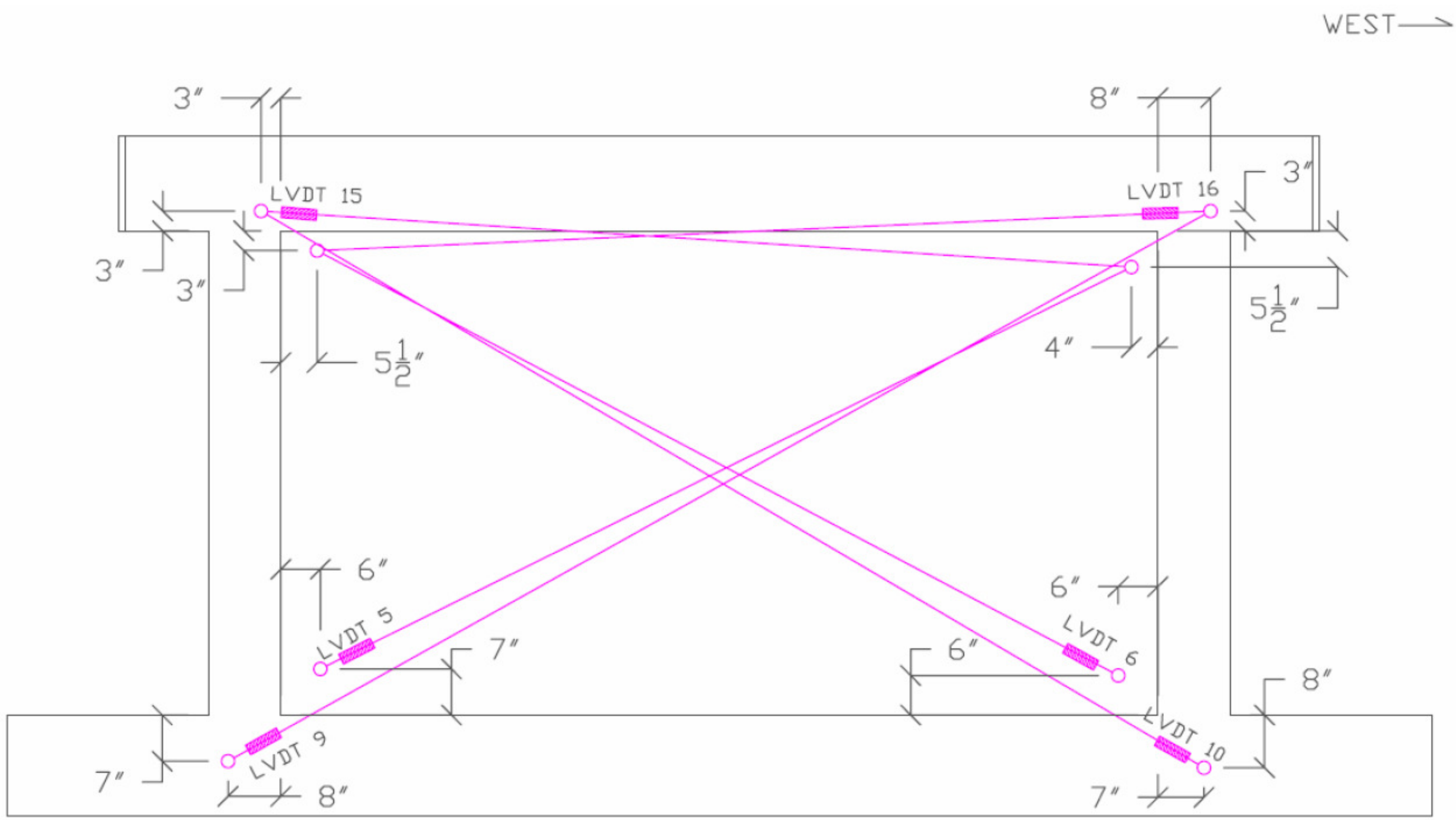

Figure 8.5: Test 4 LVDT Placement - Front

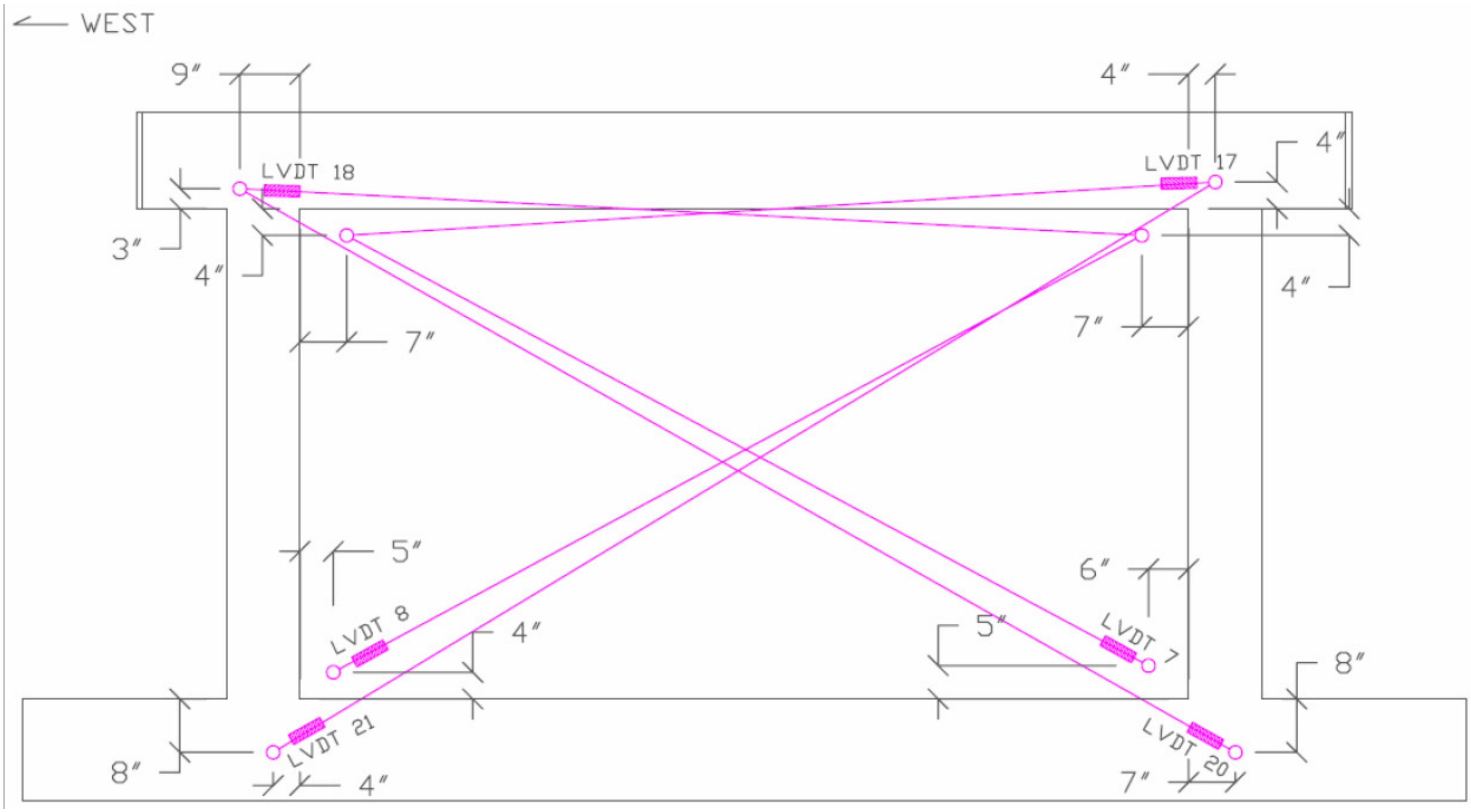

Figure 8.6: Test 4 LVDT Placement - Back

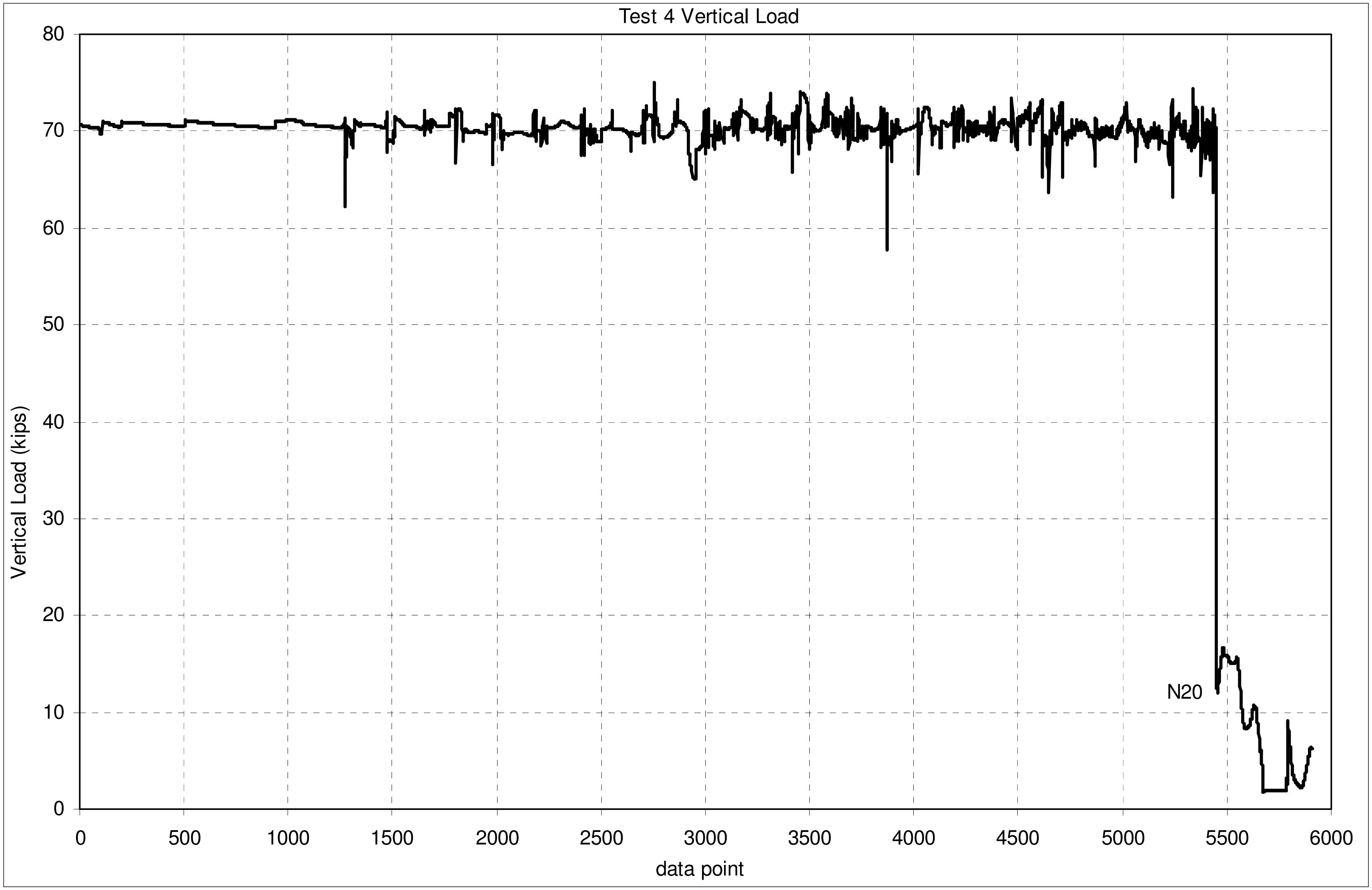

Figure 8.7: Test 4 Vertical Load

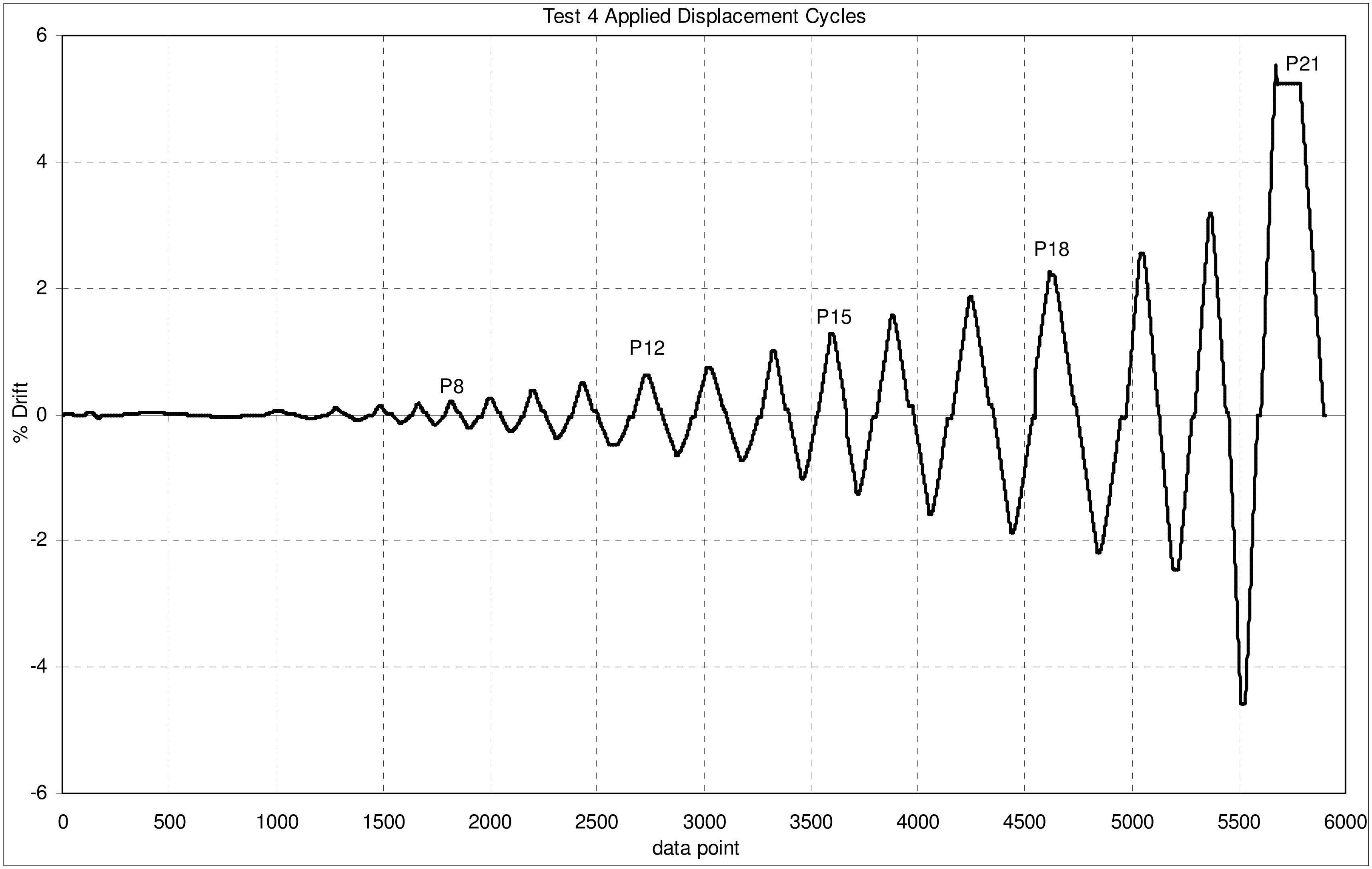

Figure 8.8: Test 4 Applied Displacement Cycles

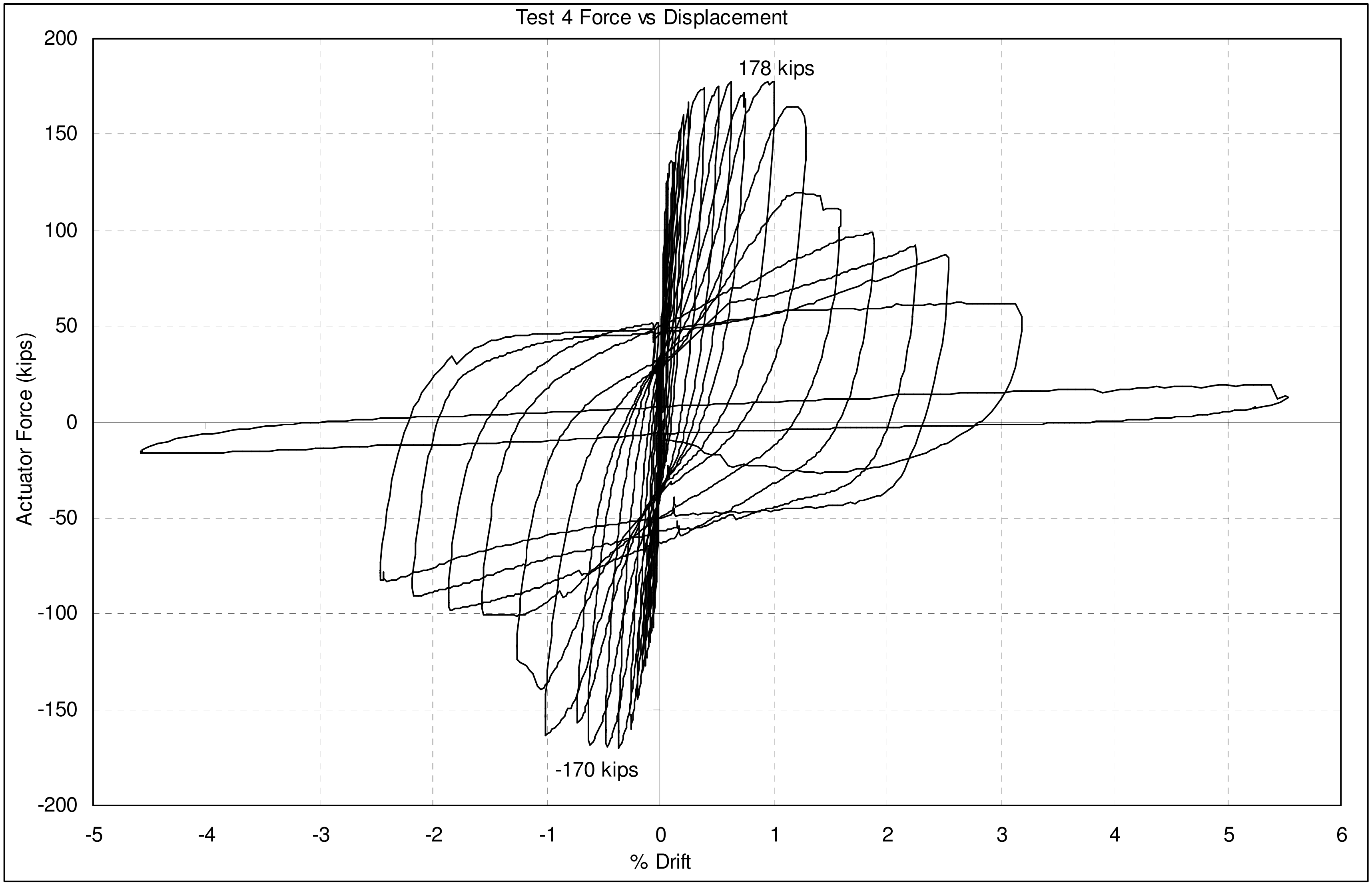

Figure 8.9: Test 4 Force vs Displacement

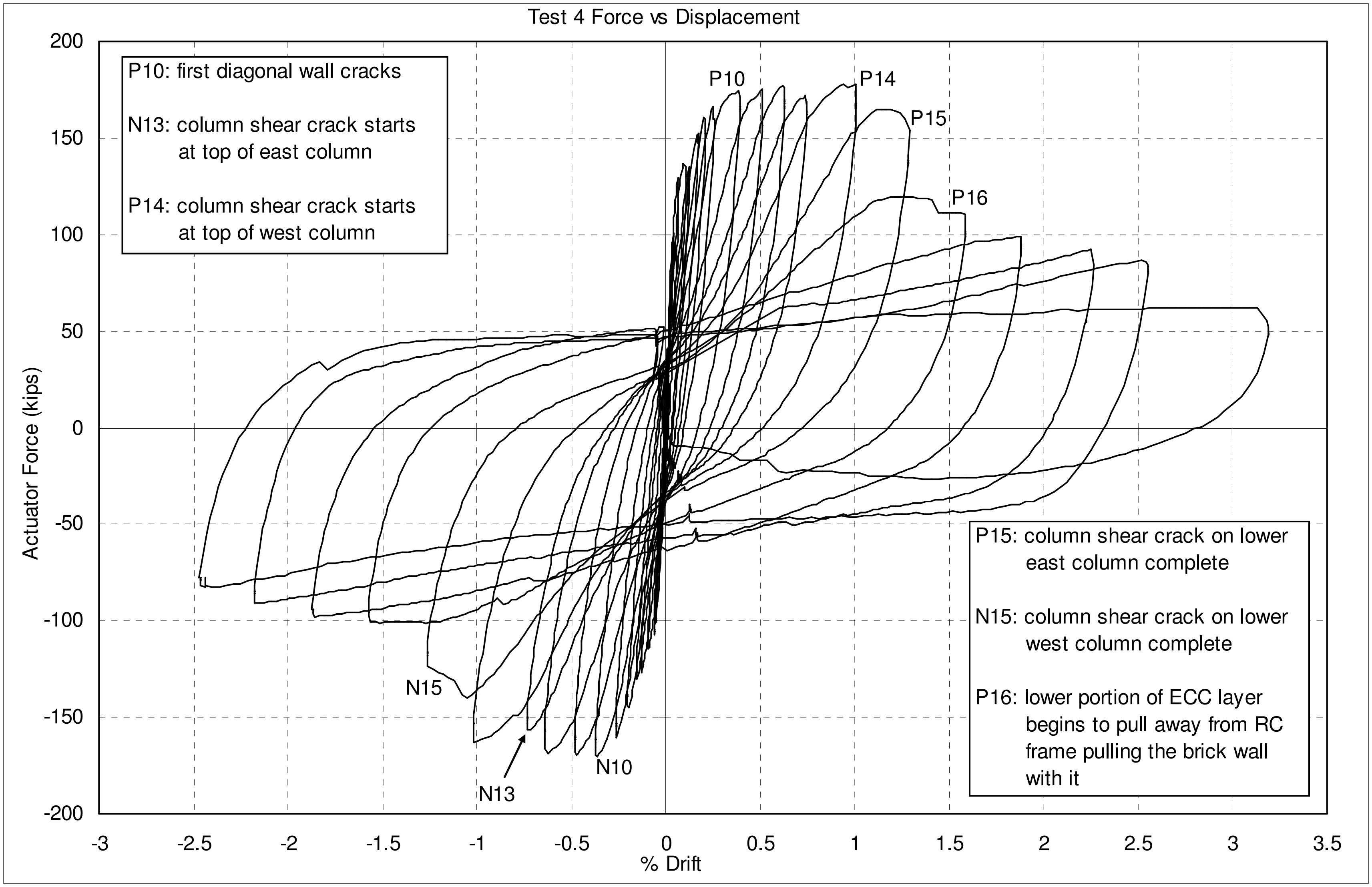

Figure 8.10: Test 4 Force vs Displacement

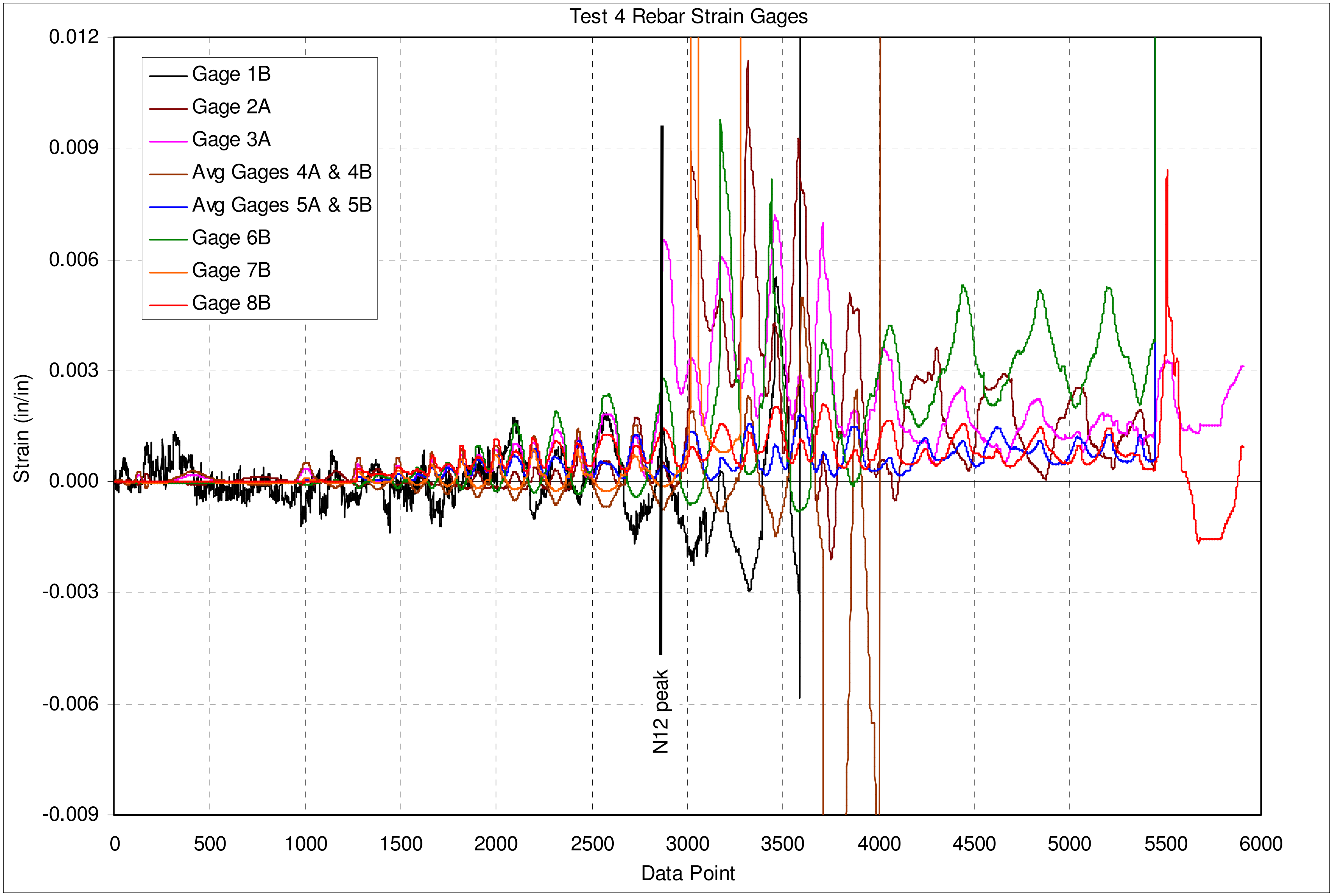

Figure 8.11: Test 4 Rebar Strains

Figure 8.12: Diagonal Wall Cracks Propagate in both Directions by Cycle N11 (Back View of Wall)

Figure 8.13: ECC Retrofit Layer Separation – Lower East Corner

Figure 8.14: ECC Retrofit Layer Separation – Lower West Corner

Lower East Corner

Lower West Corner

Figure 8.15: Final ECC Retrofit Layer Separation

Figure 8.16: #3 Dowels Behind Separated ECC Retrofit

Figure 8.17: Post Test View of the Back Side of Wall

Upper East Column

Upper West Column

Figure 8.18: Post Test View of Column Shear

Lower East Column

Lower West Column

Figure 8.20: Post Test View of Column Shear

Chapter 9: Infilled Frame Test 5

The fifth test incorporated a door opening in the masonry wall, with no retrofit. Figure 9.1 shows the dimensions of the specimen, and figure 9.2 is a photograph of it ready for testing. The material properties are listed in table 9.1 with the LVDT placement shown in figures 9.3 and 9.4. As can be seen in table 9.1, the concrete was considerably lower than the specified 3,000 psi strength.

The vertical load is displayed in figure 9.5. It was particularly difficult to keep the load constant. Toward the end of the test the specimen was simply not capable of resisting the prescribed 70 kip load.

Figure 9.6 shows the applied displacement cycles for the test. An unintentional early excursion into a higher displacement occurred at cycle P3. This was caused by a difficulty with the actuator control system that was corrected before the test resumed. The high level of displacement at this early cycle did cause a premature softening of the structure, as can be seen in figure 9.8.

The force vs displacement plots are shown in figures 9.7 and 9.8. A clear distinction between the positive and negative direction in the response is seen, more so than any of the previous tests. This structure could be classified as ductile when pushed to the right, but brittle when pushed to the left.

An interesting phenomenon unique to this test is the shear crack that formed in the top beam. Figure 9.11 shows this crack, which appeared at cycle P14. The crack did not continue to grow, and seems to have not made any significant contribution to the behavior. However, it does reveal the possibility of beam shear in this type of structure, particularly with the lack of shear stirrups in the beam. Probably the most significant occurrence is the abrupt wall crack at cycle P17, which caused the large drop in strength to the residual, see figures 9.8 and 9.9. This was followed two cycles later by the minor drop in strength at cycle N19, which was caused by a vertical crack in wall to the left of the doorway. These two cracks constituted the brittle behavior of this specimen. Both columns did shear at the bottom, but not until the residual strength had already been reached. The tops of the columns started to shear, but did not develop the large separation similar to the lower ends, see figures 9.13 and 9.14. Figure 9.12 shows the post-test crack pattern which is very similar to those in tests 2 and 3, with the oval shaped cracks around the opening.

Table 9.1: Test 5 Material Properties

Concrete Compressive Strength	2,100 psi
Mortar Compressive Strength	640 psi
Masonry Prism Compressive Strength	2,100 psi
Reinforcing Tensile Yield Strength	68,000 psi
Column Tie Yield Strength	55,000 psi

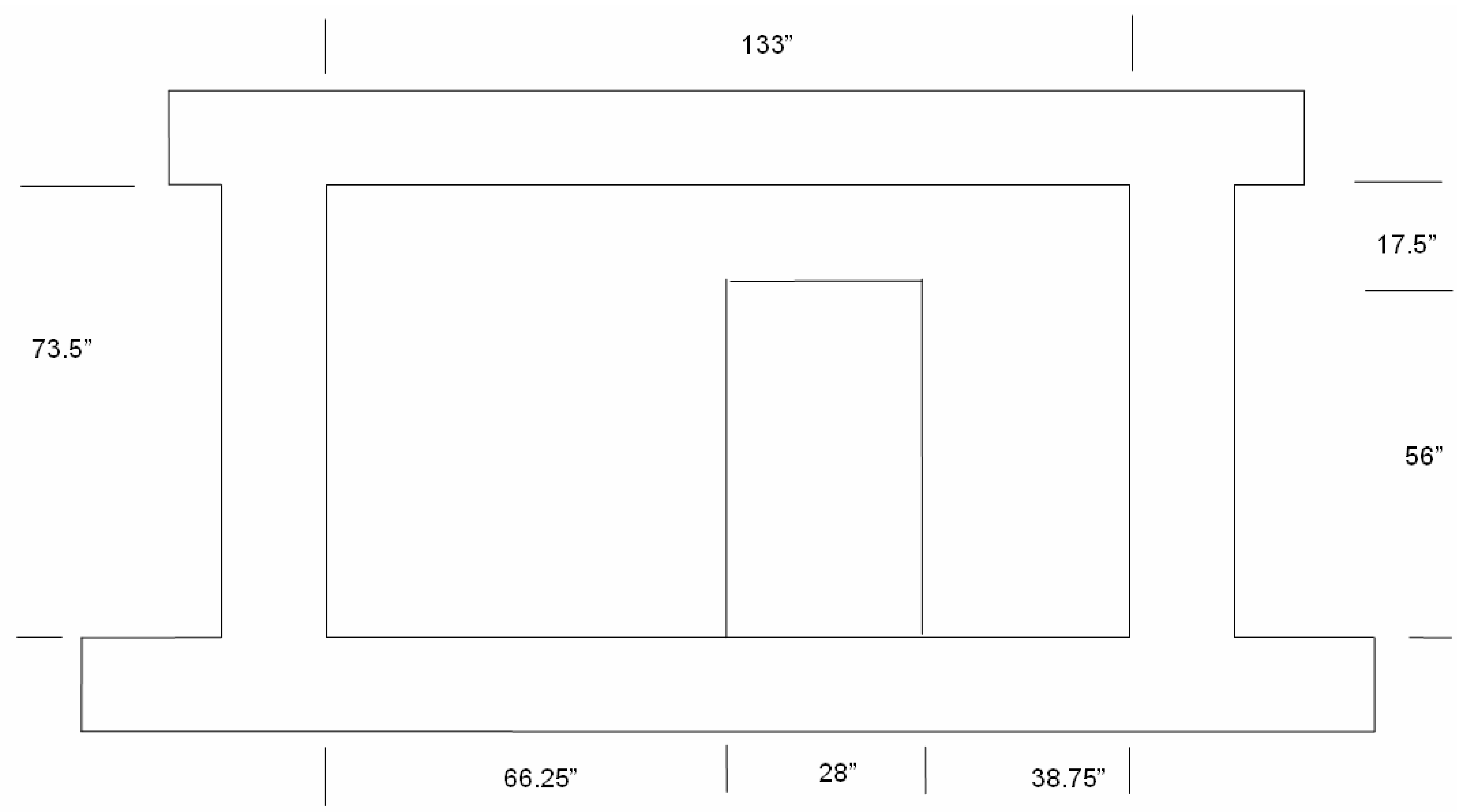

Figure 9.1: Test 5 Specimen Dimensions

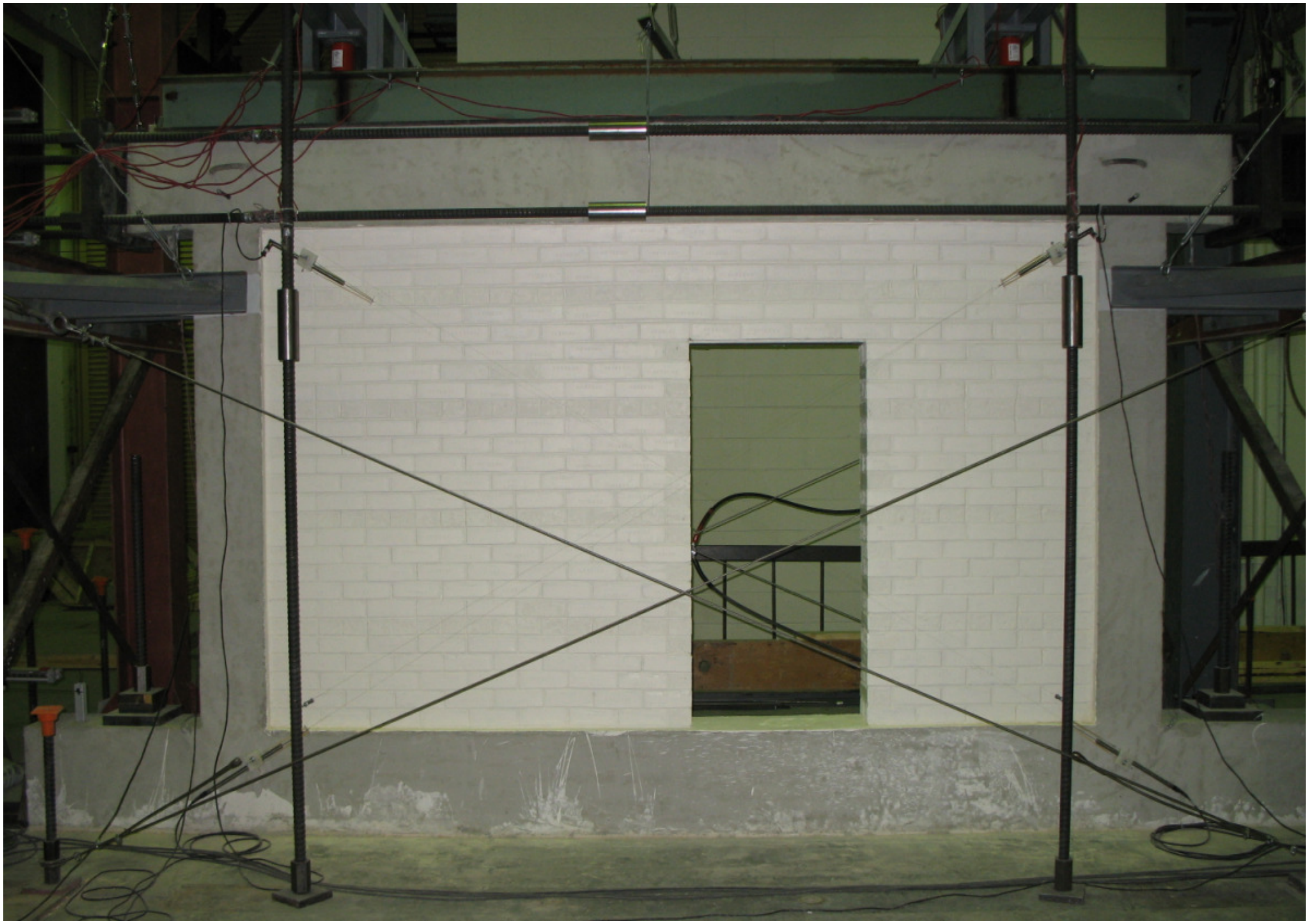

Figure 9.2: Test 5 Specimen Ready for Testing

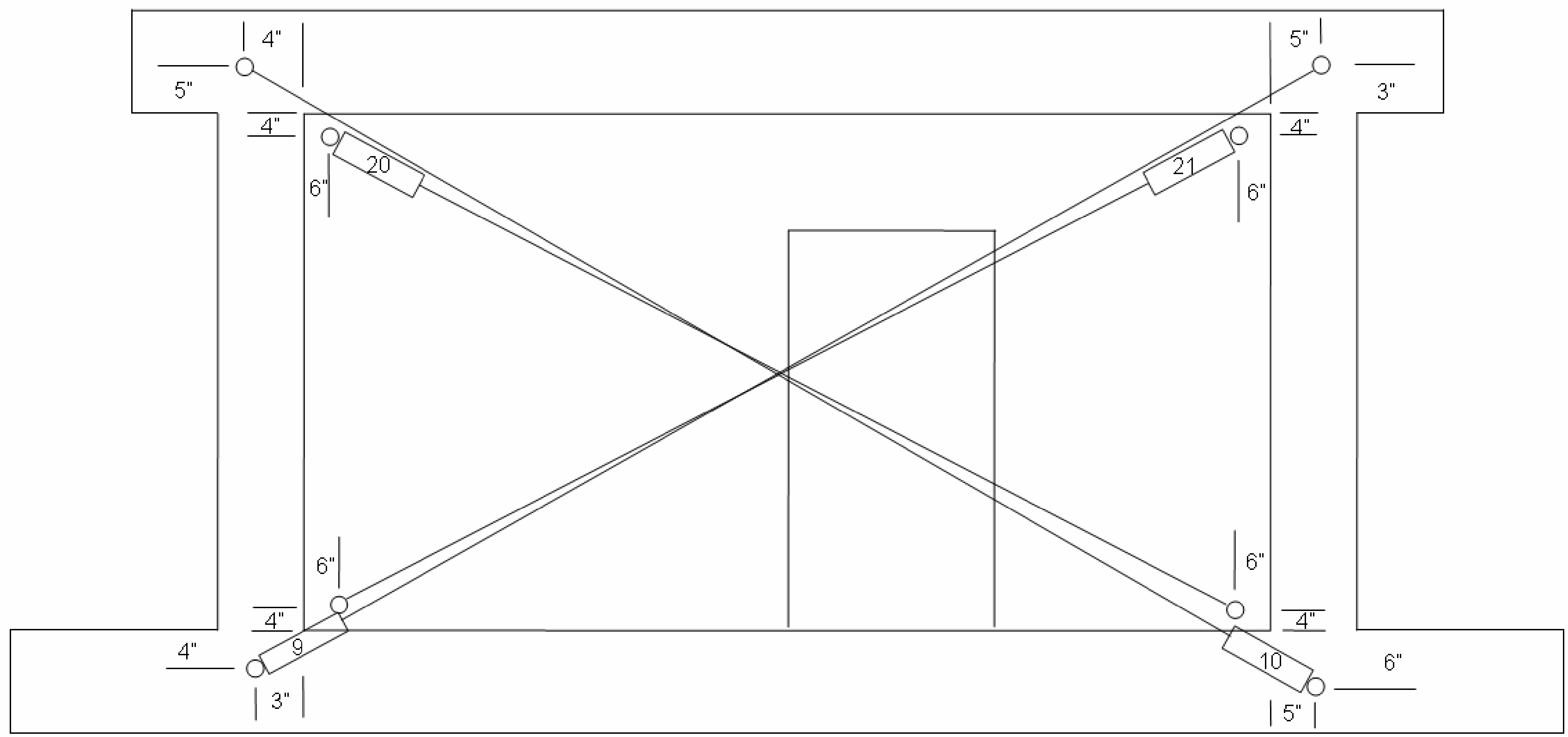

Figure 9.3: Test 5 LVDT Placement – Front View

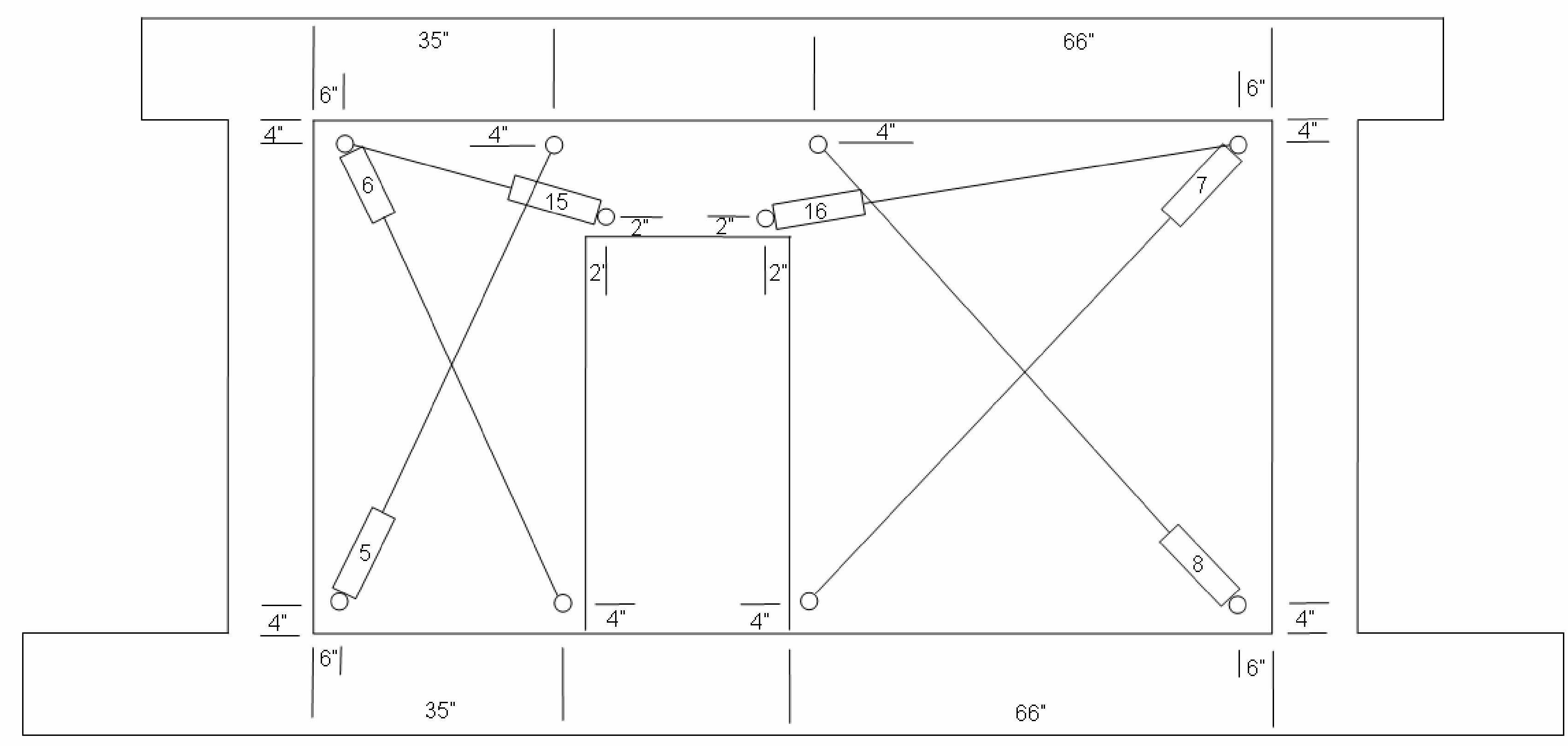

Figure 9.4: Test 5 LVDT Placement – Back View

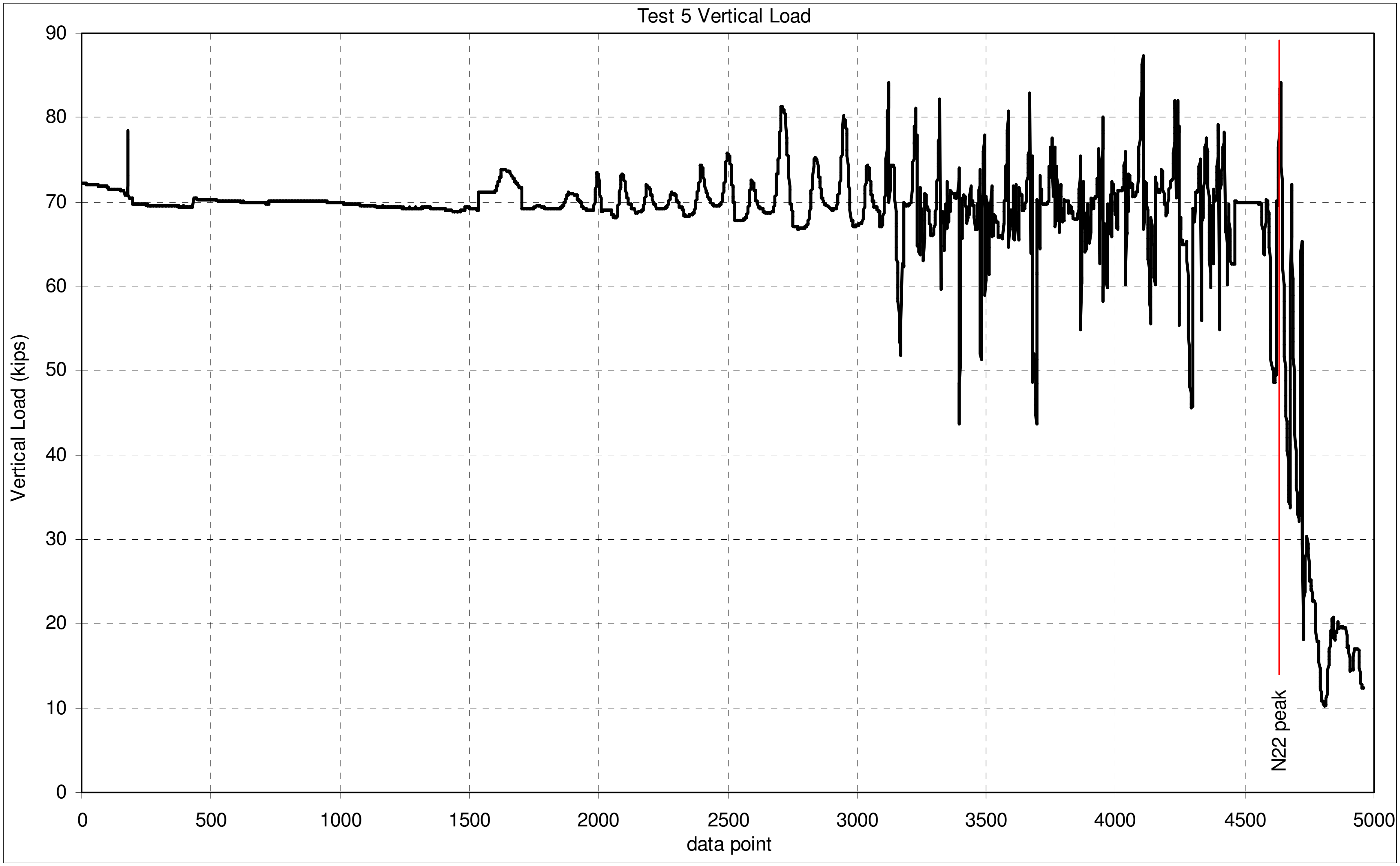

Figure 9.5: Test 5 Vertical Load

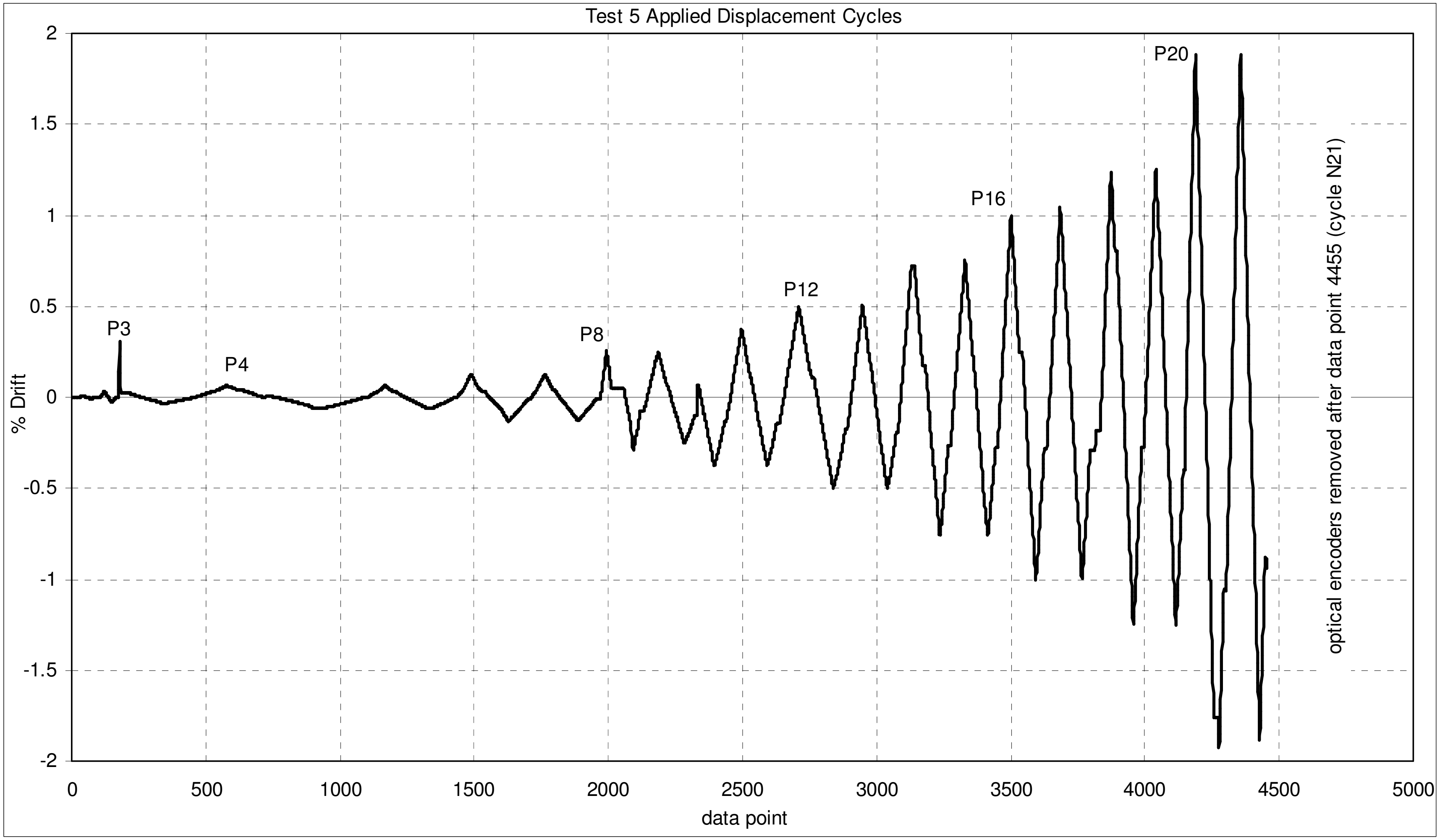

Figure 9.6: Test 5 Applied Displacement Cycles

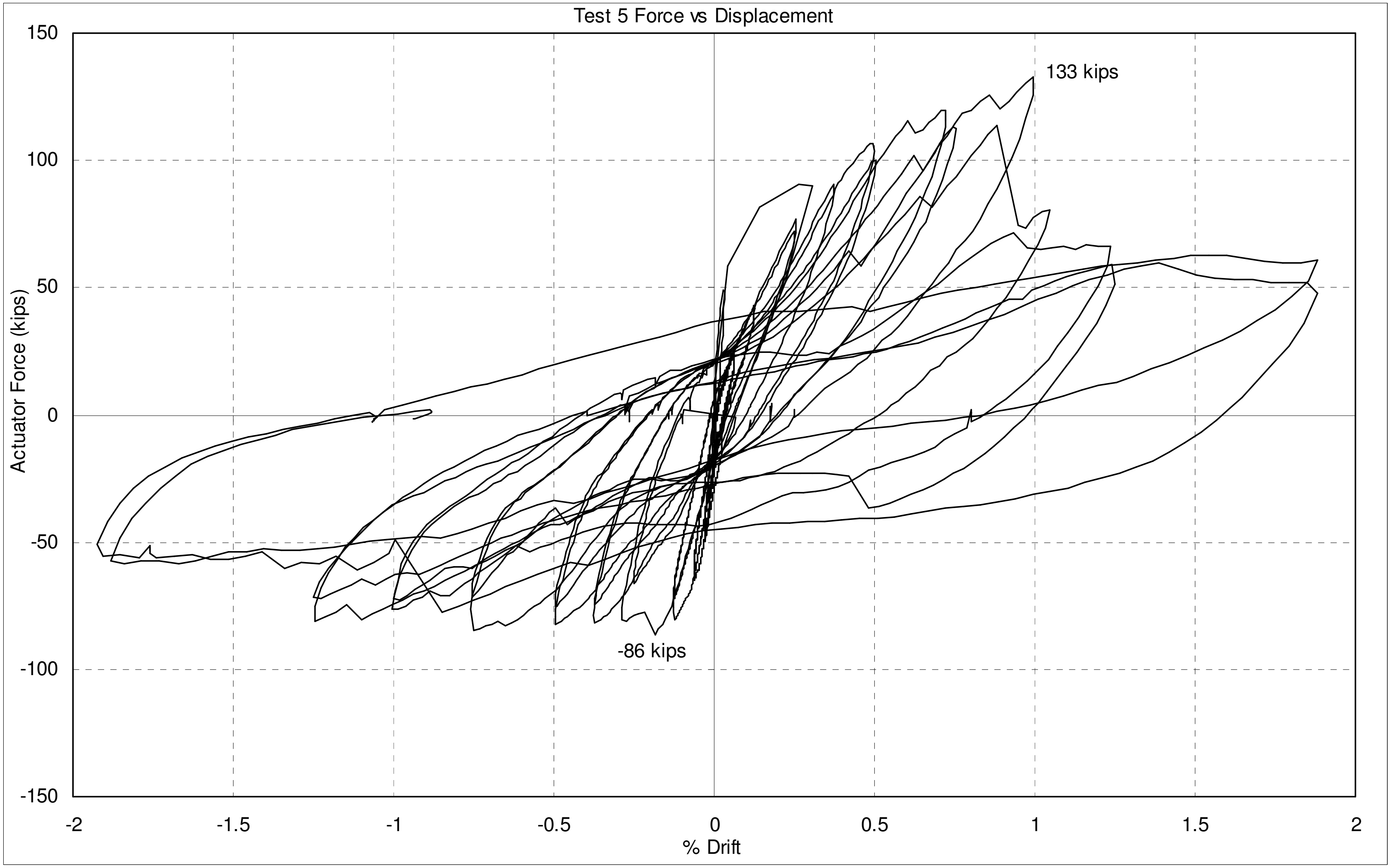

Figure 9.7: Test 5 Force vs Displacement

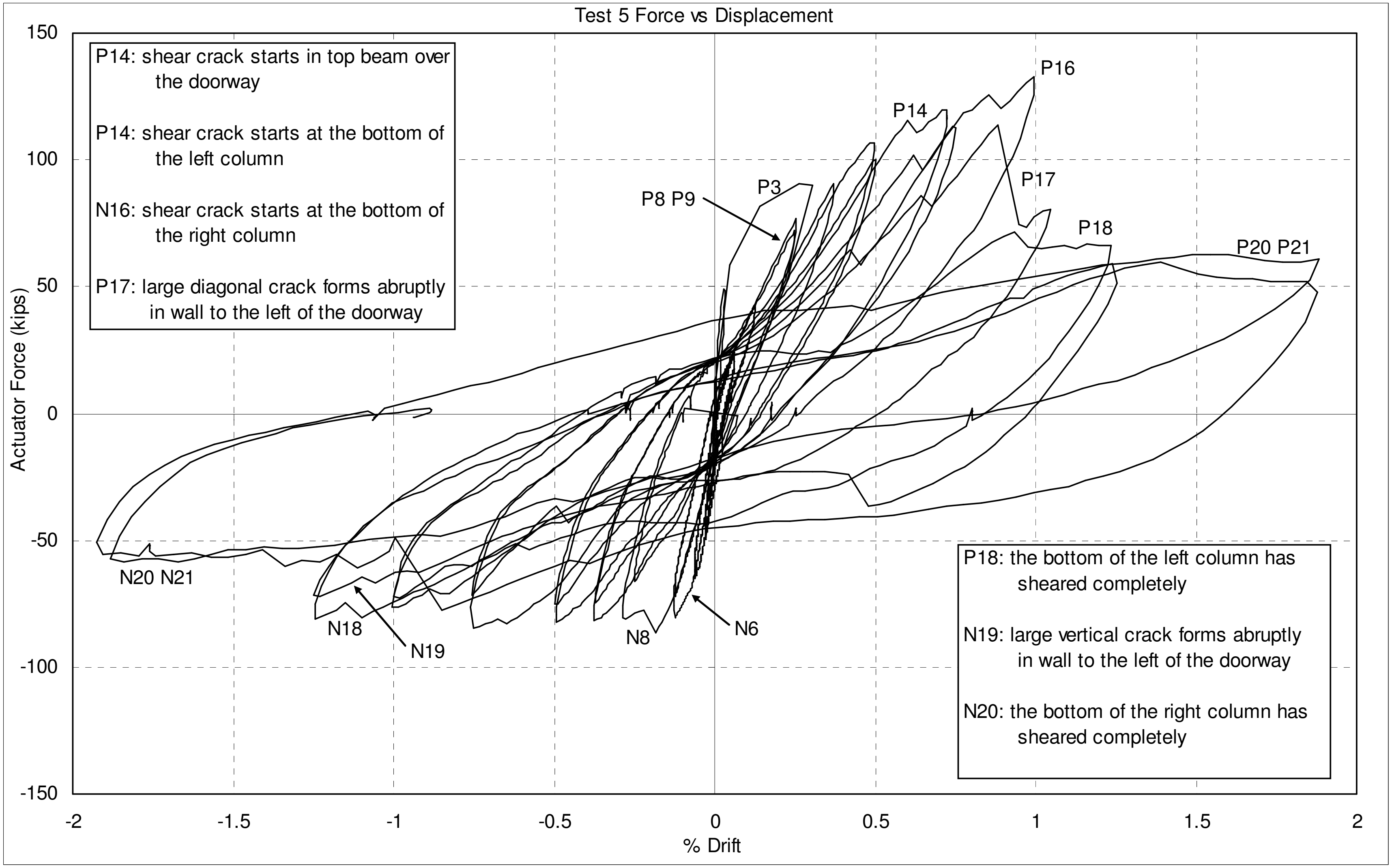

Figure 9.8: Test 5 Force vs Displacement

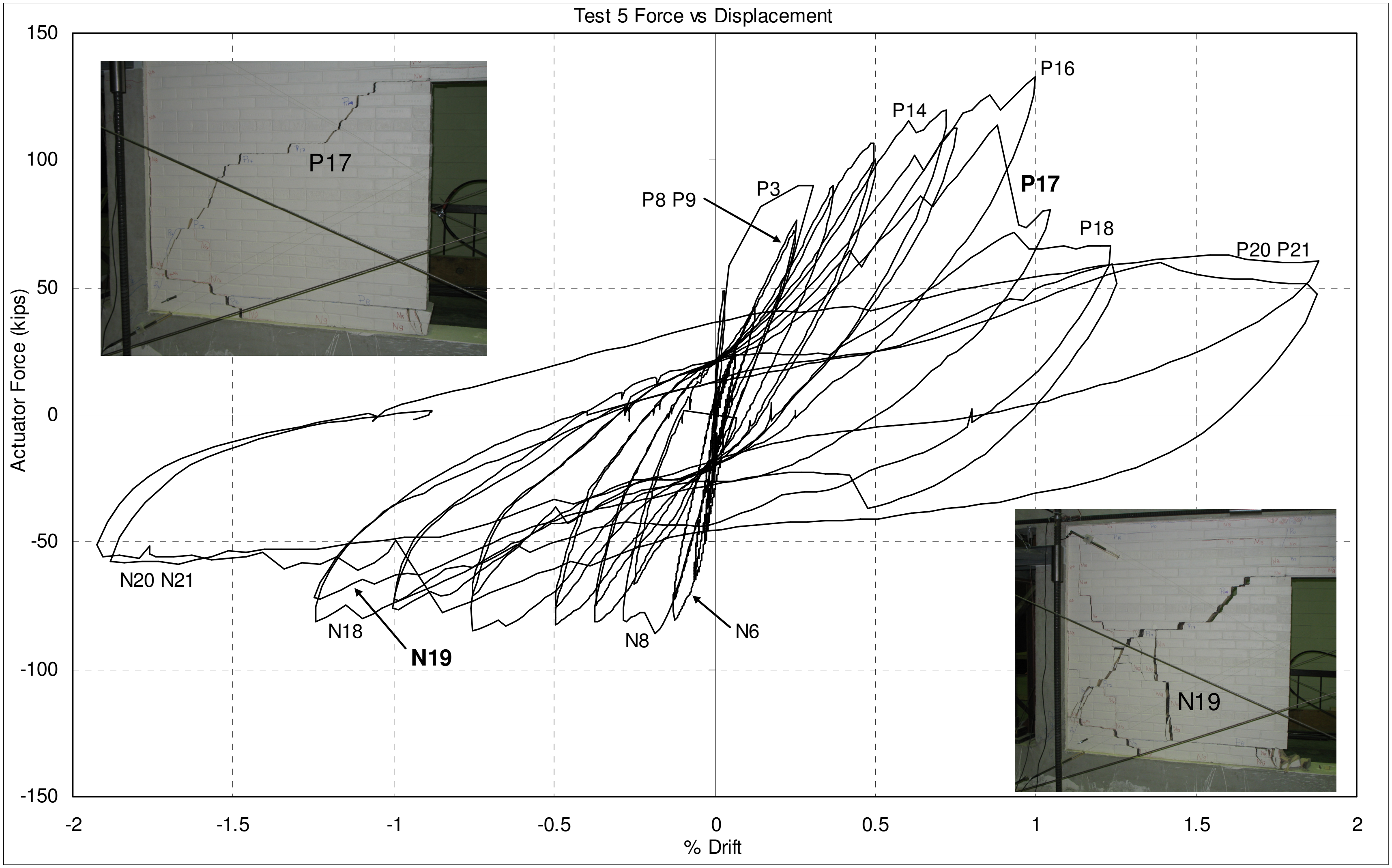

Figure 9.9: Test 5 Force vs Displacement

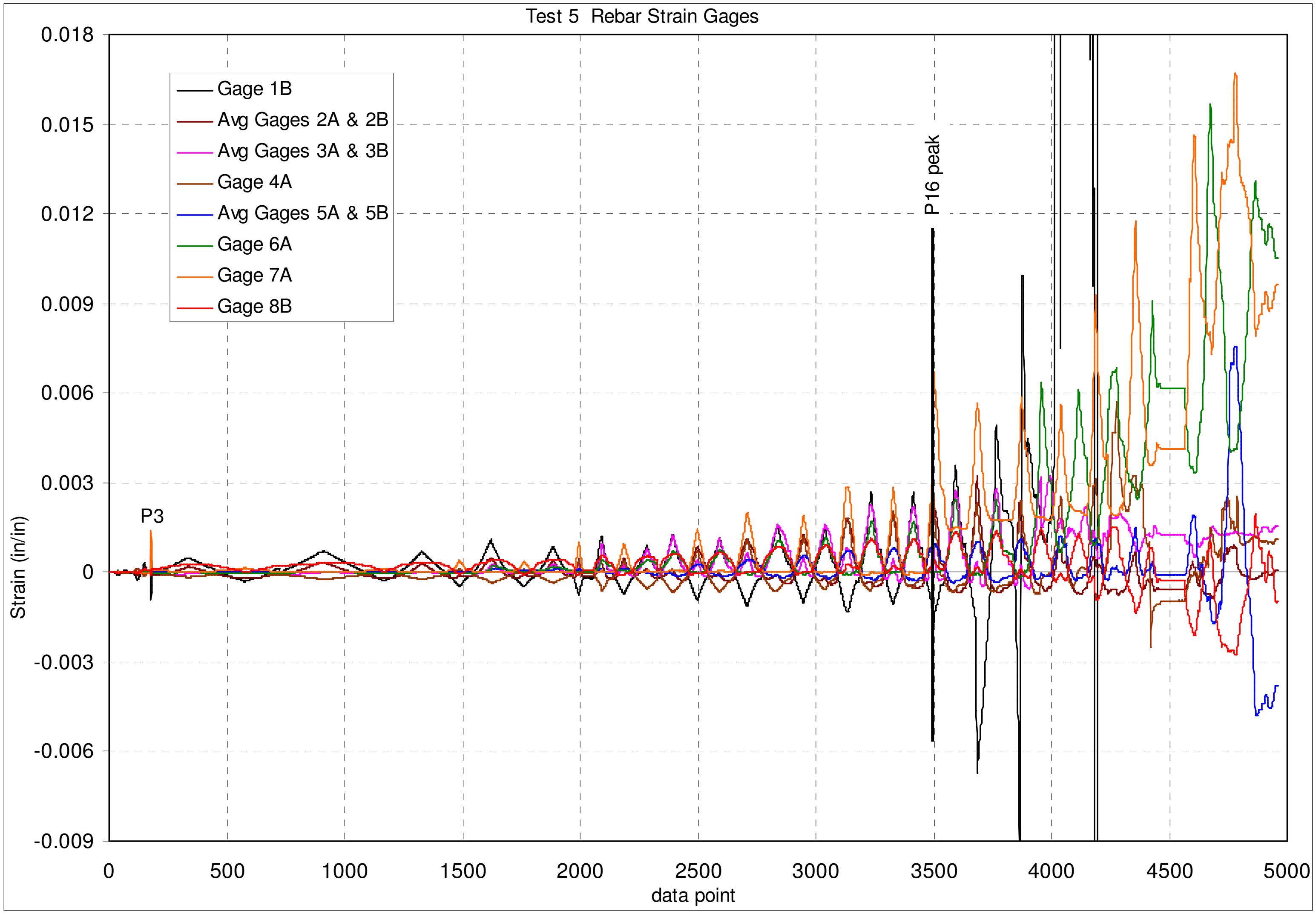

Figure 9.10: Test 5 Rebar Strain Gages

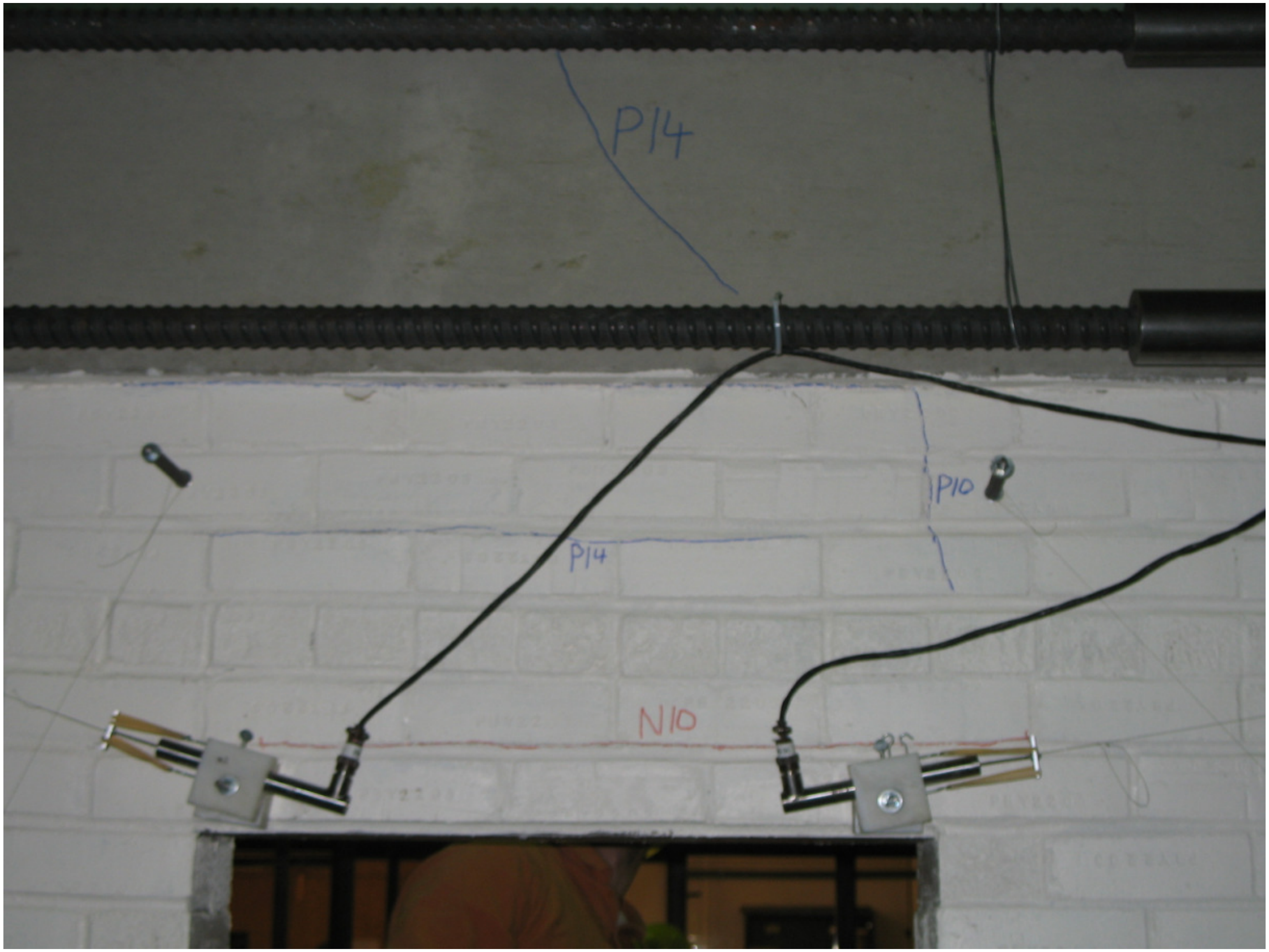

Figure 9.11: Top Beam Shear Crack

Figure 9.12: Final Crack Pattern

Lower East Column

Lower West Column

Figure 9.13: Column Shear

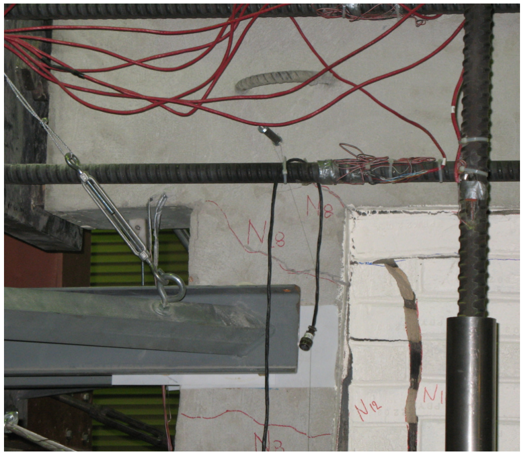

Top East Column

Top West Column

Lower East Column

Lower West Column

Figure 9.14: Post Test View of Columns

Chapter 10: Infilled Frame Test 6

The sixth infilled frame test conducted at the University of Colorado consisted of the same reinforced concrete frame as the previous tests. The brick infill wall had a window opening placed off center by the same eccentricity as that for test 2, but with larger dimensions. Figure 10.1 shows the dimensions of the specimen. Figure 10.2 is a photograph of the infilled frame with instrumentation installed. The material properties for the current test specimen are listed in table 10.1. A malfunction in the data collection system occurred which resulted in a complete lack of data for the prism tests. The instrumentation for the frame and wall are shown in figures 10.3 – 10.5.

During the anchoring process the frame was prematurely tightened to the strong floor, causing the base to crack near the bottom of the columns. These cracks can be seen in the illustrations in Figures 10.3 - 10.5. LVDTs 1, 2, 5, and 6 were installed to monitor the opening of the cracks during the test. The concern was that the base outside of the wall area may be stationary, but the main portion of the frame may be moving horizontally or rotating. As a result, following cycle N6 the bottom encoder was moved from the outer base position to a location near the center of the base (see figure 10.15). In addition, larger plates were placed at the locations of the end Dywidag anchors, as can be seen I figures 10.13 and 10.14. The final result was that the bottom encoder never measured any significant motion in either of the locations. The conclusion is that the cracks in the base did not adversely effect the test. After cycle N16 the bottom encoder was removed from the specimen because of falling debris. There was no evidence any significant movement of the base afterward, so the relative displacement after cycle N16 was calculated as the average displacement of the top two optical encoders.

The test consisted of displacement controlled cycles applied by a 220 kip MTS actuator. As with the previous tests, "positive" [half] cycles correspond to a displacement to the east (left), and "negative" half cycles to the west (right). For each cycle the positive cycle was applied first, followed by a negative cycle with the same magnitude and cycle number. Cycles were applied in pairs with the same positive and negative magnitudes, for example P8, N8, P9, N9 all have the same displacement magnitude. The magnitudes of the cycles are illustrated in figure 10.7.

Figure 10.9 shows the full set of force vs percent drift hysteresis loops for the test, along with key events noted. The response shows more ductility and lower strength than previous tests. There may be a small abrupt drop in strength after cycle P18 and N18 which would correspond to the column shear at the top and bottom of the left column. The drop in strength is fairly insignificant as compared to previous tests, yet the left column did show significant shear. The right column started to shear at the top, bottom, and near mid-height. However, these shear cracks never developed, even with a drift of nearly 2%. The final crack pattern is shown in figure 10.10, with the columns shown in figures 10.11 and 10.12.

Table 10.1: Test 6 Material Properties

Concrete Compressive Strength	2,400 psi
Mortar Compressive Strength	793 psi
Masonry Prism Compressive Strength	no data available due to a data collection malfunction with the 110 MTS test machine
Reinforcing Tensile Yield Strength	68,000 psi
Column Tie Yield Strength	55,000 psi

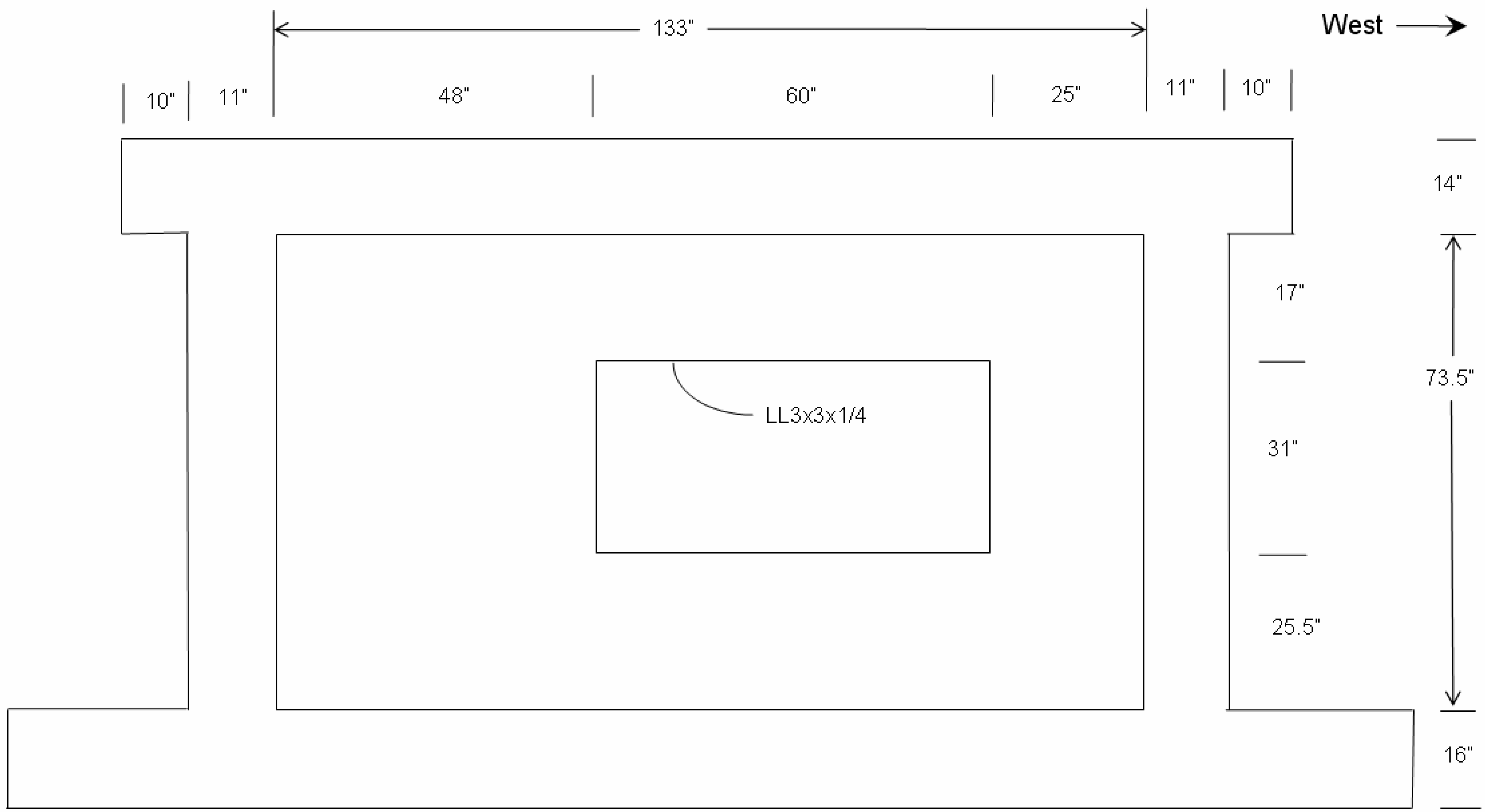

Figure 10.1: Test 6 Specimen dimensions

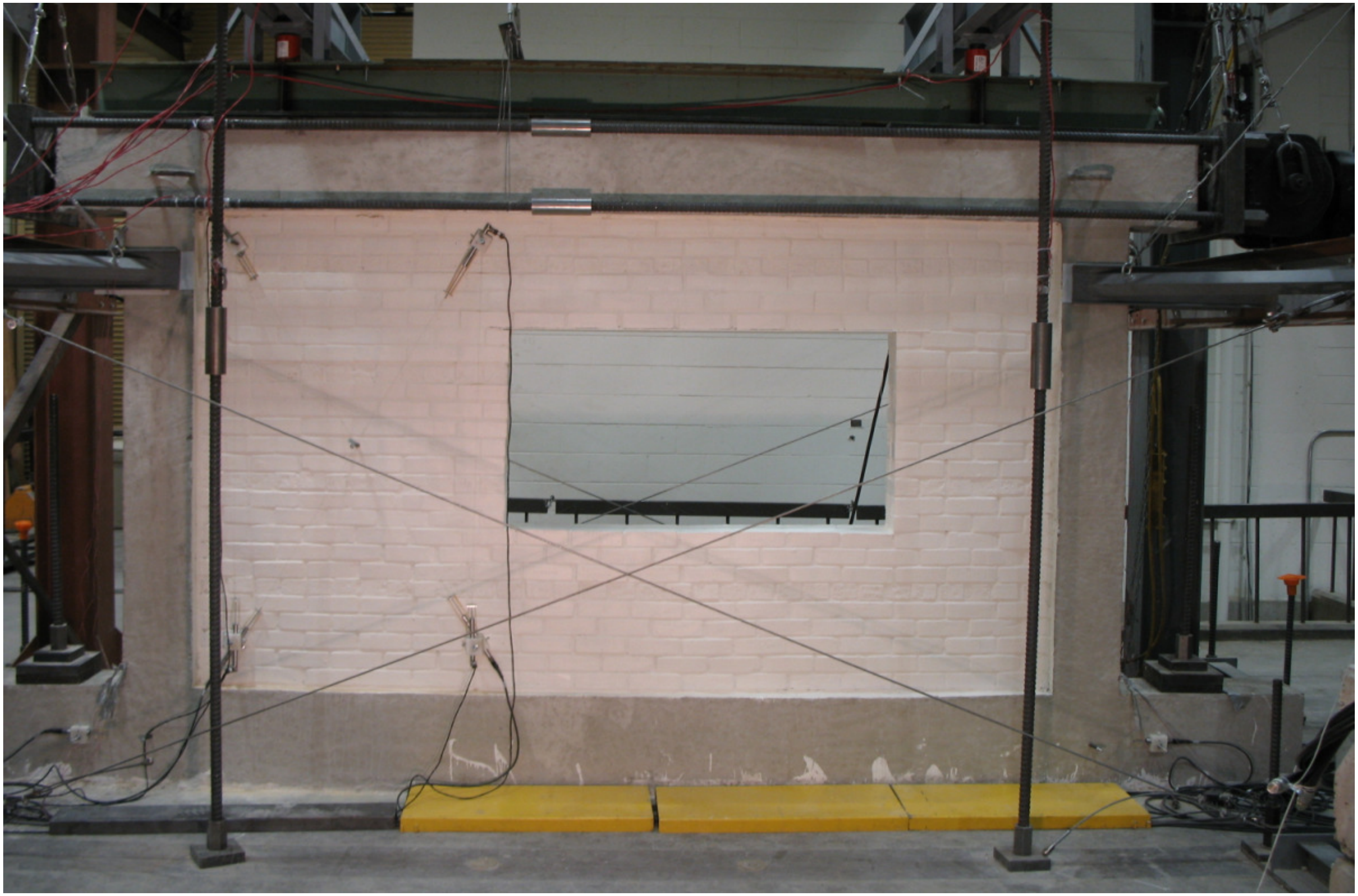

Figure 10.2: Test 6 Specimen With Instrumentation

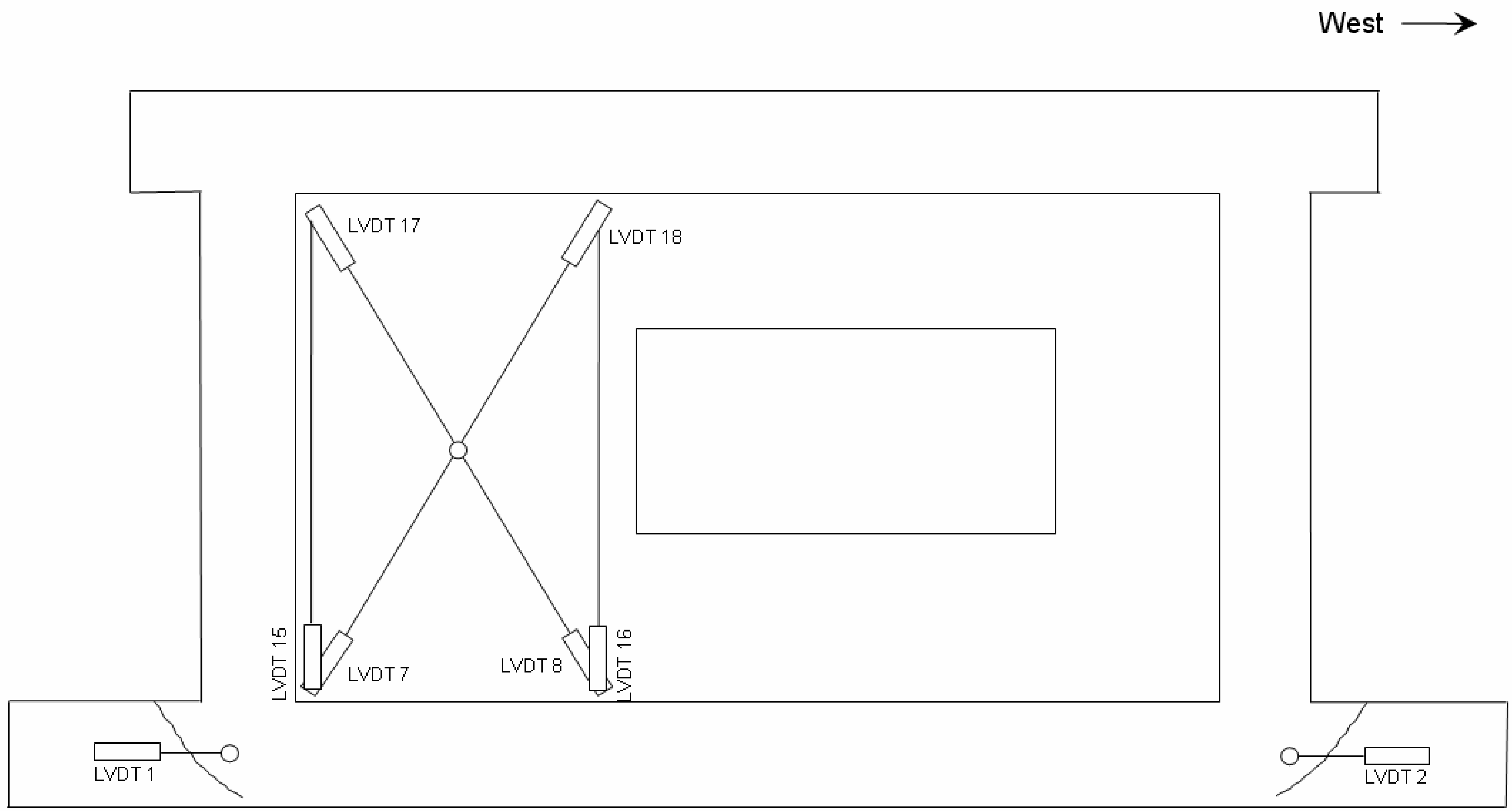

Figure 10.3: Test 6 LVDT Placement – Front View

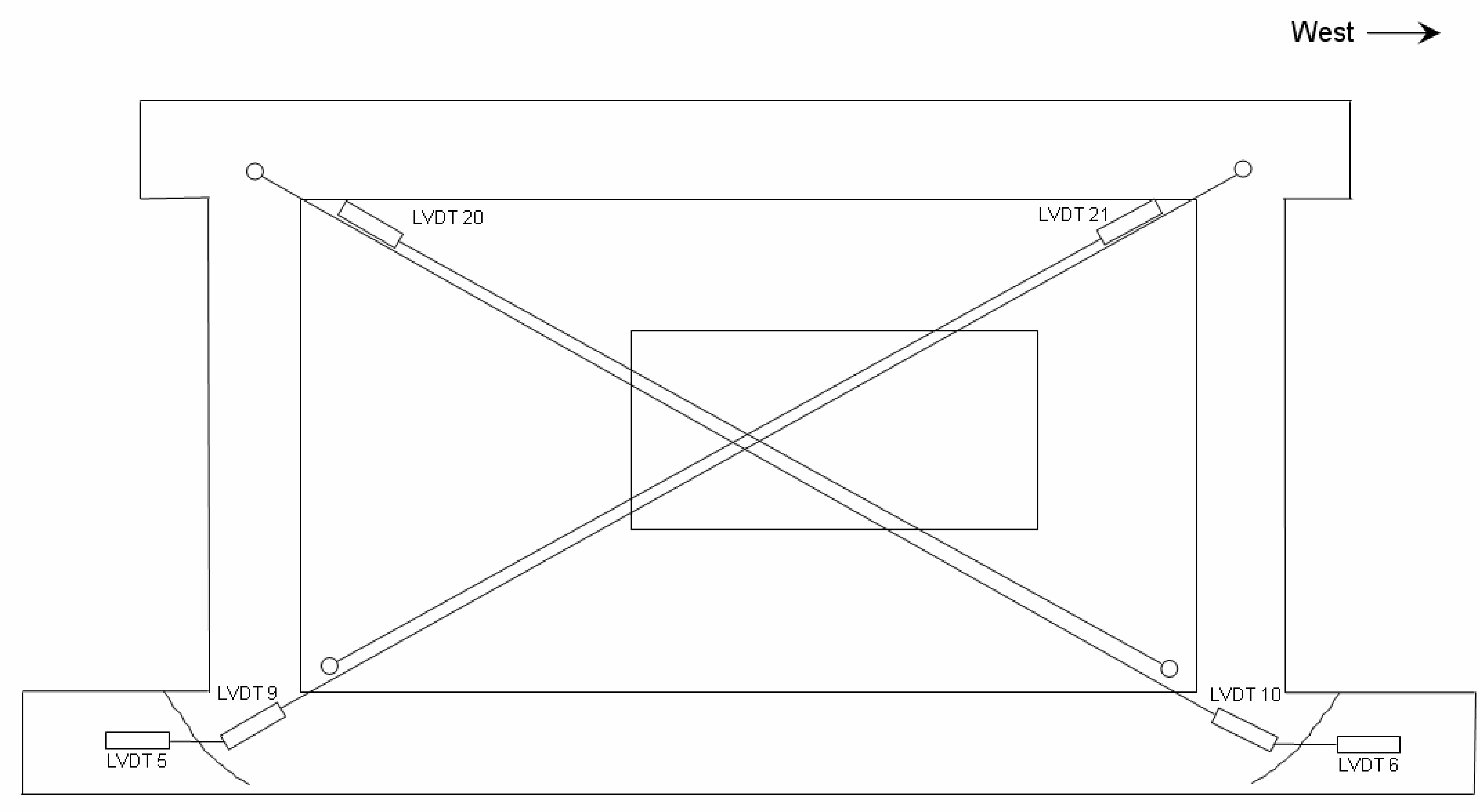

Figure 10.4: Test 6 LVDT Placement – Back of Wall as Viewed From Front

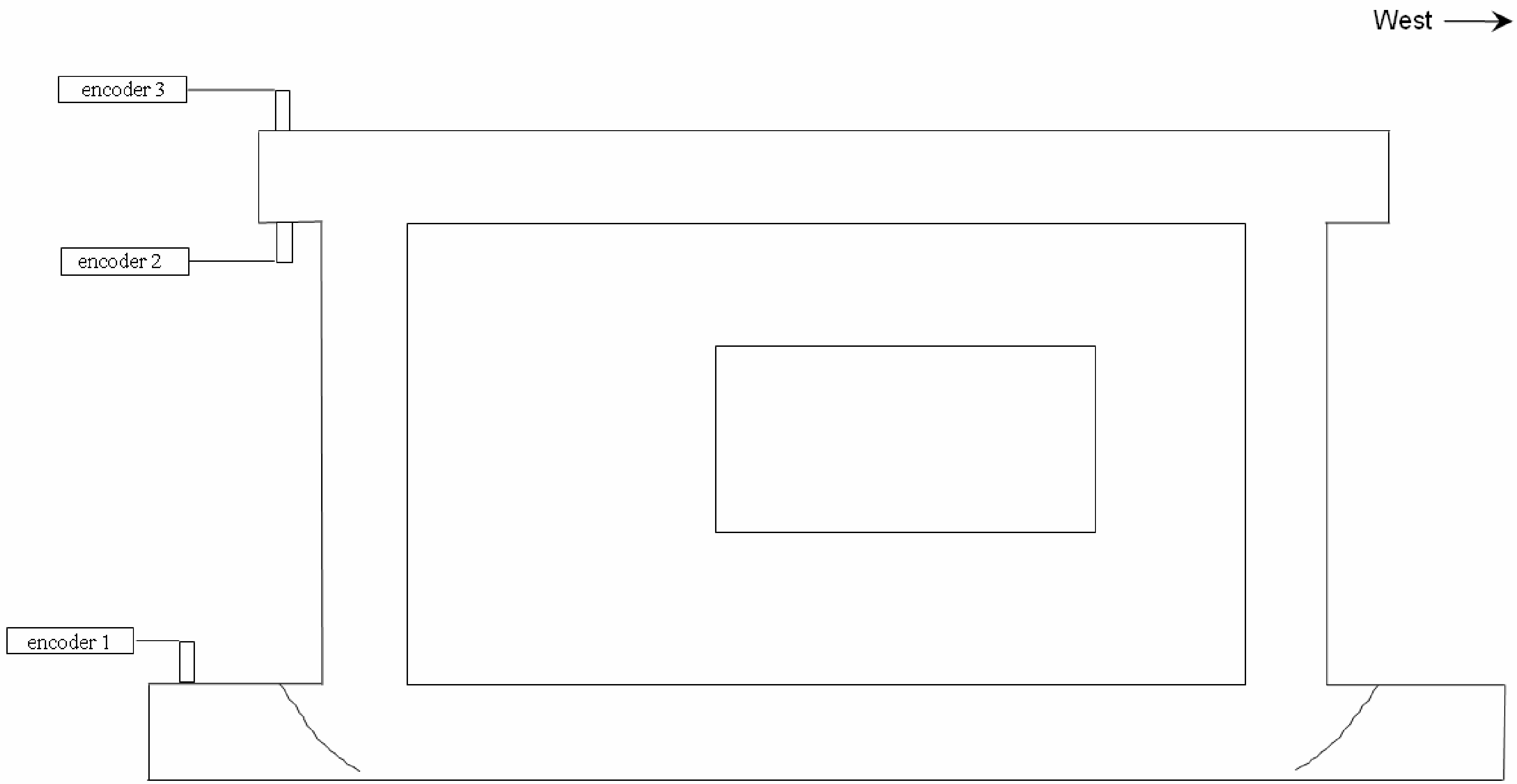

Figure 10.5: Test 6 Optical Encoder Placement

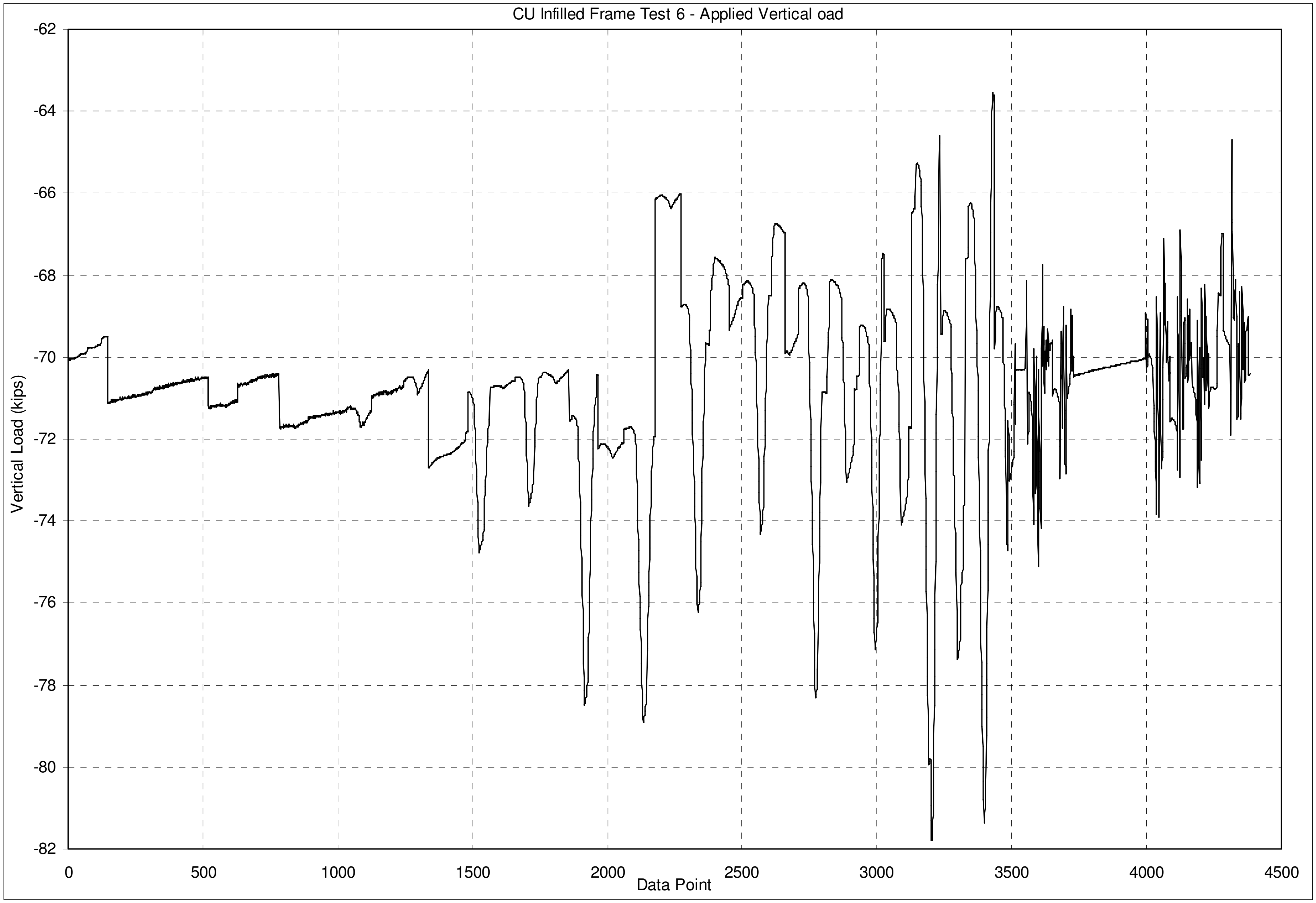

Figure 10.6: Test 6 Vertical Load

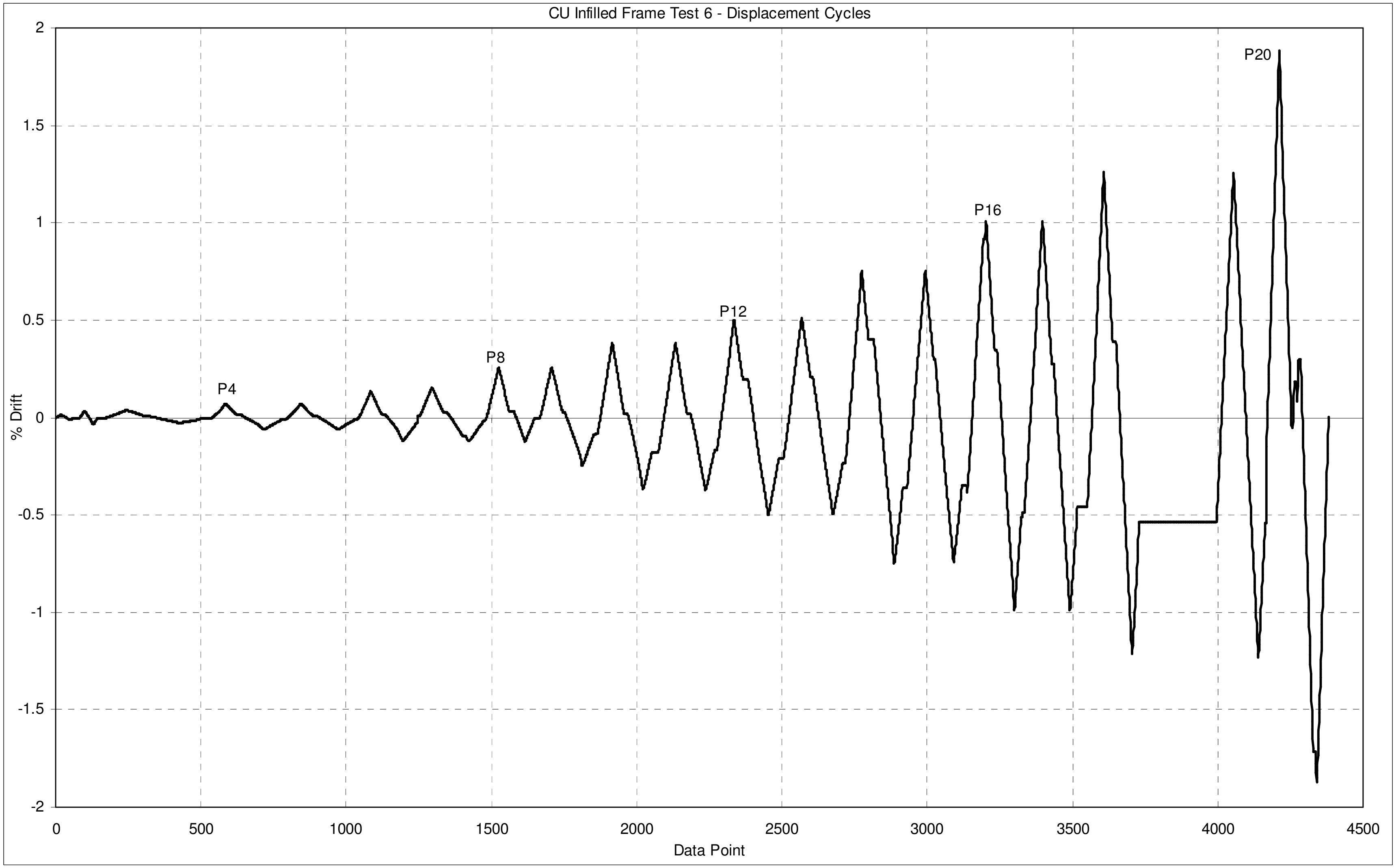

Figure 10.7: Test 6 Applied Displacement Cycles

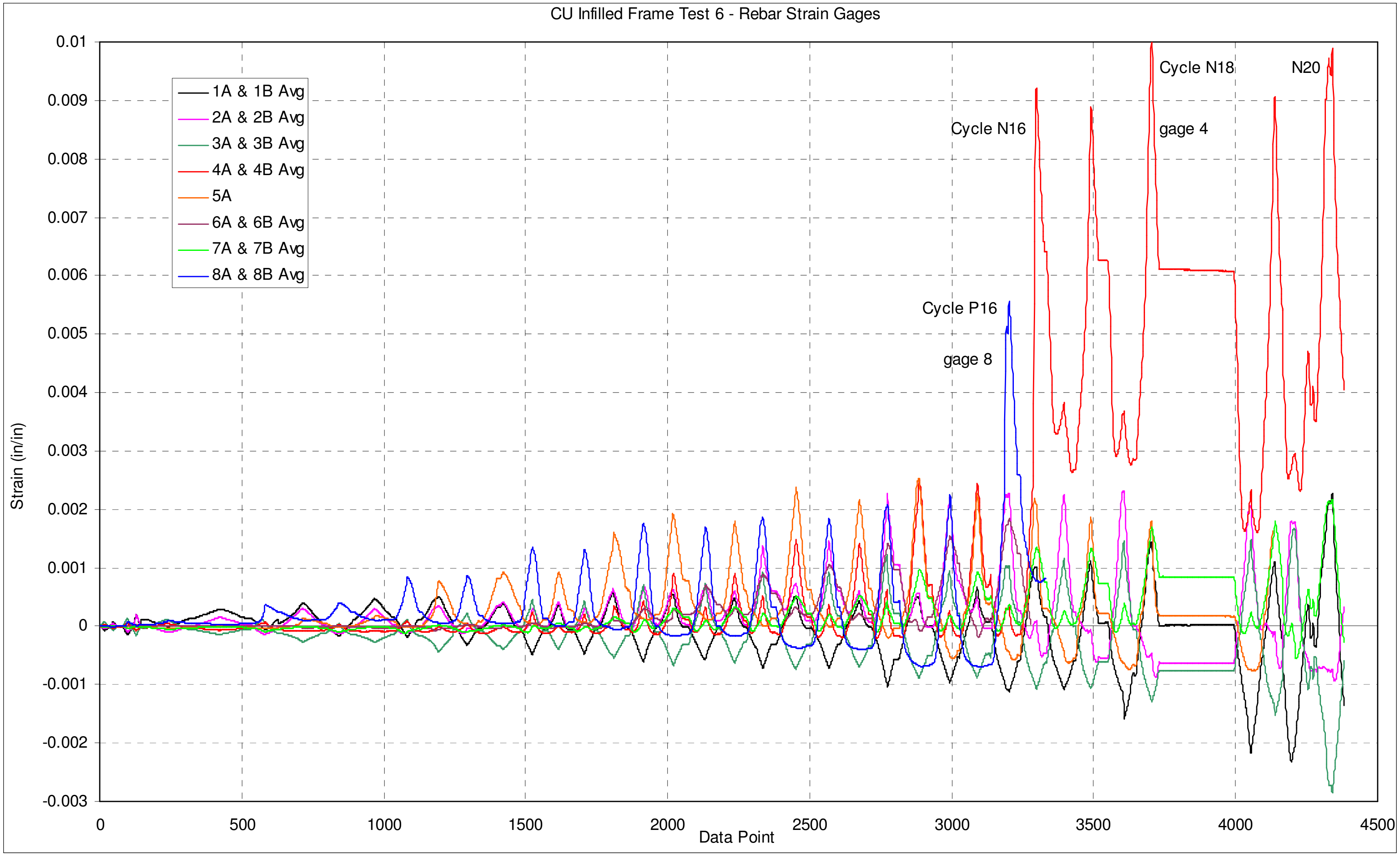

Figure 10.8: Test 6 Rebar Strain Gage Data

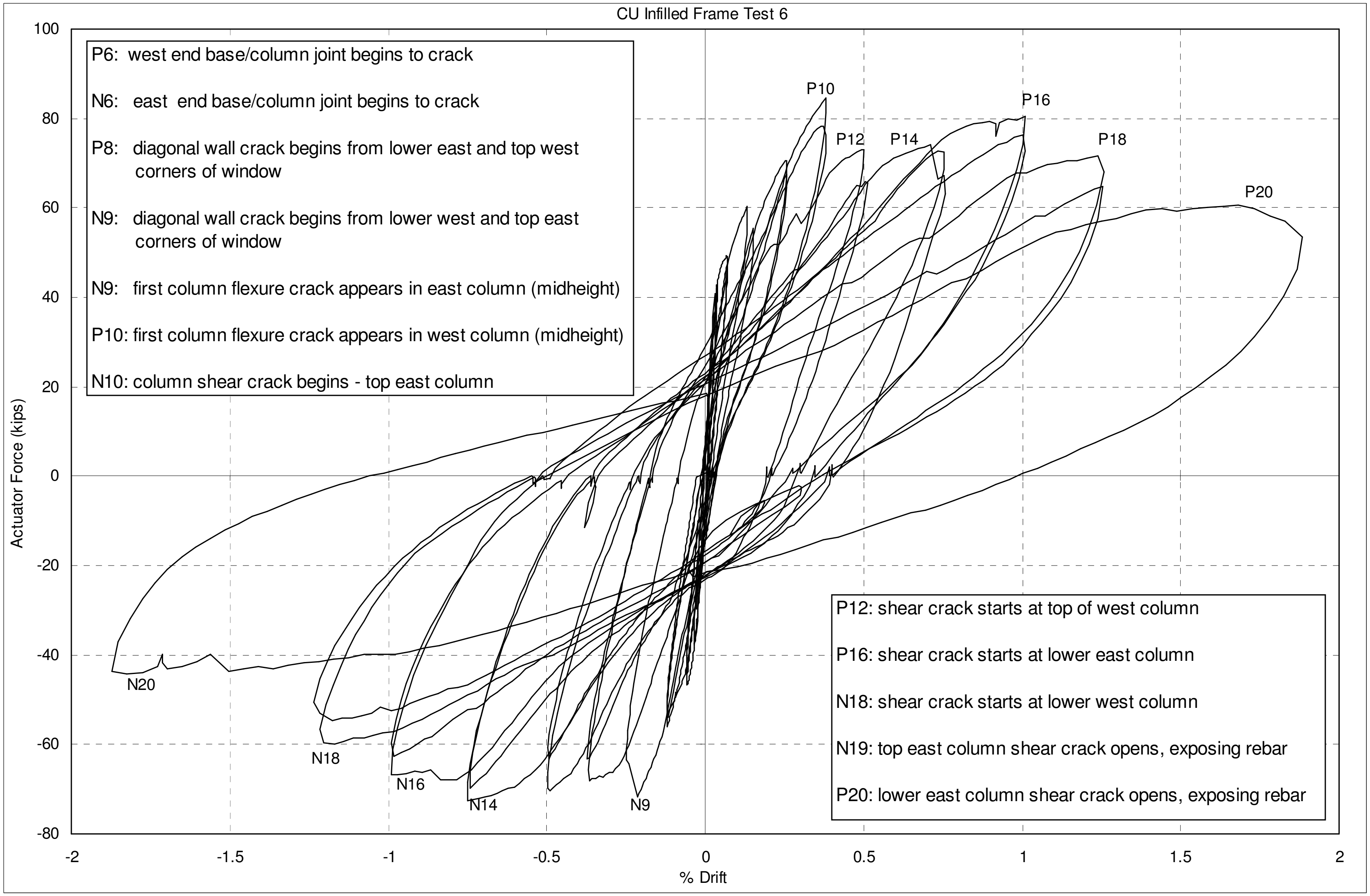

Figure 10.9: Test 6 Force vs Displacement

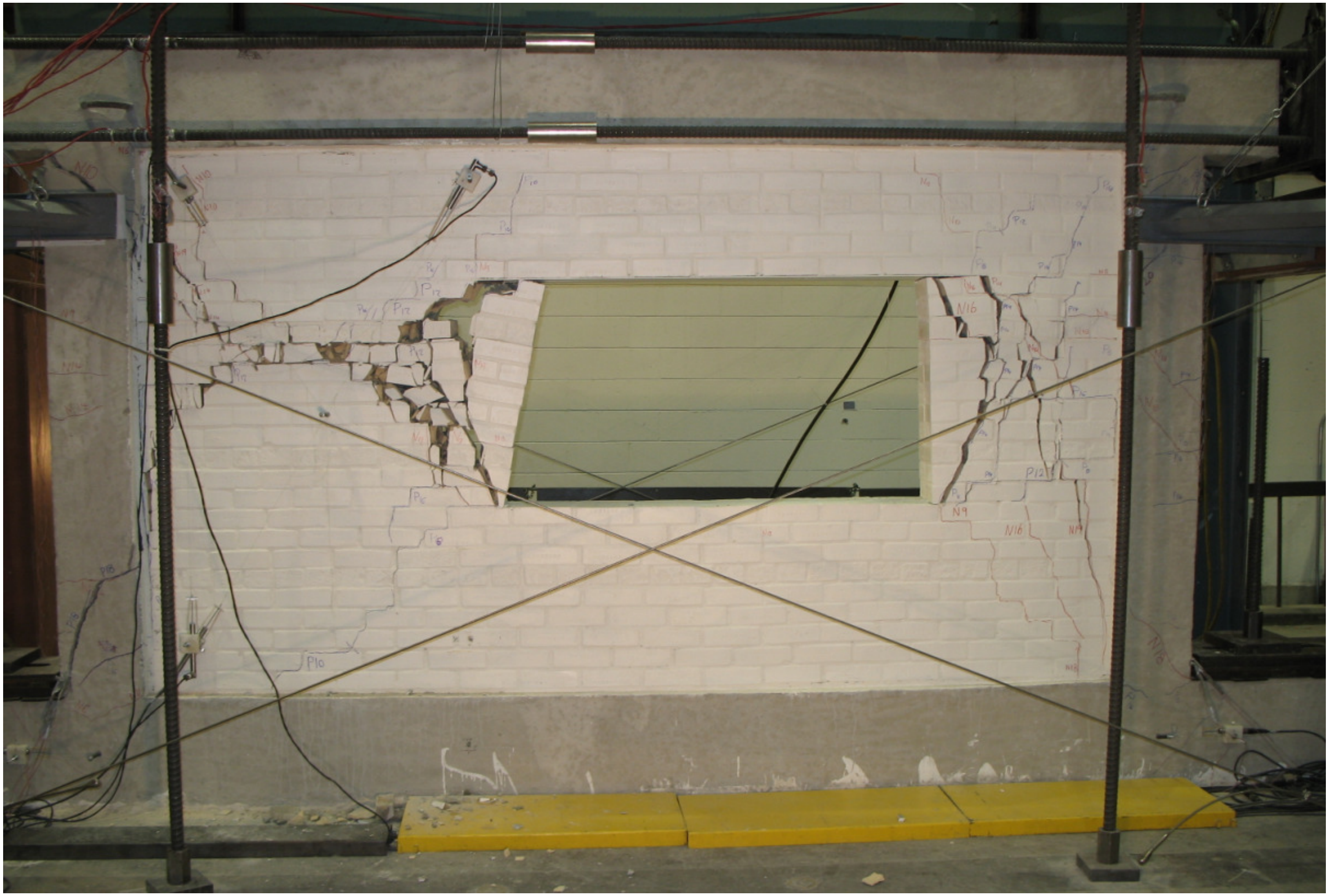

Figure 10.10: Test 6 Final Crack Pattern

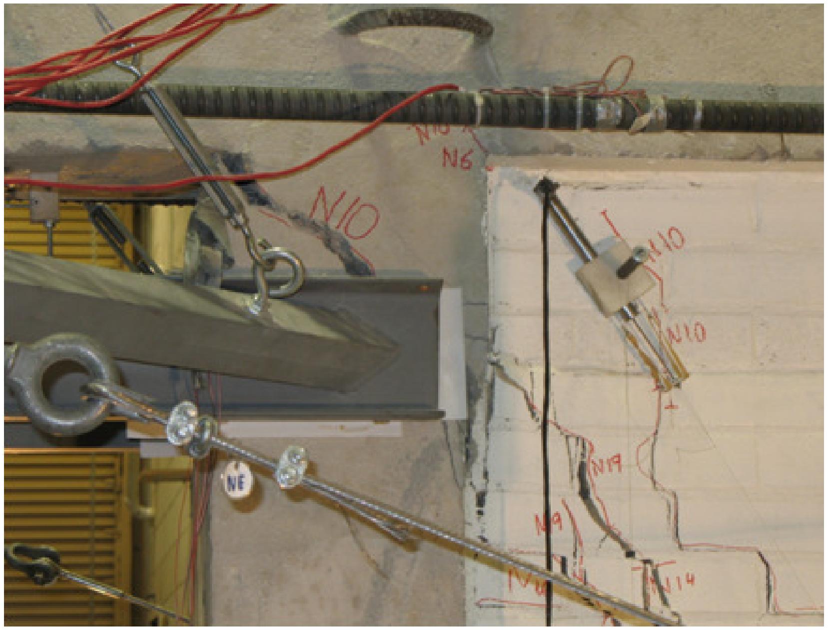

Upper East Column

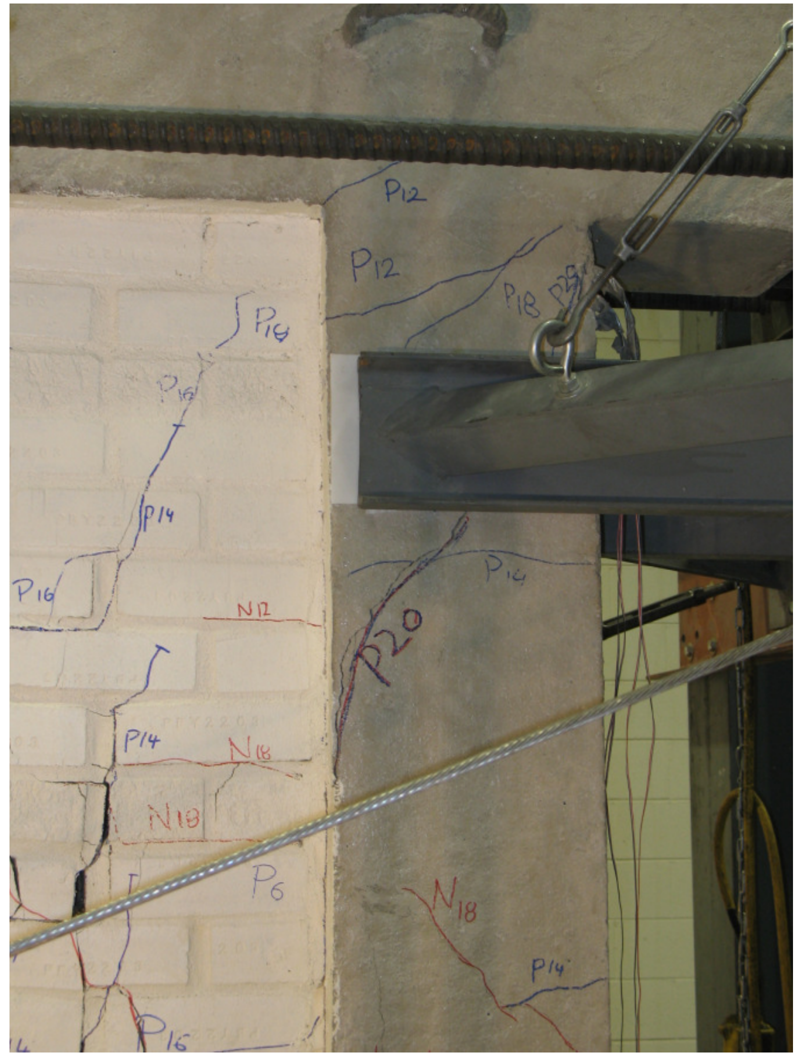

Upper West Column

Figure 10.11: Test 6 Column Shear

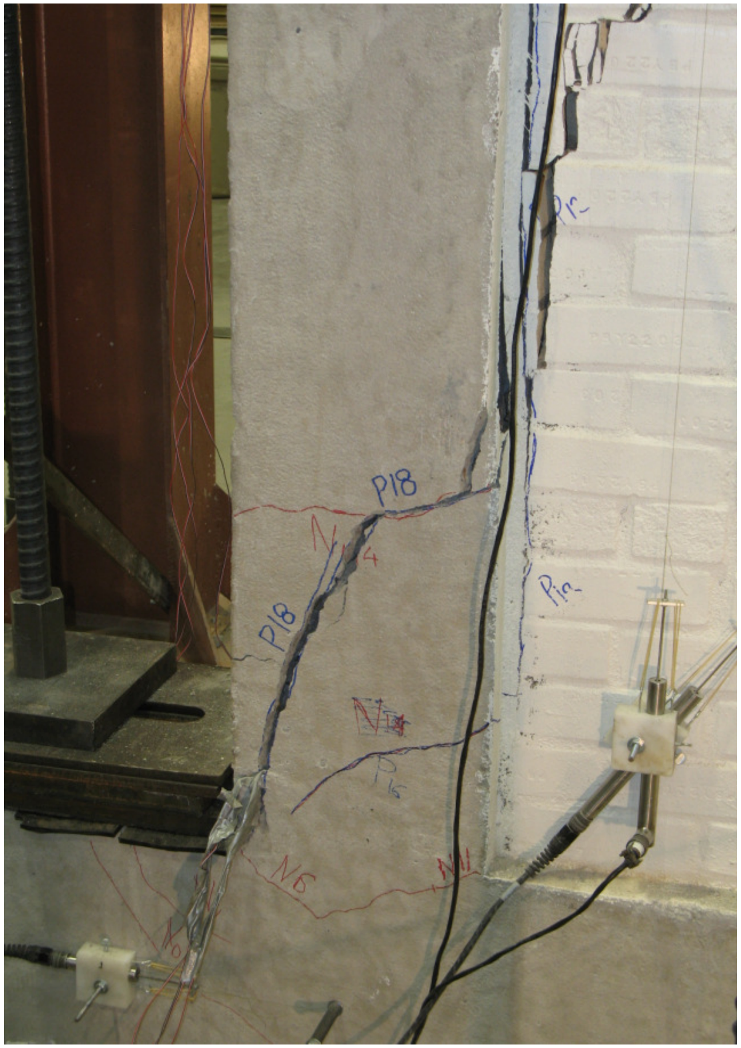

Lower East Column

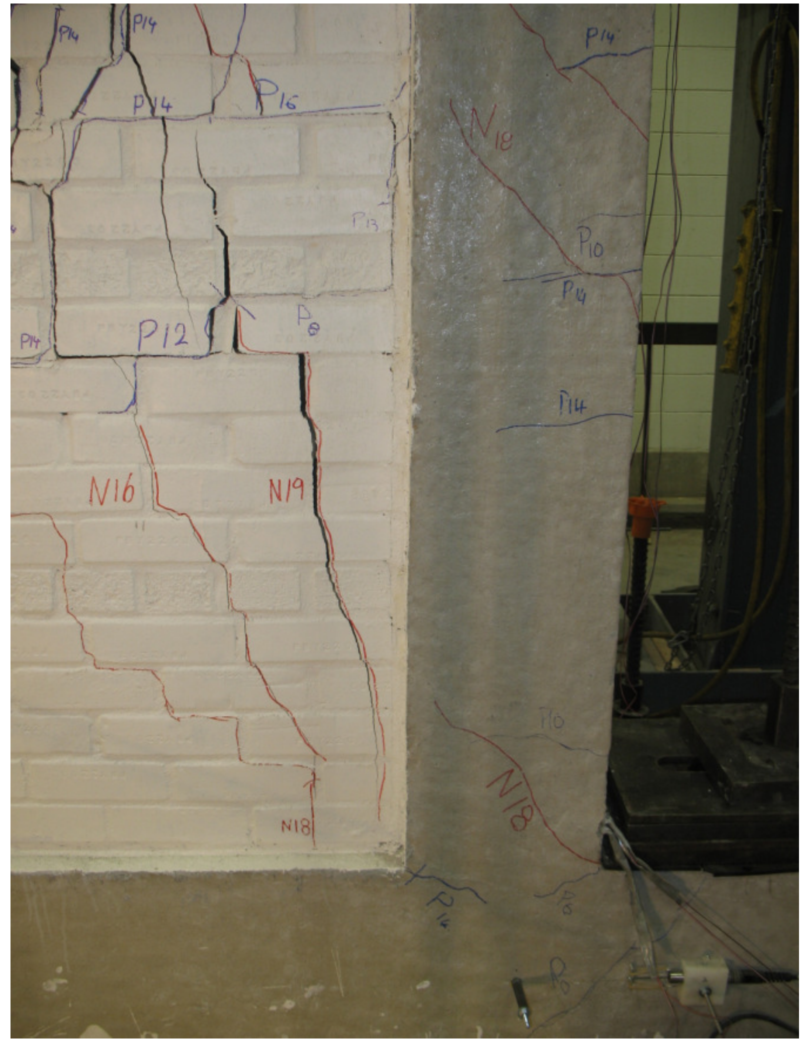

Lower West Column

Figure 10.12: Test 6 Column Shear

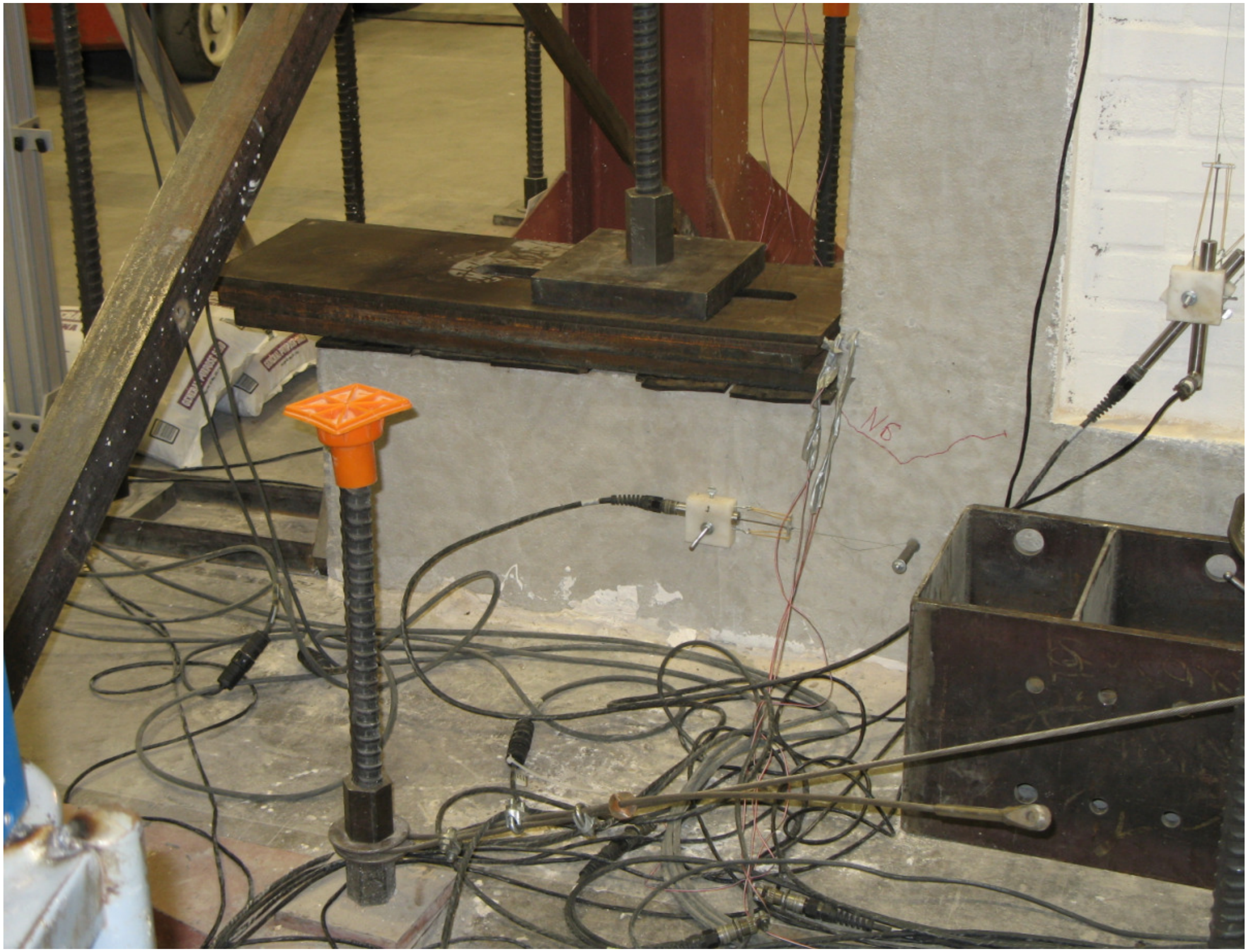

Figure 10.13: Larger East End Base Plate Installed After Cycle N6

Figure 10.14: Larger West End Base Plate Installed After Cycle N6

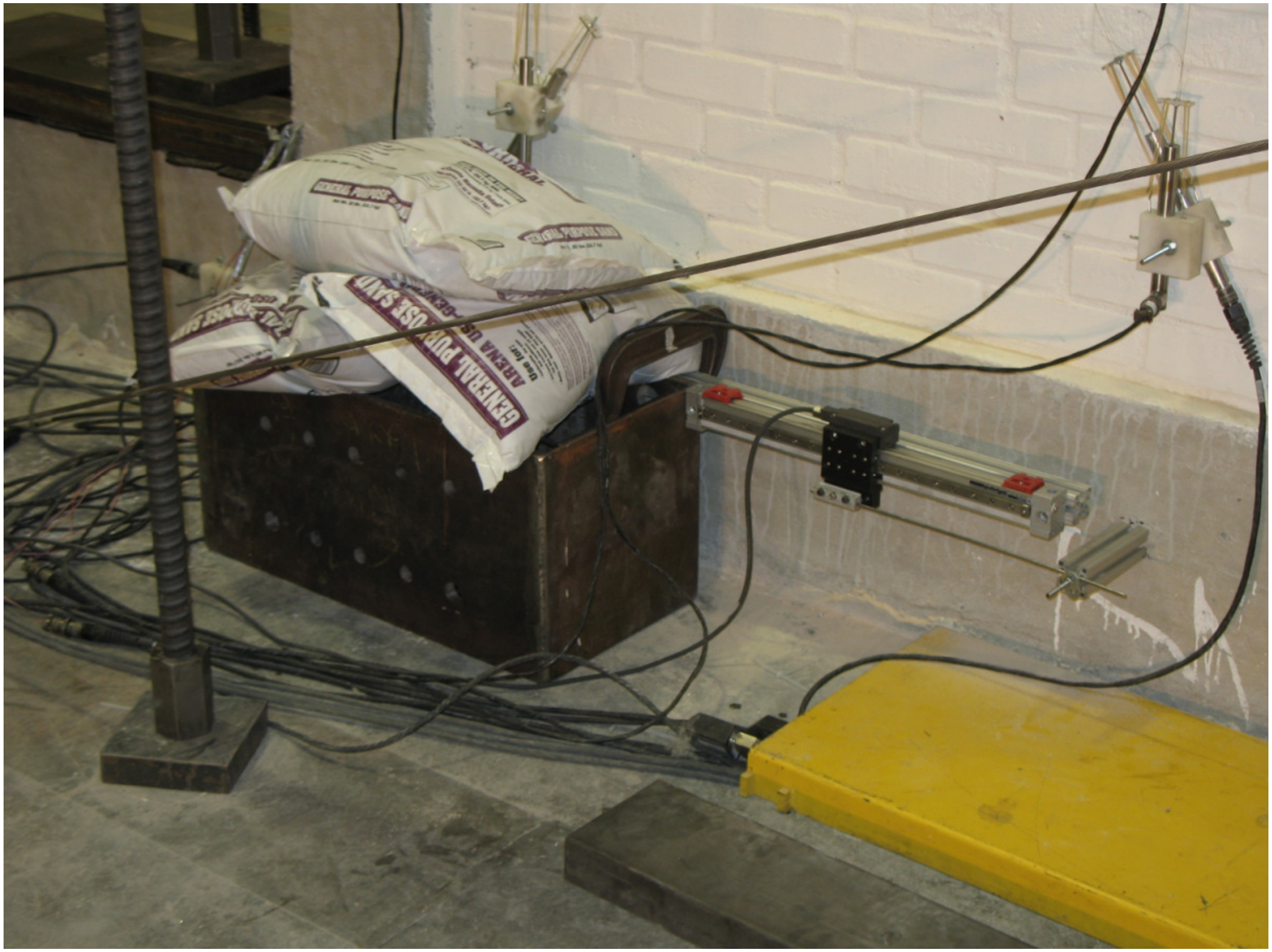

Figure 10.15: New Location For Bottom Optical Encoder After Cycle N6

Figure 10.16: Bottom Encoder Removed After Cycle N16

Chapter 11: Comparisons of the Experimental Results

A comparison of the six test results appears in figure 11.1 in the form of force vs displacement envelope plots. It is evident that a variety of behavior is displayed with regard to peak strength, ductility, and residual strength. Of particular interest to the current study is the effect of the retrofit and wall openings.

Openings

Figure 11.2 shows a comparison of the force vs percent drift for tests 1, 2, 5, and 6. The specimen for test 1 was a solid wall, for test 2 a wall with window opening, the test 5 specimen had a door opening, and test six had a larger window opening but with the same eccentricity as the test 2 window. Note that the positive direction corresponds to a right to left displacement of the actuator, as viewed from the front side of the specimen. In the positive direction the solid wall clearly shows a higher peak strength than any of the walls with an opening. Only tests 1, 2, and 5 showed brittle behavior in this direction. The wall with the larger window opening clearly shows lower strength and more ductility. Specimen 2, the other wall with window opening, shows more ductility than the solid wall or the wall with door opening. In the negative direction the solid wall and the wall with window opening show almost identical behavior. Specimens 5 and 6 show a similar response, even though the wall with the door opening shows a small brittle drop at 1.25% drift, which is not present for the wall with the large window opening.

Retrofit

Figure 11.3 shows the effect of retrofit on the specimens with window openings. The behavior of these two infilled frames is remarkably similar. A minor increase in ductility may be present in the positive direction referring to the lack of a sudden drop in strength so prevalent in the other tests. The retrofitted specimen had a very thin 0.5″ layer of ECC applied and a modest amount of reinforcing (6x6 W1.4xW1.4 WWF). In addition the retrofit was only applied to each side of the window opening, with no retrofit in the sill or lintel area. This shows that a lower bound exists for the robustness of the retrofit in order to realize any benefits.

The effect of retrofit on the solid wall appears in figure 11.4. In test 4 a 1″ thick layer of retrofit was applied with more steel (4x4 W4.0xW4.0 WWF). In this case the retrofit increased the strength and ductility. The final failure of the retrofitted specimen was still column shear, leading to a brittle failure, but at a much larger displacement than the non-retrofitted wall.

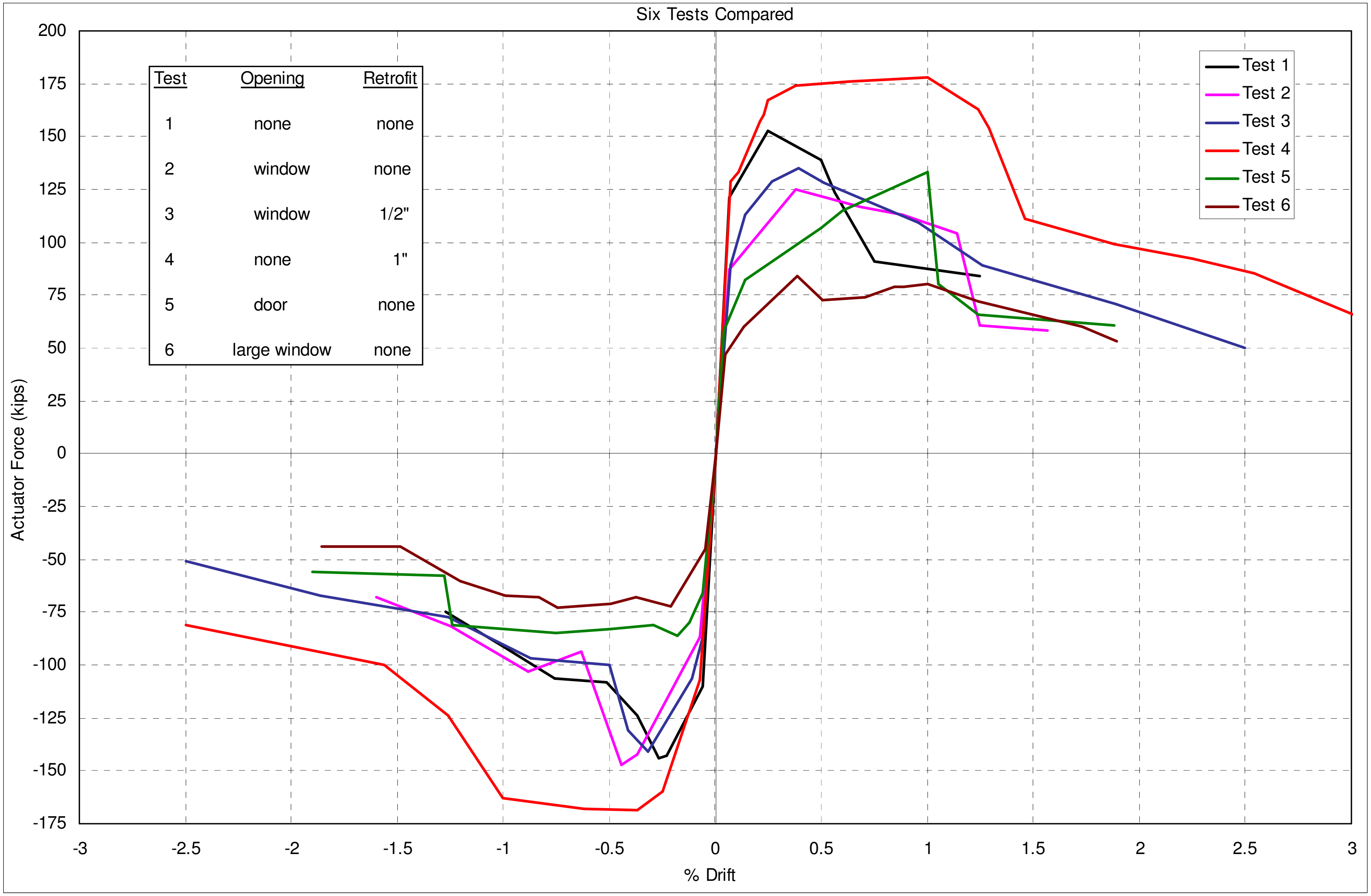

Figure 11.1: Six Tests Compared

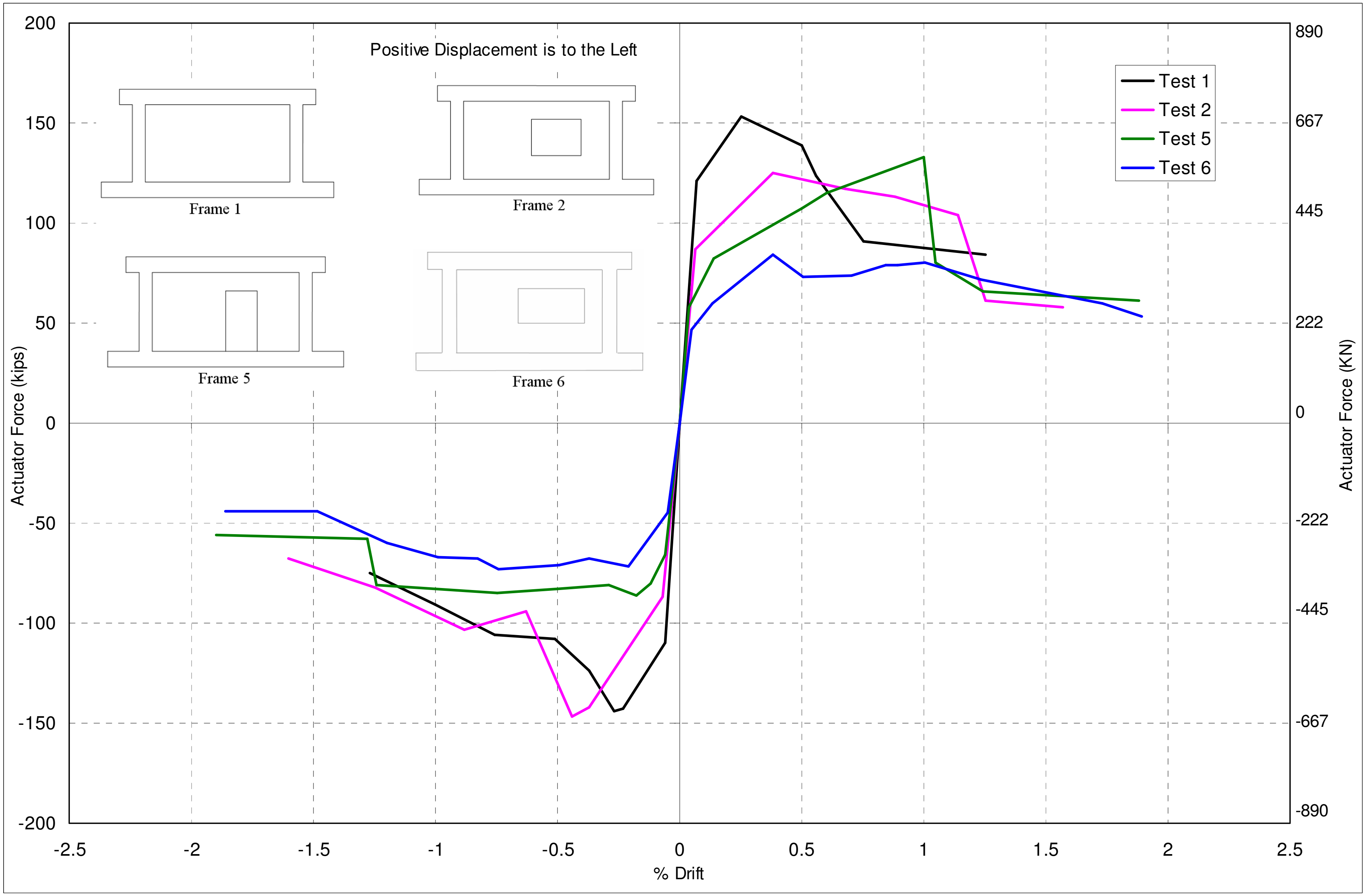

Figure 11.2: Effect of Openings

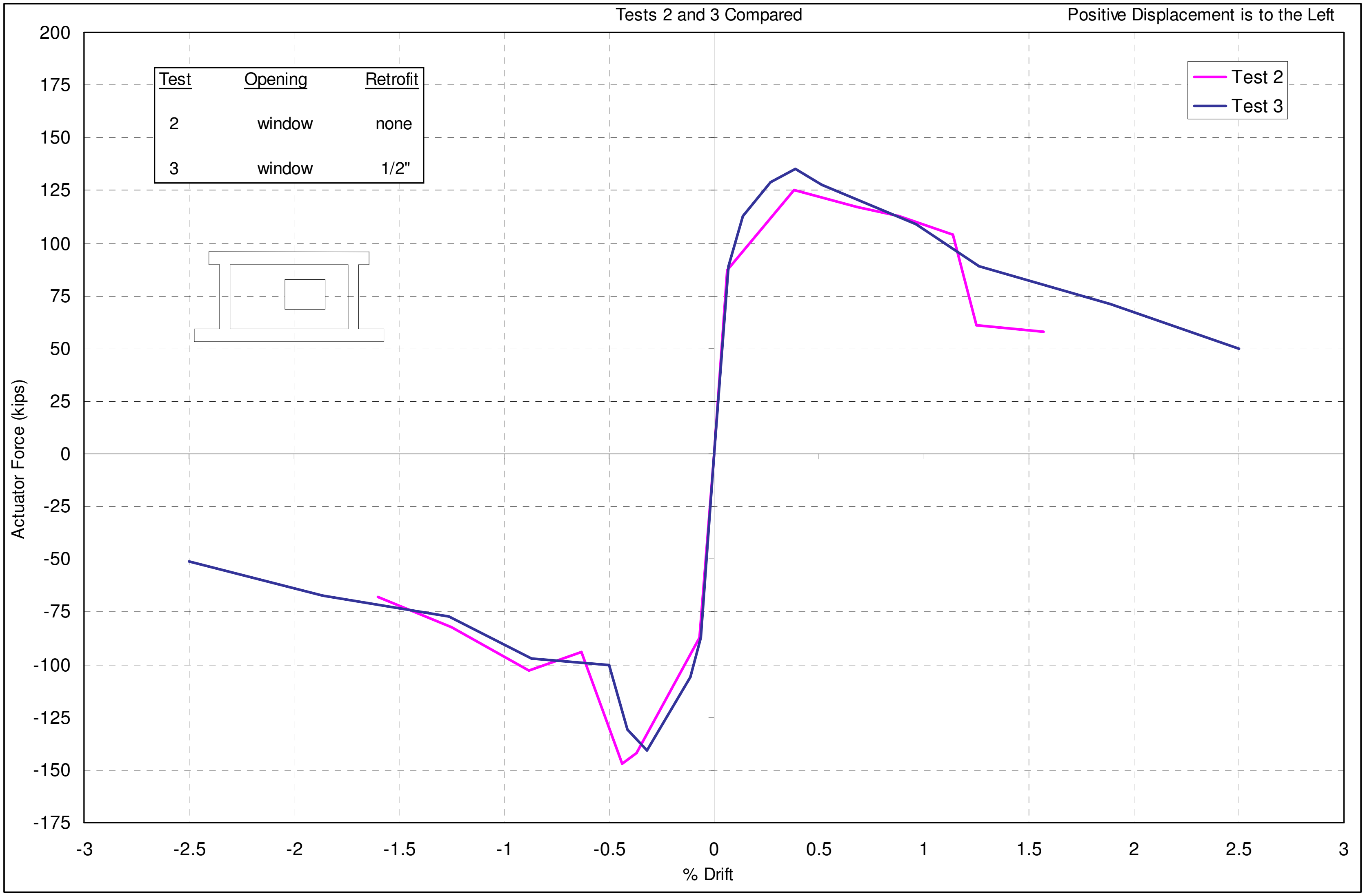

Figure 11.3: Effect of Retrofit on Infill with Window Opening

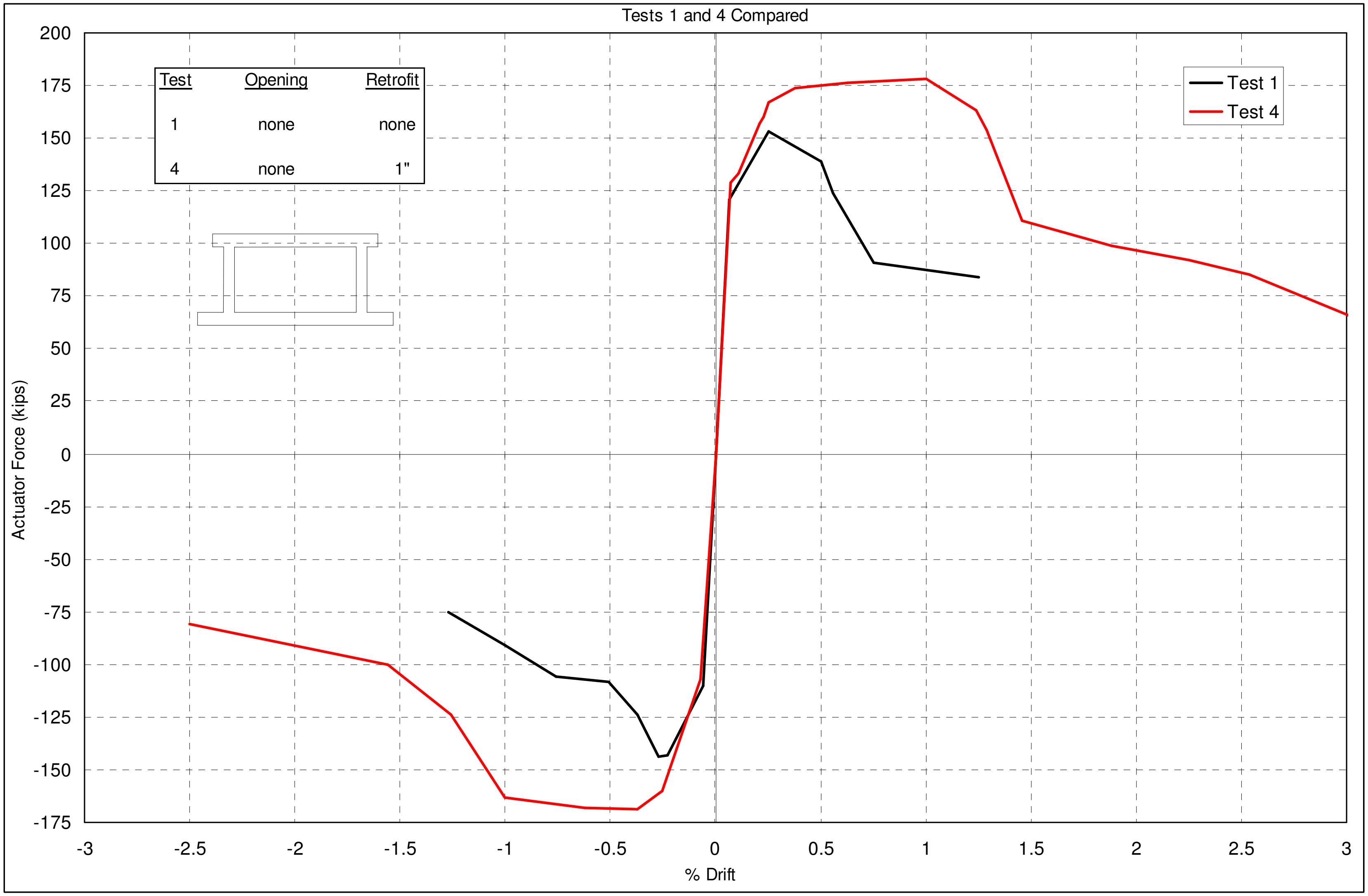

Figure 11.4: Effect of Retrofit on Solid Infill

References

ASTM C 1072-05b, Standard Test Method for Measurement of Masonry Flexural Bond Strength

ASTM E 518-03, Standard Test Method for Flexural Bond Strength of Masonry

ASTM C 952-02, Standard Test Method for Bond Strength of Mortar to Masonry Unit

Al-Chaar, G., Issa, M., Sweeney, S., Behavior of Masonry-Infilled Nonductile Reinforced Concrete Frames, Journal of Structural Engineering, Vol. 128, No. 8, August 2002, p. 1055-1063.

Al-Chaar, G., Evaluating Strength and Stiffness of Unreinforced Masonry Infill Structures, U.S. Army Corps of Engineers, ERDC/CERL TR-02-1, January 2002.

Arslan, G., Shear Strength of Reinforced Concrete Beams With Stirrups, Materials and Structures, Vol. 41, 2008, p. 113-122.

Atkinson, R., Amadei, B., Sture,S. , Saeb, S., Deformation and Failure Characteristics of Masonry Bed Joints Under Shear Loadings, Proceedings of the Fourth North American Masonry Conference, University of California, Los Angeles, California, August 16-19, 1987, p. 61.1-61.14.

Atkinson, R., Amadei,B. , Saeb, S., Sture, S., Response of Masonry Bed Joints in Direct Shear, Journal of Structural Engineering, Vol. 115, No. 9, September, 1989, p. 2276-2296.

Berto, L., Saetta, A., Scotta, R., Vitaliani, R., Failure Mechanism of Masonry Prism Loaded in Axial Compression: Computational Aspects, Materials and Structures, Vol. 38, March 2005, p. 249-256.

Blackard, B., Kim, B., Citto, C., Willam, K., Mettupalayam, S., Failure Issues of Brick Masonry, Proceedings of the Sixth International Conference on Fracture Mechanics of Concrete and Concrete Structures, Catania, Italy, June 17-22, 2007, p. 1587-1594.

Colangelo, F., Pseudo-Dynamic Seismic Response of Reinforced Concrete Frames Infilled with Non-Structural Brick Masonry, Earthquake Engineering and Structural Dynamics, Vol. 34, 2005, p. 1219-1241.

Hansen, K., Bending and Shear Tests With Masonry, Danish Building Research Institute SBI Bulletin 123, 1999.

Kakaletsis, J., Karayannis, G., Experimental Investigation of Infilled Reinforced Concrete Frames With Openings, ACI Structural Journal, Title no. 106-S14, March-April 2009, p. 132-141.

Manzouri, T. , Nonlinear Finite Element Analysis and Experimental Evaluation of Retrofitting Techniques for Unreinforced Masonry Structures, PhD Dissertation, University of Colorado, Boulder, Colorado, 1995.

Mehrabi, A., Behavior of Masonry-Infilled Reinforced Concrete Frames Subjected to Lateral Loadings, PhD Dissertation, University of Colorado, Boulder, Colorado, 1994.

Nuss, L., The Parameters Influencing Shear Strength Between Clay Masonry Units and Mortar Tested Using Shear Masonry Specimens, M.S. Thesis, University of Colorado, Boulder, Colorado, 1978.

Nuss, L., Noland, J., Chinn, J., The Parameters Influencing Shear Strength Between Clay Masonry Units And Mortar, Proceedings of the North American Masonry Conference, Boulder, Colorado, August 14-16, 1978.

van der Pluijm, R., Shear Behavior of Bed Joints, Proceedings of the Sixth North American Masonry Conference, Philadelphia, Pennsylvania, June 6-9, 1993, p. 125-136.

Rao, K., Reddy, B., Jagadish, K., Flexural Bond Strength of Masonry Using Various Blocks and Mortars, Materials and Structures, Vol. 29, March 1996, p. 119-124.

Vermeltfoort, A., Raijmakers, T., Janssen, H., Shear Tests on Masonry Walls, Proceedings of the Sixth North American Masonry Conference, Philadelphia, Pennsylvania, June 6-9, 1993, p. 1183-1193.